MODELLING THE USER-SPECIFIC HUMAN COCHLEA

by

Tiaan Krynauw Malherbe

Submitted in partial fulfilment of the requirements for the degree
Philosophiae Doctor (Electronic Engineering)

in the

Department of Electrical, Electronic and Computer Engineering
Faculty of Engineering, Built Environment and Information Technology

UNIVERSITY OF PRETORIA

July 2015

SUMMARY

MODELLING THE USER-SPECIFIC HUMAN COCHLEA

by

Tiaan Krynauw Malherbe

Supervisor: Prof T. Hanekom

Co-supervisor: Prof J.J. Hanekom

Department: Electrical, Electronic and Computer Engineering

University: University of Pretoria

Degree: Philosophiae Doctor (Electronic Engineering)

Keywords: cochlear implant; volume conduction model; FEM; CT; neural excitation; user-specific; skull model; bone resistivity

Cochlear implants have successfully been used to enable hundreds of thousands of profoundly deaf people to regain some perception of hearing. Hearing performance does, however, vary greatly among individual implant users. In order to gain a better understanding of the underlying factors that cause these inter-user performance differences, insight into the functioning of individual implant users' hearing systems is required. Some of the parameters unique to an implanted user's hearing system may be measured non-invasively using psychoacoustics or the measurement of electrically evoked compound action potentials. While these methods provide information of the macro response of a user's hearing system to stimulation, individual parameters, for example the individual neurons that are excited cannot be measured. Some individual parameters are difficult or even impossible to measure in a living human as it is not technically feasible or invasive surgery is required. When obtaining measurements inside the inner ear of a living human is not an option, an alternative that mimics the human hearing system is required from which measurements can be predicted: models.

This study describes the development of a method to construct an electrical computational three-dimensional finite element model of the implanted cochlea of a specific living individual. This method is presented as a tool for researchers to probe the cochleae of specific implanted users non-invasively. Data from a low resolution computer tomography scan is used to construct a geometric representation of the bony outer cochlear structures and augmented with histologic data to construct the smaller inner cochlear structures. A detailed skull geometry with brain and scalp volumes that includes the user's return electrode is also constructed. The user's electrode array is modelled in its intra-cochlear location and stimulation is simulated using finite element modelling. The cochleae of five individual ears were modelled and intra-cochlear and neural node potentials were predicted along with neural excitation patterns.

Having models that can predict user-specific outcomes, predictions that include the variability between implanted ears are obtained. This allowed the comparison of modelled data to common trends found in literature and enabled the investigation of questions frequently asked by modellers. These include the effect that bone resistivity, head volume shape, return electrode implementation and return electrode position have on modelled results. These findings were incorporated and contributed to higher detailed models being produced than are currently described in literature.

The models were then practically applied in two areas. The first was in the quantification of potential decay in the cochlea where a simple model is derived to predict decay at the neuron level based on the location of an electrode. The second was in the translation of the model into the clinical domain where the mismatch between the perceived pitch and mapped frequencies of specific implanted individuals were predicted. Along with these predictions it was found that neural excitation and intra-cochlear potential spread are highly dependent on individual cochlear morphology. This warrants the inclusion of user-specific morphology in volume conduction models of the implanted cochlea where user-specific outcomes are predicted.

OPSOMMING

MODELLERING VAN DIE PERSOON SPESIFIEKE KOGLEA

deur

Tiaan Krynauw Malherbe

Studieleier:	Prof T. Hanekom
Mede-studieleier:	Prof J.J. Hanekom
Departement:	Elektriese, Elektroniese en Rekenaaringenieurswese
Universiteit:	Universiteit van Pretoria
Graad:	Philosophiae Doctor (Elektroniese Ingenieurswese)
Sleutelwoorde:	koglêere inplanting; volume geleidingsmodel; eindige element modellering; X-straal tomografie; neurale aktivering; individu spesifiek; skedel model; been konduktansie

Koglêere inplantings word suksesvol gebruik om die gehoor van honderde-duisende erg-hardhorende mense tot ’n mate te herwin. Gehoorpersepsie varieer egter baie onder individuele inplantinggebruikers. Om ’n beter begrip te kry van die onderliggende faktore wat hierdie variasie in gehoorpersepsie beïnvloed, is insigte in die werking van die gehoorstelsel van ’n individu nodig. Sekere faktore wat eie aan ’n individu se gehoorstelsel is, kan nie-indringend gemeet word deur middel van psigo-akoestiek en elektries-ontlokte saamgestelde aksiepotensiale. Alhoewel hierdie metodes insae gee in die makro response van ’n gebruiker se gehoorstelsel tot elektriese stimulasie, kan individuele faktore, soos individuele neurone wat ge-aktiveer word, nie in isolasie gemeet word nie. Sekere faktore is moeilik of selfs onmoontlik om in die oor van ’n lewende individu te meet, want dit is tegnies onmoontlik, of indringende chirurgie word vereis. As die meet van faktore binne-in die oor van ’n lewendige inplantinggebruiker nie ’n opsie is nie, word ’n alternatief wat die menslike gehoorstelsel naboots verlang: modelle.

Hierdie studie beskryf hoe ŉ metode ontwikkel is om ŉ elektriese drie-dimensionele model te skep van die geïnplanteerde oor van ŉ spesifieke lewende individu. Hierdie metode word voorgelê as ŉ middel vir navorsers om die geïnplanteerde oor van ŉ lewende individu nie-indringend te ondersoek. Lae-resolusie rekenaar-tomografie data is gebruik om ŉ drie-dimensionele beskrywing van die beenagtige buite-strukture van die koglea te konstrueer. Hierdie strukture is aangevul met histologiese data van die fyner binne-strukture van die koglea. ŉ Gedetailleerde model van die skedel met brein en kopvel is ook gekonstrueer. Die gebruiker se elektrodeskikking is ook in sy posisie binne-in die koglea gemodelleer en gesimuleer deur middel van eindige element modellering. Die kogleas van vyf individuele ore is gemodelleer en spannings binne-in die koglea en op die neuronnodes is voorspel, tesame met neurale aktiveringspatrone.

Deur modelle te hê wat gebruiker-spesifieke uitkomste kan voorspel, kan voorspellings gemaak word wat die variasie tussen geïnplanteerde ore in ag neem. Dit laat weer toe dat voorspelde data met gemete data van ŉ versameling van gebruikers vergelyk kan word. Dit baan die weg sodat algemene vrae in die veld van koglêere modellering beantwoord kan word. Hierdie vrae sluit in watter effek beenresistiviteit, kopvorm, terugkeerelektrode-implementering en terugkeerelektrode-posisie op voorspellings het. Die bevindinge van hierdie vrae is geïnkorporeer en het gelei tot modelle wat meer detail bevat as wat huidiglik in die literatuur beskryf word.

Die modelle wat geskep is, is in twee praktiese areas toegepas. Die eerste is in die kwantifisering van die spanningsverval in die koglea. Hier is ŉ eenvoudige model opgestel wat spanningsverval voorspel as die posisie van ŉ elektrode bekend is. Die tweede toepassing is in die kliniese domein. Hier is die mate van wanaanpassing tussen die waargeneemde toonhoogte en toegepaste toonhoogtes voorspel. Tesame met hierdie voorspellings, is die bevinding gemaak dat die neurale aktiveringspatrone en die intra-koglêere spannings hoogs afhanklik is van die vorm van die individuele koglea. Dit motiveer dat koglêere geometrie ingesluit moet word in modelle van inplanteerde kogleas as gebruiker-spesifieke uitkomste verlang word.

ACKNOWLEDGEMENTS

I would like to extend my sincerest gratitude towards the following people and institutions for their contributions towards this study.

- First and foremost I would like to give thanks to the almighty God, our father in Jesus Christ who made this study possible and whose grandeur resonates in the infinite complexities of even the smallest created things.
- My beautiful wife, Elmien, for her love and unwavering support.
- My parents for their love, support, prayers and for providing me with a solid foundation in life.
- My study leader, Prof Tania Hanekom, for her guidance and the long hours spent on this study.
- All my friends, family and extended family for their interest, support and prayers.
- Prof Johan Hanekom and everyone I have had the privilege to get to know in the biogroup especially Stephen, Larry, Pieter, Dirk, Heinrich, Marianne, Rikus and Tiaan for pleasant memories (and lots of coffee).
- The cochlear implant users who took part in this study for their time and allowing their cochleae to be scanned.
- Erica Smith and the staff at the Steve Biko Academic Hospital radiology department.
- The following sources for providing financial assistance:
    - National Research Foundation (South Africa).
    - University of Pretoria
    - Southern Medical Pty Ltd.

LIST OF ABBREVIATIONS

%RDS	percentage of relative standard deviation
3D	three-dimensional
µ-CT	micro computed tomography
BEM	boundary element method
BM	basilar membrane
CF	characteristic frequency
CI	cochlear implant
CT	computed tomography
dB	decibel
EFI	electrical field imaging
FDM	finite difference method
FE	finite element
FEM	finite element method
fmSTC	forward masked spatial tuning curve
FVM	finite volume method
GSEF	generalised Schwartz-Eikhof-Frijns
HH	Hodgkin-Huxley
HRSCT	high-resolution spiral computed tomography
MBD	model-based diagnostic
MPM	model-predicted mapping
MRI	magnetic resonance imaging
MWR	method of weighted residuals
OC	organ of Corti
OPFOS	orthogonal-plane fluorescence optical sectioning
RT	rotational tomography

RVM	Ritz variational method
RW	round window
SG	spiral ganglion
SM	scala media
ST	scala tympani
SV	scala vestibule
TACT	tuned aperture computed tomography
VC	volume conduction

TABLE OF CONTENTS

CHAPTER 1 INTRODUCTION

1.1 PROBLEM STATEMENT

1.1.1 Context of the problem

Since the 1970's cochlear implants have been used to restore hearing to the profoundly deaf (Mudry and Mills, 2013). Despite decades of research and improvements in the technology, there still exists very large variability in hearing performance between implanted users. In order to understand such inter-user performance differences, the differences in the functioning of users' hearing systems have to be understood. One way of obtaining insight into the functioning of an individual's hearing, is to measure characteristics of that individual's hearing system. Non-invasive methods to measure these characteristics include psychoacoustics and the measurement of electrically evoked compound action potentials. These methods do not measure characteristics, such as the specific neurons that were activated, in isolation but rather give a measure of the composite response of many systems in the ear. Some characteristics are difficult or even impossible to measure in isolation in a living human as it is not technically feasible or invasive surgery is required. When measuring characteristics inside the inner ear of a living human is not an option, an alternative that mimics the human hearing system is required from which responses can be predicted: models.

Various models have traditionally been used to mimic parts of the hearing system in order to gain a better understanding of its functioning. They have mainly been in the form of animal, mathematical and computational models that describe parts of the hearing system. Models are usually generalized and do not describe the specific differences between the hearing systems of implanted individuals. In order to predict the functioning of a specific hearing system, a model of that specific user's ear has to be developed. Such a model may then be used to investigate the factors that affect inter-user variability in perception.

In this study a modelling method is developed that allows the construction of an electrical model of an implanted cochlea of a specific, living human. Models are then constructed of the cochleae of specific implant users and used to predict parameters that cannot be

measured directly such as neural excitation patterns and intra-cochlear potential fields. During the process of method development, modelling aspects that influence results are also investigated. These include the effect that bone resistivity, head volume shape, return electrode implementation and return electrode position have on modelled results. These findings contribute to higher detailed models being produced than are currently described in literature. These are then practically applied in two areas. The first is in the quantification of potential decay in the cochlea where a simple model is derived to predict decay at the neuron nodes based on the location of an electrode. The second is in the prediction of the mismatch between the perceived pitch and mapped frequencies of specific implanted individuals.

1.1.2 Research gap

Current three-dimensional (3D) cochlear models that estimate the electrical fields inside a stimulated cochlea and its effect on neural excitation are generally based on a generic human or guinea pig cochlear shape (Choi, Lai and Chen, 2004; Frijns, Briaire and Grote, 2001; Frijns, Briaire and Schoonhoven, 2000; Hanekom, 2001b; Hanekom, 2001a; Rattay, Leao and Felix, 2001a) that does not take inter-user morphological variations into account. These models have successfully been used to investigate numerous aspects about the electrophysiological functioning and characteristics of cochlear implants like the effect of electrode position, stimulus mode and site of neural excitation. To gain insight into the workings of the implanted ear of a specific individual, the morphology of that individual's cochlea has to be incorporated into the model as cochlear morphology varies among individuals (Erixon, Högstorp, Wadin and Rask-Andersen, 2009; Avci, Nauwelaers, Lenarz, Hamacher and Kral, 2014). To date, there are no user-specific human cochlear models described in literature (Kikidis and Bibas, 2014).

The focus of this study is on the development of a method to construct a 3D model of a living human individual's cochlea. Such individualized models should give better insight into the variance in the functioning of individual cochleae subjected to electrical

stimulation than models based on generic morphologies do. Such models should also allow the prediction of user-specific parameters (such as neural excitation patterns, potential spread and perceived frequencies) that cannot be obtained experimentally from living human implant users such as neural excitation patterns and intra-cochlear potential fields.

The detailed models that are produced using this method may then also be used to investigate other aspects relevant to cochlear implant modelling. These include:

- The establishment of a bone resistivity value to use in modelling as various bone values have been used in previous modelling studies.
- Investigation of the effect that head volume and return electrode implementation have on results predicted by models, as previous modelling studies have incorporated different levels of detail in this respect.

The higher detailed models resulting from incorporating these findings may then be practically applied. Two such areas include:

- The accurate description of potential decay in a cochlea based on the location of a stimulating electrode as a standard value of 3 dB/mm, which is based on decay in a homogeneous medium, is generally used to describe decay throughout a highly non-homogeneous cochlea.
- Predicting the mismatch between perceived pitch and a user's frequency map.

1.2 RESEARCH OBJECTIVES AND APPROACH

The first objective of this study is to develop a tool to probe the electrically stimulated cochlea of a specific implant user non-invasively. This is done by developing a method to construct a 3D computational model of a specific living human individual's cochlea from data that is obtainable non-invasively.

The second objective is to investigate and report factors, such as the resistivity of the cochlear bone, return electrode implementation and location, and modelled head morphology that affect model outcomes.

The third objective is to investigate the hypothesis that highly detailed 3D models of the cochleae of living implanted individuals are able to predict outcomes not predicted by models based on a generic cochlear morphology. To test this hypothesis, 3D models are constructed from standard clinical CT data of the implanted cochleae of living implanted users. These models are then used to predict potential fields and neural excitation patterns of the cochleae of each user. If it is found that user-specific cochlear geometry affects predicted potential fields and neural excitation patterns, the hypothesis is proven.

The fourth objective is to demonstrate practical applications of detailed user-specific models. These include the prediction of quantities that may be of importance in basic research in cochlear implants for example the estimation of potential decay from the location of an electrode and the translation of this modelling method to a clinical application, for example, in the prediction of the mismatch between perceived and mapped frequencies.

1.3 RESEARCH CONTRIBUTION

Models of the peripheral functioning of cochlear implants (CIs) attempt to describe the biophysical interface between the technology and the auditory nervous system and the subsequent excitation of the peripheral neural population. Cochlear models (Hanekom, 2001b; Hanekom, 2005; Frijns et al., 2000; Choi et al., 2004; Rattay et al., 2001a; Frijns et al., 2001) have focused on individual aspects of the implanted cochlea and are constantly developing to incorporate more features to improve their accuracy in predicting biological conditions. As considerable morphological variations exist among human cochleae (Erixon et al., 2009; Van Der Marel, Briaire, Wolterbeek, Snel-Bongers, Verbist and Frijns, 2014; Avci et al., 2014), including the anatomical dimensions of a specific user's cochlea in a

model is expected to allow more accurate modelling of the electrophysiology of the individual auditory periphery. Having a method to construct such a user-specific model will provide researchers with a tool to investigate user-specific differences in cochlear implant functioning.

In order to provide clinical interventions on a user-specific basis, the underlying mechanism governing stimulation of a specific person's implant needs to be understood. This may be gained from a model of that person's cochlea. The potential of this was demonstrated in the assessment of the level of mismatch between the frequency of a sound that a user perceives and the frequency map of that user. This information may be used as an aid during the mapping of an implant (also referred to as model-predicted mapping (MPM)).

Having models of individual cochlea available, enables the prediction of the responses of a population of cochleae. When investigating effects such as the effect of bone resistivity on excitation spread, a better reflection of its true effect was obtained as the variability in cochlear morphology was taken into account. Here bone resistivity values were established that are to be used in 3D finite element (FE) cochlear models as varying ranges of values have been used in cochlear models. Different resistivity values are suggested based on the implementation of the surrounding head model and neuron model used. This gives modellers with models of varying complexity a value to work from.

The detailed models produced in this study also allowed the prediction of the dependency of monopolar potential decay on electrode position. This was done as monopolar potential decay is traditionally assumed to be a constant value throughout the cochlea.

The modelling method developed here is a significant advancement in the field of cochlear implant modelling as it allows the modelling of the cochlea of a specific living implanted user. A previous model introducing subject-specificity was created for an implanted guinea pig cochlea (Malherbe, Hanekom and Hanekom, 2013), but that method required

dissection of the cochlea and a high-radiation imaging technique which is not suitable for in-vivo imaging of a human cochlea. Another study has incorporated the morphologies of different cochleae into models to introduce inter-user variance into predicted results (Kalkman, Briaire, Dekker and Frijns, 2014a) and the study by Carlyon, Macherey, Frijns, Axon, Kalkman, Boyle, Baguley, Briggs, Deeks, Briaire, Barreau and Dauman (2010) included subject specificity by scaling template models according to CT scan data; in both studies a detailed descriptions of the methods used to construct those models are not given. The present study is the first to offer a method to construct the cochlea of a specific user with the aim to predict outcomes of that specific individual. This paves the way for further research into the factors that cause the large variance in hearing performance found in cochlear implant users.

1.4 OVERVIEW OF STUDY

Figure 1.1 shows an overview of the aspects covered in this study within the context of probing user-specific cochlear implant performance. Aspects in both the theoretical research domain as well as the clinical domain are employed and predicted.

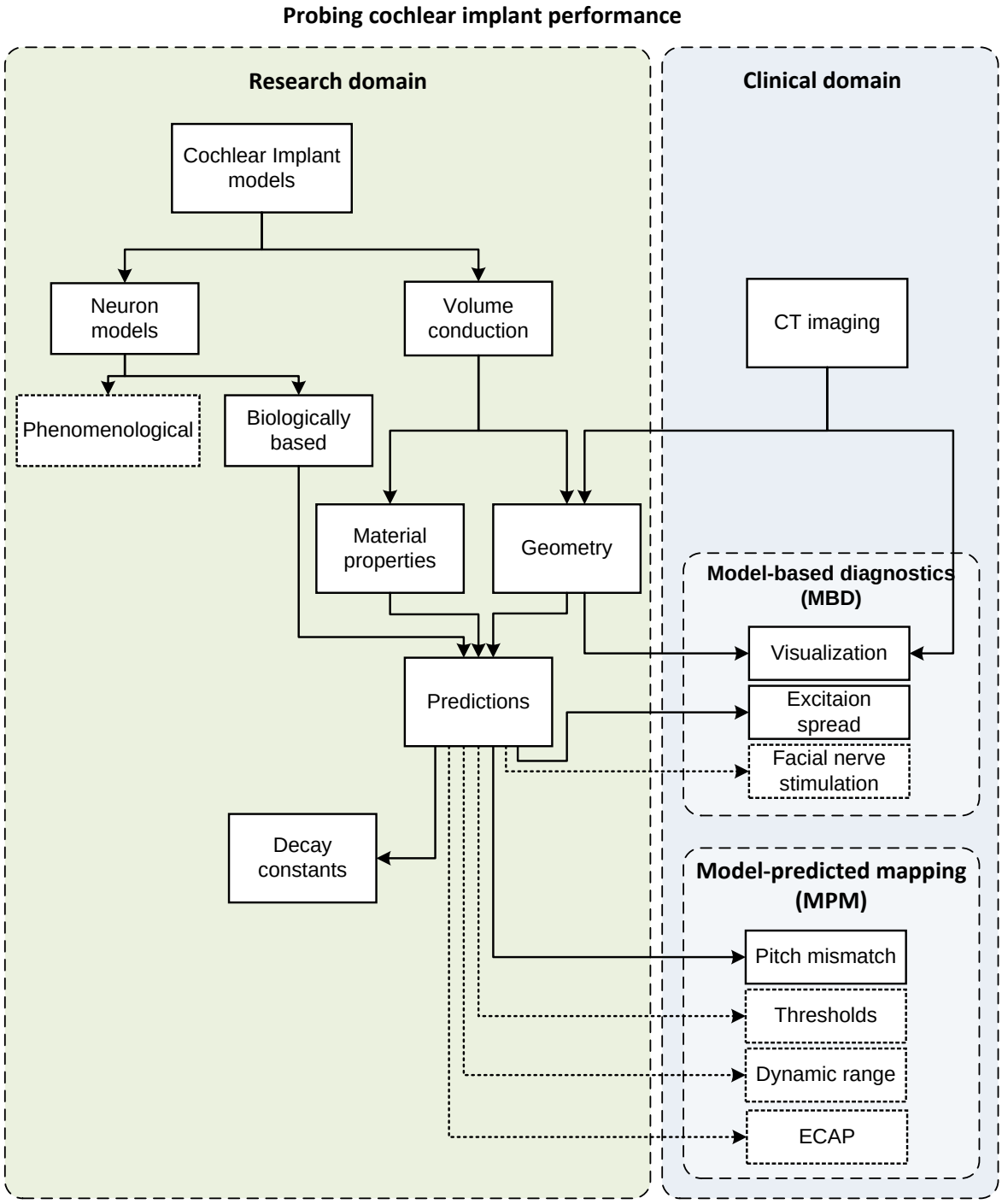

Figure 1.1. Probing user specific implant performance is done in both the theoretical research domain as well as the clinical domain. Aspects incorporated in this study are shown in solid black blocks with issues related to this study shown in dashed blocks

Figure 1.2 shows a functional diagram indicating how the aspects incorporated into this study fit together.

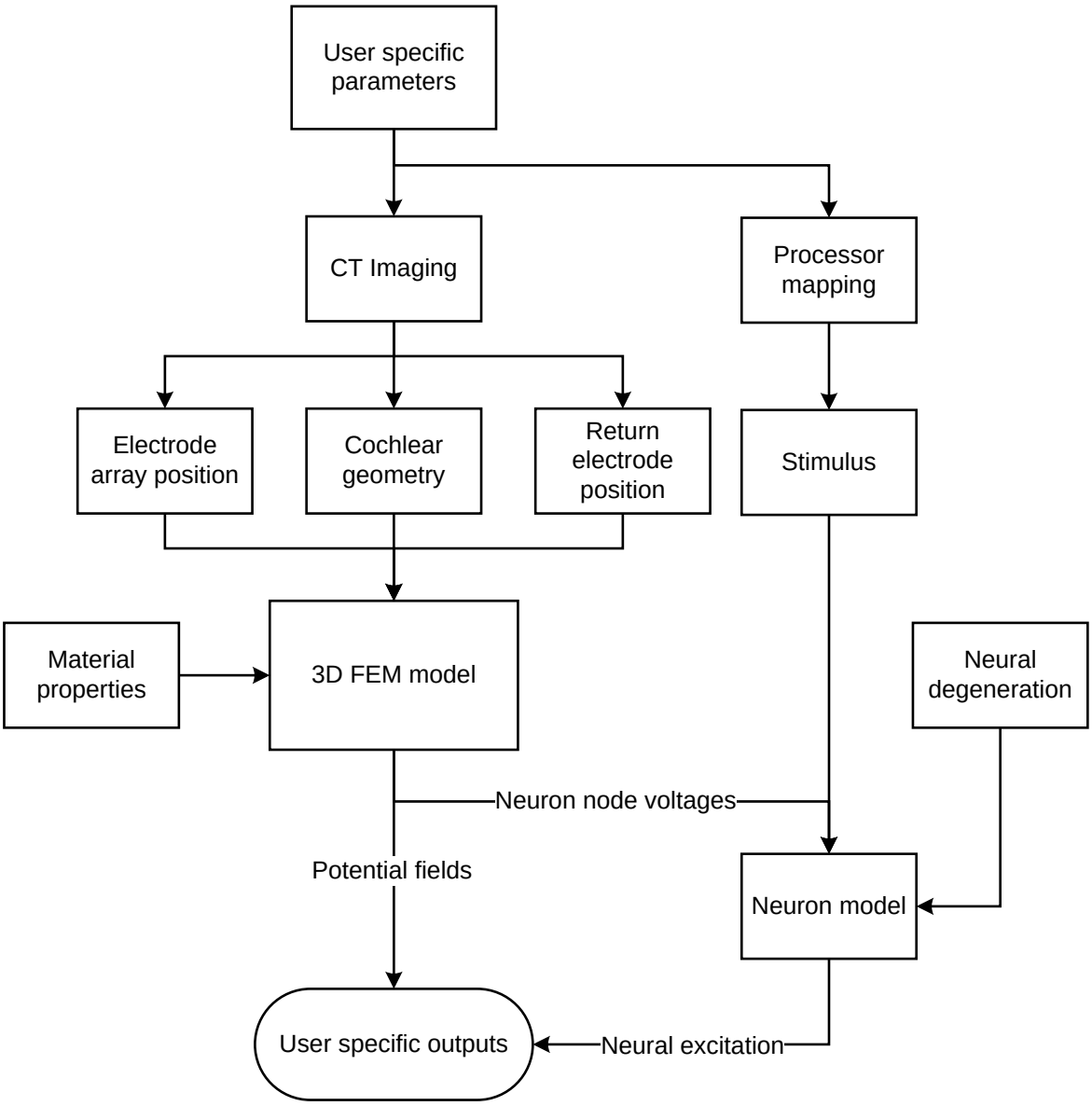

Figure 1.2. Functional diagram of the study. The aspects around cochlear implant modelling that have been incorporated in this study are shown

This thesis is divided into the following sections.

Chapter 2. Literature study

The literature pertaining to the different aspects of this study is explored.

Chapter 3. Methods

The methodology followed to construct a model of the implanted cochlea of a specific live human implant user is described.

Chapter 4. Bone resistivity estimation

A bone resistivity value for use in volume conduction models of a cochlear implant is derived using models constructed with the method described in Chapter 3.

Chapters 5 and 6. Model applications

Two applications of the detailed models that were constructed are demonstrated. The first is the derivation of a simple function to determine potential decay in a cochlea based on the position of the electrode. The second is the application of a user-specific model to predict the mismatch between the perceived pitch and the mapped frequency of specific individuals.

Chapter 7. General discussion

Chapter findings are summarized and discussed in the context of the research objectives and literature. Future direction of this research is also discussed.

Chapter 8. Conclusion

Final thoughts and a summary of the conclusions from this study are given.

1.5 RESEARCH OUTPUTS

A summary of work from this study that has been presented elsewhere is listed here.

1.5.1 Published peer-reviewed journal articles

Malherbe, T. K., Hanekom, T. and Hanekom, J. J. (2015). The effect of the resistive properties of bone on neural excitation and electric fields in cochlear implant models. Hearing Research, 327:126-135.

1.5.2 Peer-reviewed journal articles in review

Malherbe, T. K., Hanekom, T. and Hanekom, J. J. (In review) Constructing a three-dimensional electrical model of a living cochlear implant user's cochlea. International Journal for Numerical Methods in Biomedical Engineering.

1.5.3 Conference outputs

Hanekom, T., Malherbe, T.K., Gross, L., Baron, R., Asvat, R., Badenhorst, W., and Hanekom, J.J., "Design and application of user-specific models of cochlear implants" 2015 Conference on Implantable Auditory Prostheses, Granlibakken Conference Grounds, Tahoe City, California, July 12-17, 2015, p. 25

Badenhorst, W., Malherbe, T.K., Hanekom, T. and Hanekom, J.J., "Investigating the effect of cochlear geometry and neural models on the thresholds when modelling the cochleae of specific implant users" 2013 Conference on Implantable Auditory Prostheses, Granlibakken Conference Grounds, Tahoe City, California, July 14-19, 2013, p. 132

Hanekom, T., Asvat, R., Baron, R., Malherbe, T.K., Badenhorst, W. and Hanekom, J.J., "Cochlear implants: quantifying user-specificity in peripheral neural responses", University of Pretoria 4th Neuroscience Day, University of Pretoria, Pretoria, 9 May 2013.

* Hanekom, J.J. and Hanekom, T." New topics in cochlear implant research", 2013 SACIG Conference, Discovery Health, Sandton, Johannesburg, 4 to 5 May 2013.

* Hanekom, J.J. and Hanekom, T., "What underlies variation in performance with a cochlear implant?", presented at "Cochlear Implants: Do they meet their expectations?", half day course presented at the Department of Communication Pathology, University of Pretoria, Main Campus, 1 August 2013.

Hanekom, T., Hanekom, J.J. and Malherbe, T.K., "Using high-resolution cochlear imaging and computer modelling to investigate peripheral auditory neural excitation", 2012 SACIG Conference, Tygerberg Hospital, Cape Town, 12 to 13 May 2012.

Hanekom, T., Malherbe, T.K. and Hanekom, J.J., "Probing auditory neural excitation using high-resolution imaging and modelling", University of Pretoria 3nd Neuroscience Day, University of Pretoria, Pretoria, 10 May 2012.

Hanekom, T., Malherbe, T.K., Jönsson, A.E.R. and Hanekom, J.J., "Modeling of peripheral factors that affect neural excitation in the electrically stimulated cochlea", 2011 Conference on Implantable Auditory Prostheses, Asilomar Conference Grounds, Pacific Grove, California, July 24-29, 2011, p. 272

Hanekom, T., Malherbe T.K., Jönsson, A.E.R. and Hanekom, J.J., "Modelling of peripheral factors that affect neural excitation in the electrically stimulated cochlea", University of Pretoria 2nd Neuroscience Day, University of Pretoria, Pretoria, 19 May 2011.

Malherbe, T.K., Hanekom, T. and Hanekom, J.J., "Constructing 3D models of subject specific human cochleae from CT-scans", 11th International Conference on Cochlear Implants and Other Implantable Auditory Technologies, Stockholm Sweden, June 30- July 3, 2010, p. 67

* Talks presented included work presented in this thesis.

1.5.4 Other publications

Malherbe, T., Hanekom, T. and Hanekom, J.J. (2014). “Peering into a cochlear implant user’s head”, Innovate, (9).

Govindasamy, R., Malherbe, T., Hanekom, T. and Hanekom, J.J. (2011). “Subject-specific modelling of neural responses to electrical stimulation of the auditory system”, Innovate, (6).

CHAPTER 2 LITERATURE STUDY

The aim of this chapter is to explore the literature pertaining to the different aspects of this study. As this study combines different research fields and disciplines, each is covered separately.

2.1 BACKGROUND ON COCHLEAR IMPLANTS

Cochlear implants are prosthetic devices that restore variable levels of auditory perception to persons with little or no hearing. This is achieved by stimulating surviving cochlear neurons via an electrode array implanted into the cochlea. The pulses applied to the electrodes are provided by an external speech processor which encodes sound picked up by an external microphone into short pulses. The external speech processor communicates with the implanted electronics via a transcutaneous link.

The first documented case of electrically induced hearing was that of Alessandro Volta in the late 18th century. When inserting two metal rods connected to a battery of electrolytic cells (which he invented) into his ears, he heard a “loud boom within the head” followed by a “boiling sound”. Throughout the years other attempts at electric hearing were made but it was only until the middle of the 20th century that electrical stimulation of the auditory nerve became well understood and cochlear implants came into being.

Some of the seminal work on cochlear implants were done by Doyle, Doyle Jr and Turnbull Jr (1964) and Simmons (1966) during the 1960’s. They were of the first to surgically implant electrodes into or near the cochlea. The electrodes they implanted did not succeed in enabling the patients to perceive speech, but did pave the way for further research.

Since then numerous advances in this field were made which led to the first commercial cochlear implant, the House 3M single-electrode implant, becoming available in 1972. Some of these first single channel implants allowed users to perceive environmental sounds and identify a few words, but speech perception was poor (Brackmann, 1976; Michelson, Merzenich, Pettit and Schindler, 1973). Today, multichannel electrode arrays with advanced speech encoding and stimulation strategies allow some users to perceive

speech without visual cues and enable them to use the telephone. In some cases implants have allowed pre-lingual deaf children to learn language skills at close to the same rate as normal hearing children (Bouchard, Ouellet and Cohen, 2009) and have provided a large improvement in the quality of life of the users (Klop, Briaire, Stiggelbout and Frijns, 2007; Schorr, Roth and Fox, 2009).

Despite these advances there still remains large variability in speech perception performance between individual users (Firszt, Holden, Skinner, Tobey, Peterson, Gaggl, Runge-Samuelson and Wackym, 2004; Kunisue, Fukushima, Kawasaki, Maeda, Nagayasu, Kataoka, Kariya, Fukutomi, Takami and Nishizaki, 2007). Some of the contributing factors of this variability are the duration of deafness and duration of cochlear implantation (Blamey, Arndt, Bergeron, Bredberg, Brimacombe, Facer, Larky, Lindstr"m, Nedzelski, Peterson, Shipp, Staller and Whitford, 1996; Bouchard et al., 2009; Dawson, Blamey, Rowland, Dettman, Clark, Busby, Brown, Dowell and Rickards, 1992; Friedland, Venick and Niparko, 2003; Geers, Tobey, Moog and Brenner, 2008; Mosnier, Sterkers, Bebear, Godey, Robier, Deguine, Fraysse, Bordure, Mondain, Bouccara, Bozorg-Grayeli, Borel, Ambert-Dahan and Ferrary, 2009; Rubinstein, Parkinson, Tyler and Gantz, 1999), age of implantation (Hassanzadeh, Farhadi, Daneshi and Emamdjomeh, 2002; Mahmoud and Ruckenstein, 2014), speech perception before implantation (Friedland et al., 2003; Rubinstein et al., 1999), speech processing algorithm used (Kim, Shim, Chung, Chang and Choi, 1997; Loizou, Stickney, Mishra and Assmann, 2003; Skinner, Holden, Whitford, Plant, Psarros and Holden, 2002), stimulation mode used (Mesnildrey and Macherey, 2015), unilateral or bilateral implantation (Sparreboom, Langereis, Snik and Mylanus, 2015), electrode insertion depth (Buchman, Dillon, King, Adunka, Adunka and Pillsbury, 2014), design of the electrode array (Rebscher, Hetherington, Snyder, Leake and Bonham, 2007) and position of the electrode array in the cochlea (Finley, Holden, Holden, Whiting, Chole, Neely, Hullar and Skinner, 2008).

Animal studies have shown that cochlear neurons start to degenerate if they are not stimulated for a prolonged period of time (Schuknecht, 1993; Vollmer, Beitel, Snyder and

Leake, 2007). Studies based on human data (Nadol Jr, 1990; Nadol Jr, 1997), however, suggest that this may not be the case for human cochlear neurons. Another study has shown that neural degeneration is dependent on the cause of deafness (Teufert, Linthicum and Connell, 2006). The hearing performance of a user, including speech perception, is directly dependent on the state of the neurons and the ability of the electrodes to excite them. In order for an electrode to excite a neuron, the neuron has to fall within the voltage distribution area of the electrode. This is especially true for the neuron terminal which has been shown to be especially sensitive to external potentials (Rubinstein, 1993). This voltage distribution is determined by the geometry of the cochlea as well as the geometry and position of the electrode array in the cochlea (Rebscher et al., 2007). It is thus necessary to develop a cochlear model that accurately models the geometry and conductive properties of the cochlea (also referred to as a volume conduction model in some literature).

2.2 COCHLEAR MODELS

The hearing system is immensely complex and consists of different subsystems working together. One way to gain better insight into the workings of these systems is to use models. A model predicts the behaviour of a system under certain conditions. The purpose of a model may be twofold. First, a model may be used to predict outcomes that are impractical or even impossible to measure on a real implant user. Secondly, the development of a model may be used to gain better insight into the system it is modelling; if a model is able to predict outcomes of a system accurately, it can be assumed that the underlying biological systems it is modelling is sufficiently understood.

Different aspects of the cochlea have been incorporated in different models. In this study an electrical model is used to determine the current patterns induced in a cochlea by a stimulating electrode. These current patterns are then used as an input to a neuron model to predict neural excitation patterns. Some of the contributions of others pertaining to these two broad areas of modelling are summarized here.

2.3 ELECTRICAL COCHLEAR MODELS

A variety of electrical models have been developed for use in cochlear implant research. These models vary in complexity and scope of problems they can be used for. The following techniques have been used to predict the current patterns induced by a stimulating electrode inside a cochlea to varying degrees.

2.3.1 Lumped parameter models

Lumped parameter models represent the geometric properties of a volume conductor with a resistor and capacitor network (Suesserman and Spelman, 1993). This method has the advantage that resistive and capacitive effects are relatively easy to incorporate because of the simple network structure. Another advantage is that computer simulations are faster and less complex than some of the other methods listed here.

The lumped parameter modelling technique may be applied to find the potential distribution in a cochlea (Strelioff, 1973; Vanpoucke, Zarowski and Peeters, 2004). In its simplest form, this is done by dividing the unrolled cochlea into sections and modelling each section as a network of resistors, capacitors and voltage sources. These sections are then joined together to form a circuit that represents the potential distributions across the entire cochlea. The potential at any point in the cochlea may then be obtained by analysing this circuit using a computer circuit simulation program such as SPICE (Vladimirescu, 1994).

These models are, however, not refined because circuit elements represent large areas of tissue and fluids (Suesserman and Spelman, 1993). They are thus more suited to modelling global effects in biomedical applications and not effects on a neuron level (Briaire and Frijns, 2000a). By adding more elements, improved approximations of the potentials in the cochlea may be obtained. However, in more complex networks such as the one implemented by Vanpoucke et al. (2004) where cross turn conductances were implemented by additional resistors, increasing the number of elements causes the elements to lose their

physical meaning and elements can no longer be directly ascribed to physical areas in the cochlea making the assignment of material values to elements problematic. In order to obtain higher resolution potentials at the neuron level while incorporating cross turn effects, the potentials inside a three-dimensional spiralling representation of the cochlea have to be determined.

2.3.2 Three-dimensional cochlear models

3D models aim to incorporate the geometric structure of the cochlea in order to obtain a more accurate and detailed prediction of current patterns induced by a stimulating electrode. Generally a geometric mesh of the cochlea is constructed from measured data (described in section 2.5), material properties are assigned to the different modelled substructures (see section 2.7) and potentials in the cochlea are then calculated. These potential fields may be obtained using one of the following methods.

2.3.2.1 Finite element method (FEM)

Finite element modelling have been used in various models of the implanted cochlea (Malherbe et al., 2013; Hanekom, 2001b; Choi et al., 2004) and is one of the more popular methods to estimate three-dimensional electrical fields. To apply the finite element method, a continuous domain is discretized into a set of smaller sub domains (Clough, 1990) that can be described by their own partial derivative equations. This process is also known as meshing. The finite element method is then used to find approximate solutions to these equations. A disadvantage of this method is that mesh generation may be difficult and the entire volume has to be rediscretized when a small change is made to the geometry. In the present study electrical effects are modelled that do not require the cochlear structure to change, this eliminates the need for rediscretization. In other applications where cochlear mechanics are modelled (Skrodzka, 2005), the geometry constantly changes shape causing the mesh to be rediscretized. An advantage of FEM is that capacitive effects and anisotropic materials may be incorporated in a biological model (Briaire and Frijns, 2000a).

To solve a FEM problem the following operations have to be completed (Burnett, 1987):

- construction of a trial solution,
- application of an optimizing criterion and
- estimation of accuracy.

A trial solution $\overline{U}$ is a solution that approximately satisfies solution. It is generally in the following form:

$$\overline{U}(x;a) = \phi_0(x) + a_1\phi_1(x) + a_2\phi_2(x) + ... + a_N\phi_N(x) \tag{2.1}$$

where *x* represents the independent variables in the problem, $\phi_0(x)$ to $\phi_N(x)$ are known functions called *trial* or *basis* functions and the coefficients a_0 to a_N are undetermined parameters called *degrees of freedom*.

An optimizing criterion determines the best values of the undetermined parameters a_0 to a_N. There are two types of optimizing criterion namely *Method of weighted residuals* (MWR) which is used when the governing equations are differential equations and the *Ritz variational method* (RVM) which is used when the governing equations are integral equations.

An estimation of accuracy is needed to determine how close the approximate solution is to the exact solution. In most theoretical cases the exact solution is not known. The accuracy may then be estimated by comparing the solutions obtained from different optimizing criteria. The closeness and convergence of these results may give insight into the accuracy of the obtained solution (Burnett, 1987).

Powerful commercial software like Comsol Multiphysics and ANSYS that employ FEM to solve volume conduction problems are readily available.

2.3.2.2 Finite difference method (FDM)

The finite difference method is similar to the finite element method but has distinct differences. The FDM is an approximation to the differential equation where the FEM is an approximation to the solution. The advantage of FDM is that it is easy to implement. The disadvantage is that it is restricted to simple rectangular shapes and simple alterations thereof. This makes it undesirable for use in complex biomedical modelling. When modelling a cochlea using FDM, a very small mesh has to be used to avoid leakage from the modelled membranes (which are very thin). This leads to large memory requirements and long computation times (Briaire and Frijns, 2000a).

To implement the FDM, it can be considered as a subset of FEM with its basis functions chosen as piecewise constant functions or Dirac delta functions. To calculate the potential distribution in a biomedical application, the Taylor expansion of the Poisson equation along a fixed structure of points is calculated and then solved via an iterative process (Briaire and Frijns, 2000a).

2.3.2.3 Finite volume method (FVM)

The finite volume method is used to represent partial differential equations as algebraic equations and to evaluate them. A mesh is created from a geometry just as in the FDM. The value of each node of the mesh is then calculated. The volume around each node is known as a finite volume.

To implement this method, governing partial differential equations are first used to describe each node of a geometric mesh. If a volume integral in a partial differential equation contains a divergence term, it is converted to a surface integral using the Divergence theorem. The values of the nodes are then determined by estimating solutions to the partial differential equations.

2.3.2.4 Boundary element method (BEM)

The boundary element method is used to solve linear partial differential equations that have been formulated as integral equations (Cheng and Cheng, 2005). In this method only the boundary values are calculated instead of the values of the entire space described by the partial differential equation. This makes it a more computer resource efficient method than volume discretisation methods for some problems (FEM, FDM and FVM) (Cheng and Cheng, 2005). In some instances the BEM becomes less efficient. This is because BEM results in fully populated matrices that cause storage requirements and computing time to grow according to the square of the problem size. Whereas volume discretization methods result in banded matrices that cause storage requirements and computing time to rise linearly to the problem size.

To obtain the potential distribution caused by a current source in a piecewise homogeneous volume conductor, Green's second theorem is used in the BEM (Briaire and Frijns, 2000a). This results in a differential equation to be solved. The BEM requires that only the boundaries between volumes with different conductivities be used in calculations. Equations describing these boundaries are then solved simultaneously. Cochlear models employing the BEM method mainly include those of Frijns and co-workers (Briaire and Frijns, 2000a; Briaire and Frijns, 2000b; Frijns et al., 2000).

2.3.3 Applicability to present study

FEM was chosen for use in this study because of its suitability to the present problem where potentials in very large (in terms of mesh elements) volumes have to be determined. It is also easy to implement as the Comsol Multiphysics software package is readily available. Comsol Multiphysics also has the added benefit of having an interface to Matlab via the Livelink interface. Using the Livelink interface, the 3D geometry of the model, which was created in Matlab from measured data, could be directly translated to a Comsol Multiphysics compatible 3D geometry from where it was meshed.

2.4 COCHLEAR MORPHOLOGY

To construct a geometric representation of an implanted cochlea of a specific user, the dimensions of that cochlea and position of the electrodes have to be estimated accurately. It has been shown that cochlear morphology differs between persons and ears (Erixon et al., 2009; Avci et al., 2014). The extent of these variations is investigated here.

2.4.1 Cochlear dimensions

Table 2.1 shows a summary of measured human cochlear dimensions from literature. Brief measurement details are also listed. A diagram indicating the positions where the measurements were taken is shown in Figure 2.1. As the measurements were obtained between different landmarks using different techniques, the values reported by the studies are not directly comparable. What is of interest is the magnitude in variation in measurements within each of the studied samples. This is indicated by the percentage of relative standard deviation (%RSD) that is calculated as follows:

$$\%RSD = \frac{SD}{mean} \tag{2.2}$$

It is evident from the relatively high %RSD that width, height, length and canal width vary greatly among cochleae. Individual variation is especially prominent (%RSD around 20%) among the cochleae measured in the Teissier, Van Den Abbeele, Sebag and Elmaleh-Berges (2009) study. In that study the cochleae of children with hearing loss were measured and significant differences to the control group of normal hearing children were found. The larger difference of morphology in persons with abnormal hearing to normal hearing persons was also used by Dimopoulos and Muren (1990) to identify abnormal pathology. As cochlear implant users are profoundly deaf, it is reasonable to expect their morphology will vary with a %RSD in the order of 20%.

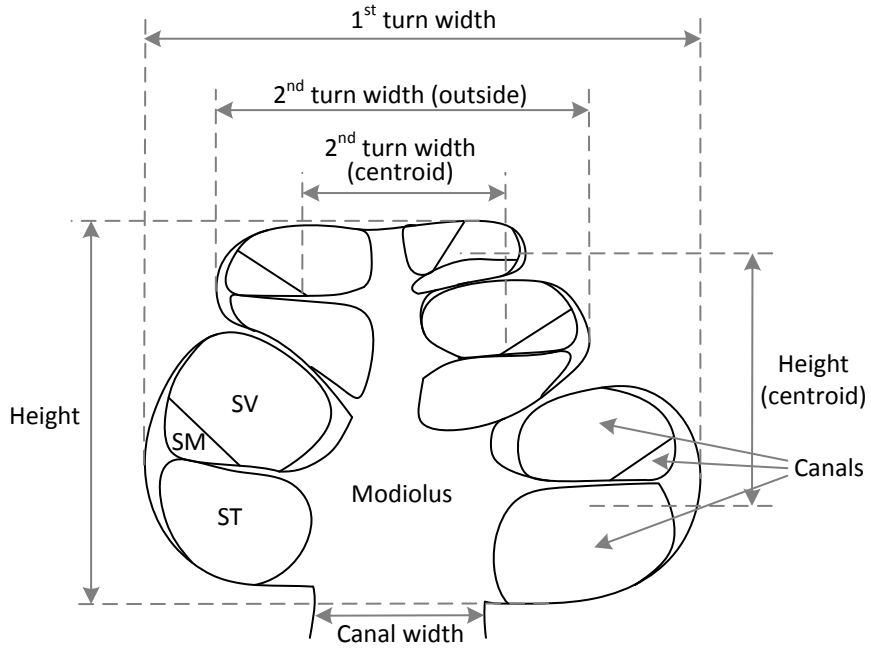

Figure 2.1. Axial slice through the cochlea indicating where the measurements in Table 2.1 were obtained

Other variations in cochlear morphology have also been observed. Biedron, Westhofen and Ilgner (2009) found the number of turns of the cochlea to range between 2 and 3 turns. They found that 65% of cochleae have more than 2.5 turns, with 11% of those cochleae having more than 2.75 turns. Another interesting observation from their data is that left and right cochleae of the same person may vary up to 0.25 turns. They also noted that the number of cochlear turns is similar for both genders as was also found by Wysocki (1999). No correlation between age and cochlear dimensions was also found (Dimopoulos and Muren, 1990; Wysocki, 1999; Teissier et al., 2009) indicating that cochleae are fully developed at birth.

Based on these findings, the incorporation of the dimensions of an individual cochlea into a model is warranted.

Table 2.1. Summary of measured human cochlear dimensions indicating inter-cochlear variations

Measurement	**Measurement detail**	**Mean [mm]**	**SD**	**%RSD**	**Source**	**Sample size**	**Reference**
Transverse[1] width base	Across basal turn on outside of canals	8.85	0.45	5.1	Plastic casts	95	(Dimopoulos and Muren, 1990)
Axial[2] width base	Across basal turn on outside of canals	6.77	0.35	5.2	Plastic casts	95	(Dimopoulos and Muren, 1990)
	Across basal turn between canal centroids	7.91	0.53	6.7	CT	20	(Ketten, Skinner, Wang, Vannier, Gates and Neely, 1998)
Axial width 2nd turn	Across second turn between canal centroids	4.27	0.54	12.6	CT	20	(Skinner, Ketten, Vannier, Gates, Yoffie and Kalender, 1994)
Axial width 2nd turn. Children with conductive hearing loss.	Across second turn on outside of canals	5.75	0.31	5.4	CT	103	(Teissier et al., 2009)
Axial width 2nd turn. Children with sensorineural hearing loss.	Across second turn on outside of canals	5.61	0.51	9.1	CT	71	(Teissier et al., 2009)
Axial width apex	Across apical turn between canal centroids	1.46	0.26	17.8	CT	20	(Skinner et al., 1994)
Height	Base to helicotrema	3.93	0.4	10.2	Plastic casts	95	(Dimopoulos and Muren, 1990)
Height	Basal centroid to apex centroid	2.75	0.25	9.1	CT	20	(Ketten et al., 1998)
Height. Children with conductive hearing loss.	Narrowing of modiolus to helicotrema	3.70	0.29	7.8	CT	103	(Teissier et al., 2009)

[1] Measured across cochlea from RW across helicotrema (Stenvers' view).

[2] Measured across cochlea from the axial-pyramidial view (Polsch view) that is perpendicular to the Stenvers' view.

Height. Children with sensorineural hearing loss.	Narrowing of modiolus to helicotrema	3.71	0.33	8.9	CT	71	(Teissier et al., 2009)
Length (BM)	Canal centroids from hook to apex	33.01	2.31	7.0	Spiral model from CT	20	(Ketten et al., 1998)
Length (BM)	Top of pillar cells base to apex	33.31	2.38	7.1	Photomicrograph	7	(Sridhar, Stakhovskaya and Leake, 2006)
Length (Spiral ganglion)	Centre of spiral ganglion base to apex	13.9	0.79	5.7	Photomicrograph	6	(Sridhar et al., 2006)
Length(duct)	2D duct reconstruction	30.8	2.6	8.3	Histologic section		(Lee, Nadol Jr and Eddington, 2010)
Length of 1st turn	0-360^{o} of outer wall of cochlea	20.3	1.2	5.9	CT of temporal bones	8	(Adunka, Unkelbach, Mack, Radeloff and Gstoettner, 2005)
Axial canal width. Children with conductive hearing loss.	Width of narrowing of modiolus	2.16	0.25	11.6	CT	103	(Teissier et al., 2009)
Axial canal width. Children with sensorineural hearing loss.	Width of narrowing of modiolus	2.12	0.55	25.9	CT	71	(Teissier et al., 2009)

2.5 OBTAINING COCHLEAR DIMENSIONS

In order to construct a geometric representation of an individual implanted cochlea, the dimensions of that cochlea have to be accurately measured. Non-invasive methods suitable for imaging the cochlea of a living implanted human, however, have a lower resolution than other more invasive techniques. This limits the cochlear structures that can be visualized from the imaging data to large structures such as the bony structure of the cochlea as well as the electrode contacts. If the geometry of bony structure of an individual's cochlea is known, the geometry of the smaller inner structures may be estimated by scaling a detailed description of these smaller structures according to the

cochlear bone. The techniques that may be used to image cochleae in-vivo (bony geometry) and ex-vivo (small internal structures) are discussed here.

2.5.1 In-vivo imaging

The following techniques are suitable for in-vivo imaging of the bony structures and electrode contacts of the implanted cochlea. A description of each method is given along with its strengths and disadvantages.

2.5.1.1 Radiography

The position of an electrode array inside an implanted cochlear array may be determined using conventional radiography (Cohen, Saunders and Richardson, 2003; Skpizner, Holliday, Roland, Cohen, Waltzman and Shapiro, 1995). This method is commonly used during implant surgery to assess the insertion depth and placement of the array (Chen, Farb, Hanusaik, Shipp and Nedzelski, 1999; Cohen, Xu, Xu and Clark, 1996; Xu, Xu, Cohen and Clark, 2000). The position of individual electrodes relative to the cochlear walls are clearly visible on radiographs (Skpizner et al., 1995) but smaller 3D structures are not clearly distinguishable (Verbist, Frijns, Geleijns and van Buchem, 2005). Phase-contrast radiography (Xu, Stevenson, Gau, Tykocinski, Lawrence, Wilkins, Clark, Saunders and Cowan, 2001) is a modality of conventional radiographs that produces more detail of the bony structure of the cochlea but still lacks the ability to distinguish between internal cochlear structures.

By using these methods it only takes a few seconds to obtain an image and is suitable for *in vivo* imaging. *In vivo* imaging using radiography does however expose the patient to radiation.

2.5.1.2 Rotational Tomography (RT)

Rotational tomography (also referred to as Digital Volume Tomography) is based on 3D digital subtraction angiography (Aschendorff, Kubalek, Turowski, Zanella, Hochmuth, Schumacher, Klenzner and Laszig, 2005). This technique has been successfully used post-operatively in imaging the electrode array placement of patients (Aschendorff et al., 2005). A study by Aschendorff, Kubalek, Hochmuth, Bink, Kurtz, Lohnstein, Klenzner and Laszig (2004) suggests that this method predicts the position of the electrode array in the scala tympani and scala vestibuli more accurately than using a 16-slice CT scanner. The disadvantage of this method is that it exposes the patient to radiation.

2.5.1.3 Magnetic Resonant Imaging (MRI)

Magnetic resonant imaging is particularly well suited to estimate fluidic structures inside the cochlea as was done in the guinea pig cochlea (Ghiz, Salt, DeMott, Henson, Henson and Gewalt, 2001; Koizuka, Seo, Murakami, Seo and Kato, 1997; Thorne, Salt, DeMott, Henson, Henson and Gewalt, 1999). Presently the best MRI scanners can achieve a resolution in the order of 3 µm. Studies by Thorne et al. (1999) and Koizuka et al. (1997) used a 25 µm scanner to image the scala vestibuli, scala tympani and cochlear duct. The boundaries between these structures were used to estimate the position of Reissner's membrane. Ghiz et al. (2001) have successfully imaged the round window membrane in temporal bones of six specimens.

When imaging implanted ears using MRI, large artefacts arise due to the presence of the magnet in the implant. This magnet is used to keep the external processor worn by the patient in alignment with the implanted coil transcutaneously. This artefact can be in the order of 7 cm wide and totally obstructs the cochlea (Vincent, Ruzza, Vaneecloo and Dubrulle, 2008). Some implants allow the magnet to be removed surgically before an MRI scan. These implants include the HiRes90K from Advanced Bionics (Advanced Bionics, Sylmar, CA) and the CI24M, CI24R (CS) Nucleus Freeform and CI24ABI devices from Cochlear Corporation (Cochlear Corporation, Melbourne, Australia) (Majdani, Leinung, Rau, Akbarian, Zimmerling, Lenarz, Lenarz and Labadie, 2008).

MRI can also cause the implant to heat up. Tests have shown that this temperature rise is below 0.5 °C and within safety limits using 1.5 T and 3 T MRI scanners (Chou, 2007; Majdani et al., 2008). Serious demagnetization of the magnet can also occur during 3 T MRI scans which can lead to the external processor not lining up properly with the internal coil (Majdani et al., 2008).

MRI has successfully been used in the pre-operative imaging of cochleae to assess implant feasibility. Studies have however shown that in some cases CT scans provide superior results (Bettman, Beek, Van Olphen, Zonneveld and Huizing, 2004; Chaturvedi, Mohan, Mahajan and Kakkar, 2006) due to the difficulty of displaying bony structures using MRI. MRI data may, however, be combined with CT data to obtain a better overall description of the cochlea.

2.5.1.4 Computed tomography (CT)

CT scanners work by passing x-rays through a patient where they are attenuated and subsequently measured by detectors. The x-ray tube and detectors rotate around the scanned area while scanning. The signals measured by the detectors are then passed to a computer where image reconstruction takes place (Seeram, 2001).

There are different types of CT scanners two of which are direct CT and spiral CT scanners. Direct CT scanners work by scanning a single slice at a time and then moving on to the next slice. Each slice is scanned by rotating the x-ray tube and detectors through 360 degrees. Spiral CT continually rotates the x-ray tube and detectors while it is moved along the axis of the scanned subject (Seeram, 2001). This result in faster scanning times for high volume subjects and lower radiation dosages.

High resolution thin-section direct CT scanners are commonly used for temporal bone imaging (Sorn and Curtin, 1996; Swartz, 1989). These type of scans often require extensive neck extension by the patient which is not always possible (Caldemeyer, Sandrasegaran, Shinaver, Mathews, Smith and Kopecky, 1999). Spiral CT scans, however,

is less dependent on the body position of the patient (Kaste, Young, Holmes and Baker, 1997; Luker, Lee and Erickson, 2007). A study conducted by Caldemeyer et al. (1999) compared spiral CT with conventional direct CT scans of temporal bones. They concluded that using spiral CT scans resulted in higher detailed representations of temporal structures.

Newer methods that produce higher resolution scans with smaller inherent artefacts have also been developed. These involve the use of more advanced scanners and include Tuned Aperture Computed Tomography (TACT) (Sakata, Hareyama, Heil, Henson, Henson Jr, Webber, Nair and Smith, 2007), high-resolution spiral computed tomography (HRSCT) (Seemann, Seemann, Bonel, Suckfull, Englmeier, Naumann, Allen and Reiser, 1999), flat panel CT scanners (Gupta, Bartling, Basu, Ross, Becker, Pfoh, Brady and Curtin, 2004), Multisection CT (Verbist et al., 2005) and Microcomputed Tomography (μ-CT) (Lane, Driscoll, Witte, Primak and Lindell, 2007).

The metal of the implanted cochlear electrode arrays cause artefacts on CT scans and cause the resulting images to be blurred (Ketten et al., 1998; Whiting, Bae and Skinner, 2001; Yang, Wang, Skinner, Rubinstein and Vannier, 2000). Numerous techniques have been used to reduce blurring (Wang, Vannier, Skinner, Cavalcanti and Harding, 1998; Xu et al., 2000; Jiang, Wang, Skinner, Rubinstein and Vannier, 2003; Wang, Vannier, Skinner, Kalender, Polacin and Ketten, 1996; Whiting et al., 2001). In previous study where a guinea pig cochlea was imaged (Malherbe et al., 2013), a simple method of augmenting the blurred CT scan data with a histologic slice of a healthy cochlea proved successful in dealing with artefacts.

2.5.1.5 Suitability criteria

In assessing the suitability of an in-vivo imaging technique for the present study, the following constraints have to be taken into account.

- The technique should allow imaging of living human cochlea.

- The technique should allow the estimation of the electrode array relative to other cochlear structures.
- The standard deviations in cochlear measurements between individuals are between 0.25 and 1.2 mm (Table 2.1). In order to accurately measure cochlear differences of the cochlear structures listed, the imaging technique used should have a resolution that is better than 0.25 mm.

CT meets these constraints. It also has the added benefit of being used as a standard clinical method to obtain cochlear morphology. The data obtained from these CT measurements may then be used to construct the 3D geometrical representation of the bony structures of an individual cochlea. As conventional CT does not allow the imaging of the smaller cochlear structures such as Reissner's membrane, the location of these structures will have to be estimated by augmenting the CT data with data obtained using another higher resolution method. Photomicroslice data may provide this detail, but as it is not suited for in vivo imaging, data from a different cochlea will have to be used. This will cause the inner structures of the modelled geometry to deviate from the specific geometry of the user. Scaling of the photomicrograph data according to the CT data may reduce this deviation.

2.5.2 Imaging finer cochlear structures

The following techniques may be used to obtain detail of the fine inner cochlear structures with which in-vivo data of the larger cochlear structures may be augmented.

2.5.2.1 Physical dissection

In 1952 Fernández (Fernandez, 1952) dissected six guinea pig cochleae and measured the dimensions of the cochlear structures. Measurements were done by magnifying the structures with a camera lucida. This method required that each specimen be stained with hematoxylin-eosainn to highlight histological features. One disadvantage of this method is

that small structures such as Reissner's membrane cannot be studied because it gets damaged during dissection because of its thin and fragile membranous structure. Another disadvantage is that measurements from physical dissection cannot be obtained from living implant users.

2.5.2.2 Histologic Sectioning

Histologic sectioning involves segmentation of the cochlea into thin slices. Before slicing the cochlea it undergoes a chemical preparation which includes decalcification and dehydration. It is then sliced into slices about 25 µm thick and observed using light microscopy (Nadol Jr, 1990). This method provides highly detailed images with a very high resolution of the internal cochlear structures. The disadvantage is that measurements cannot be obtained *in vivo*. Also the Reissner's membrane can sometimes be damaged during dehydration making the boundary between the scala media and scala vestibuli unresolvable. This method is time consuming and requires considerable technical expertise.

2.5.2.3 Video fluoroscopy

Video fluoroscopy has been used in the imaging of cadaveric cochleae (Balkany, Eshraghi and Yang, 2002; Roland, Fishman, Alexiades and Cohen, 2000). This method also involves extensive chemical preparation of the cochlea. The resolution obtained using this method is insufficient to distinguish fine cochlear structures and is more suited to determining the position of the electrode contacts relative to the cochlear wall.

2.5.2.4 Orthogonal-plane Fluorescence Optical Sectioning (OPFOS)

Orthogonal-plane fluorescence optical sectioning was used by Voie (2002) to obtain detailed images of the inner ear and small cochlear structures such as Reissner's membrane. Hofman, Segenhout and Wit (2009) used OPFOS to create a 3D model of the guinea pig

inner ear. This method also involves fixation, decalcification and dehydration of the cochlea and is not suited for *in vivo* applications.

2.5.2.5 Micro Computed Tomography (µ-CT)

µ-CT scanners works on the same principal as conventional CT but can provide high resolution slices that can attain voxel sizes as small as 1 μm^3. The disadvantages of µ-CT are that size constraints usually require histologic sectioning of the sample being scanned. The scanned sample is also exposed to high levels of radiations for prolonged periods of time. This rules out its use for in-vivo human imaging.

2.5.2.6 Suitability criteria

In assessing the suitability of an ex-vivo imaging technique for the present study, the following constraints have to be taken into account.

- The technique should allow imaging of the fine inner structures of a human cochlea.
- The smallest structure that governs the shape of the cochlear ducts is the Reissner's membrane. As this membrane is 12 µm thick (Shibata, Matsumoto, Agishi and Nagano, 2009), the imaging method should have a resolution of at least 12 µm.

All the mentioned methods meet these constraints. A photomicroslice of a histologic section was used to estimate the positions of the fine inner cochlear structures in this study mainly because of its availability and high resolution.

2.6 ESTIMATING ELECTRODE LOCATION

The methods used in the previous section focus on extracting images from temporal CT scans. To accurately construct a model from these images, the position of the electrode array relative to the inner ear structures should be clear.

Using high resolution µ-CT with additional staining, small structures such as the basilar membrane, organ of Corti and Reissner's membrane may be imaged (Poznyakovskiy, Zahnert, Kalaidzidis, Schmidt, Fischer, Baumgart and Yarin, 2008). As these structures are not resolvable using conventional CT scanners on live subjects, their positions have to be estimated using known geometric data of the cochlea. This was done in a study of the human cochlea by Skinner, Ketten, Holden, Harding, Smith, Gates, Neely, Kletzker, Brunsden and Blocker (2002) where the position of these structures were estimated using data obtained by Ketten et al. (1998). Other studies that include electrode location within the cochlea measure the electrode locations relative to the cochlear walls (Czerny, Steiner, Gstoettner, Baumgartner and Imhof, 1997; Ruivo, Mermuys, Bacher, Kuhweide, Offeciers and Casselman, 2009; Cohen, 2009). A recent study by Noble, Gifford, Hedley-Williams, Dawant and Labadie (2014) determined the electrode location relative to the neural elements of individual users using CT data.

2.7 MATERIAL PROPERTIES

In an electrically stimulated cochlea, current flows from a stimulating electrode to a return electrode via the cochlear tissues. The shape and resistivities of these tissues determine the path that the current will follow (Micco and Richter, 2006). Obtaining an accurate geometric representation of cochlear structures will not result in more accurate predictions of current patterns if the resistivities assigned to those structures are not accurately represented in the model.

Table 2.2 lists the resistivities commonly used in electrical models of the cochlea. The majority of these values were obtained from guinea pig or gerbil animal models as human data are not available. Some of these values, like that of perilymph, can be assumed to be fairly representative of the human case as the chemical composition of perilymph is fairly universal across mammals. Other values, such as that of bone, may differ greatly from the human case as the density and porousness of bone varies between species. Micco and Richter (2006) ascribed the difference in bone resistivity between the guinea pig and gerbil

to this difference where the guinea pig has compact bone and the gerbil has thin and porous bone. This variation in values may be the reason why a large range of values have been used to describe cochlear bone in modelling studies.

Table 2.2. Resistivities of cochlear structures used in models[1]

Structure	Resistivity [Ohm.cm]	Method	Species	Reference
Cochlear wall				
ST	353-643	Electrode-reflection coefficient	Gerbil	(Kumar, Chokshi and Richter, 2010)
ST	475-574		Gerbil	(Micco and Richter, 2006)
SV	353-616	Electrode-reflection coefficient	Gerbil	(Kumar et al., 2010)
SV	475-543		Gerbil	(Micco and Richter, 2006)
SM	432-759	Electrode-reflection coefficient	Gerbil	(Kumar et al., 2010)
SM	470-616		Gerbil	(Micco and Richter, 2006)
Modiolus				
	228-487	Electrode-reflection coefficient	Gerbil	(Kumar et al., 2010)
			Gerbil	(Micco and Richter, 2006)
Perilymph (ST,SV)				
	47		Guinea pig	(von Békésy, 1951)
	62		Gerbil	(Kumar et al., 2010)

[1] Abbreviations used in the table: ST: scala tympani, SV: scala vestibuli, SM: scala media.

	71.9		Guinea pig	(Misrahy, Hildreth, Shinabarger and Gannon, 1958; Strelioff, 1973)
	70		Guinea pig	(Finley, 1989; Frijns et al., 2000; Hanekom, 2001b)
Endolymph (SM)				
	59.8		Guinea pig	(Misrahy et al., 1958; Strelioff, 1973)
	60		Guinea pig	(Frijns et al., 2000; Hanekom, 2001b; Finley, 1989)
Bone				
	641 ±203		Guinea pig	(Micco and Richter, 2006)
	641		Guinea pig	(Frijns, de Snoo and Schoonhoven, 1995; Finley, Wilson and White, 1990; Hanekom, 2001b; Malherbe et al., 2013; Govindasamy, 2012)
	630		Guinea pig	(Finley, 1989; Spelman, Clopton and Suesserman, 1987)
	6400		Used in model	(Rattay et al., 2001a)
	7143		Used in model	(Kalkman et al., 2014a)
	6250		Used in model	(Frijns, Kalkman and Briaire, 2009a)
	100:1 bone to scalar fluid conductivity ratio		Used in model	(Mens, Huiskamp, Oostendorp and Van Den Broek, 1999; Whiten, 2007)
Reissner's membrane				
	60480		Guinea pig	(Finley, 1989)
	1020408			(Hanekom, 2001b)

Basilar membrane				
	1800		Guinea pig	(Finley, 1989)
	8000			(Hanekom, 2001b)
Neural tissue axial				
	300		Guinea pig	(Finley, 1989; Hanekom, 2001b)
Neural tissue transverse				
	1500			(Finley, 1989; Hanekom, 2001b)
Spiral ganglion				
	300		Guinea pig	(Finley, 1989)
Stria vascularis				
	18900			(Frijns et al., 2000; Hanekom, 2001b)
Organ of Corti				
	8330			(Frijns et al., 2000; Hanekom, 2001b)

Based on the variance in values of the same structures, different models incorporating different values may lead to different results. Care has to be taken in choosing values for the modelled cochlear structures in the 3D volume conduction models in order to produce realistic voltage distribution patterns.

2.8 NEURON MODELS

The 3D volume conduction methods are capable of estimating the voltage distribution in the cochlea but not capable of estimating the highly non-linear response of nerve fibres. A separate neural model has to be used to translate the voltage distribution patterns of the 3D model into neural responses. The inputs of such a model are the potentials that are produced at the locations of the nodes of Ranvier of each modelled neuron.

2.8.1 Node positions

Most 3D cochlear models have assumed neurons to emanate radially from the modiolus through the spiral lamina to the organ of Corti (Malherbe et al., 2013; Malherbe, 2009; Hanekom, 2001b; Briaire and Frijns, 2000b). In reality neurons follow a "bicycle-spoke" pattern from the modiolus into the spiral lamina (Sridhar et al., 2006; Stakhovskaya, Sridhar, Bonham and Leake, 2007). This pattern starts off radially in the base of the cochlea and then resembles more of a "bicycle-spoke" pattern apically. The implication of this is that the tonotopic configuration of inner hair cells as described by Greenwood (1990) does not necessarily apply to the spiral ganglion cells located at the same angles medially to the hair cells. Using a purely radial pattern may cause a mismatch in frequencies predicted by a model where degenerate neurons with only spiral ganglion cells and axons are modelled. Thus care has to be taken in translating predicted neural firing patterns into perceived pitch. As the trajectories of neurons are more radial towards the base of the cochlea, pitch induced by basal electrodes should still be predicted correctly using the assumption of purely radial neurons. Another study (Kalkman, Briaire and Frijns, 2014b) further improved neuron positioning by arranging cell bodies according to an anatomically realistic spatial distribution in the spiral ganglion.

The voltages extracted from the volume conduction model at the locations of these neuron nodes are then used as the input to a neuron model.

2.8.2 Neuron models

The seminal work on neural modelling was done by Hodgkin and Huxley (1952). The Hodgkin-Huxley (HH) equations were derived through experimental work done on giant squid axons during the 1950's. Since that time various other neural models such as the Frankenhaeuser-Huxley (Frankenhaeuser and Huxley, 1964), Fitzhugh (FitzHugh, 1969), Chiu et. al. (Chiu, Richie, Rogart and Stagg, 1979), Sweeney et. al. (Sweeney, Mortimer and Durand, 1987) and Schwarz-Eikhof (Schwartz and Eikhof, 1987) models have been developed. The Hodgkin-Huxley model is however still widely used as it is one of the few

models that can produce multiple spikes during low frequency sinusoidal stimulation (Hartmann, Topp and Klinke, 1984) as well as produce an action potential when successive sub-threshold pulses are applied (Rattay, Lutter and Felix, 2001b). It is especially used when modelling human cochlear neurons where it has been found that a warmed Hodgkin-Huxley model (where gating has been accelerated to more closely match mammalian neurons) matches the behaviour of a cochlear neuron the closest out of all the above mentioned models (Rattay et al., 2001b).

These models however only model the dynamics of a single membrane patch of a neuron. To model complex cochlear neurons that consist of various nodes with different properties, a neural cable model should be used. Models incorporating such cable equations include a cochlear neuron model developed by Rattay et al. (2001b) and the Generalized Schwarz-Eikhof-Frijns (GSEF) model (Frijns et al., 1995). These models have successfully been used in combination with volume conduction (VC) models to investigate cochlear neural excitation patterns (Rattay et al., 2001a; Frijns et al., 2000).

2.9 CURRENT COCHLEAR MODELS

Existing 3D cochlear models that predict the electrical fields inside a stimulated cochlea (using volume conduction) and their effect on neural excitation (using neuron models) are generally based on a generic human or guinea pig cochlear shape (Hanekom, 2001b; Frijns et al., 2000; Choi et al., 2004; Rattay et al., 2001a; Frijns et al., 2001) that does not take inter-user morphological variations into account. These models have been used successfully to investigate numerous aspects that affect the biophysical interface between the implant technology and the cochlear tissues, such as the design and intra-cochlear location of the electrode and their effects on neural excitation characteristics, e.g. dynamic range and spread of excitation. However, generic models fail to provide insight into the detailed biophysics of and neural response to a specific user's implant. Only user-specific models are expected to shed light on, among others, variations in threshold level and pitch perception observed in users implanted with electrode arrays with the same design in similar intra-cochlear locations. The prediction of person-specific outcomes therefore

necessitates the inclusion of model parameters that describe inter-personal variance. A recent study recognized this limitation of generic models and used four general human cochlear morphologies in an attempt to introduce inter-user variations in the model predictions (Kalkman et al., 2014a). While the approach simulates user variance, its objective is not to predict neural excitation for a specific user. To describe the cochlear environment and its response to electrical stimulation for a specific live human, it is necessary to represent the individual's cochlear morphology and electrode placement in a user-specific model.

2.10 POTENTIAL USES FOR A USER-SPECIFIC COCHLEAR MODEL

Having a cochlear model based on the morphology and electrode placement of an individual cochlea has the potential of describing the inner workings of an implanted cochlea better than a model based on a general morphology. Such a detailed model may be used to shed light on other aspects related to cochlear models in general.

One such aspect is the selection of a bone resistivity value to use in cochlear models. As a large range of resistivities (641 to 7143 Ω.cm) have been used to describe cochlear bone in VC models (see Table 2.2), the selection of a single value to use is not clear. Cochlear models that accurately describe the cochlear morphology as well as surrounding structures may be used to find a suitable bone resistivity value by varying the resistivity of the surrounding bone until model predictions match measured data.

Another use of cochlear models may be to shed light on the rate of current decay of a stimulating electrode. Generally a monopolar decay rate of 3 dB/mm is assumed as it has been measured in physical models containing electrodes in salt solutions (Kral, Hartmann, Mortazavi and Klinke, 1998) as well as in animal models (Kral et al., 1998; O'Leary, Black and Clark, 1985). Neural excitation spread measured in animal models was also found to exhibit a similar monopolar decay rate of around 3 dB/mm (Hartmann and Klinke, 1990; Kral et al., 1998). Many implant processor analysis filter slopes are chosen according to

this value. As this value has been derived from animal models and salt bath experiments, this single value may not accurately describe the decay of current from a stimulating electrode in a human cochlea as measured at the location of the neural elements. Using VC models that incorporate detailed descriptions of human cochlear morphologies to investigate current decay from a stimulating source may shed light onto how well the 3 dB/mm decay rate generally holds in a human cochlea and further more may be able to give an estimate of the decay rate of a specific electrode in a specific implanted cochlea.

Also a model based on the morphology of the cochlea of a specific user will give insight into the sound perceptions of specific implant users. A user-specific model may be used to predict the mismatch between a user's programming map and perceived pitch. This is a valuable tool investigating the effects of very deep electrode insertions (Hochmair, Hochmair, Nopp, Waller and Jolly, 2015) such as those offered by MED-EL electrode arrays.

2.11 CONCLUSION

Predicting the functioning of an implanted cochlea involves modelling various aspects of a cochlea. These include predicting the potential distribution induced by a stimulating electrode as well as the resulting neural excitation patterns. In order to predict user-specific outcomes from a cochlear model, user-specific parameters have to be incorporated into the model. As cochlear morphology varies between cochleae, incorporation of a user's cochlear morphology into a model should elicit a more user-specific response.

The following section describes the methodology to construct a user-specific cochlear model within the context of the background given here.

CHAPTER 3 METHODS

The contents of this chapter is included in the following article:

Malherbe, T. K., Hanekom, T. and Hanekom, J. J. Constructing a three-dimensional electrical model of a living cochlear implant user's cochlea. International Journal for Numerical Methods in Biomedical Engineering. (In review)

This chapter explains the methodology followed to construct a model of the implanted cochlea of a specific living human implant user.

3.1 INTRODUCTION

Modelling the complete functioning of a system as intricate as the human inner ear is a daunting challenge. The modelling process requires simplification of the system through assumptions of the underlying mechanisms to enable its description through a set of mathematical equations. However, while models provide only an approximate description of a system, they do provide a tool to probe the modelled system in ways that are not necessarily possible in a living system. Models of the peripheral functioning of cochlear implants (CIs) attempt to describe the biophysical interface between the technology and the auditory nervous system and the subsequent excitation of the peripheral neural population. Cochlear models (Hanekom, 2001b; Hanekom, 2005; Frijns et al., 2000; Choi et al., 2004; Rattay et al., 2001a; Frijns et al., 2001) have focused on individual aspects of the implanted cochlea and are constantly developing to incorporate more features to improve their accuracy in predicting biological conditions. As considerable morphological variations exist among human cochleae (Erixon et al., 2009; Van Der Marel et al., 2014), including the anatomical dimensions of a specific user's cochlea in a model is expected to allow more accurate modelling of the electrophysiology of the individual auditory periphery. Such a model, in combination with perceptual and measured electrophysiological data from a living implant user, may then be used to gain insight into the parameters that cause hearing performance to vary so greatly among users (Firszt et al., 2004).

Existing three-dimensional (3D) cochlear models that predict the electrical fields inside a stimulated cochlea and their effect on neural excitation are generally based on a generic human or guinea pig cochlear shape (Hanekom, 2001b; Frijns et al., 2000; Choi et al., 2004; Rattay et al., 2001a; Frijns et al., 2001) that does not take inter-user morphological variations into account. These models have been used successfully to investigate numerous aspects that affect the biophysical interface between the implant technology and the cochlear tissues, such as the design and intra-cochlear location of the electrode and their effects on neural excitation characteristics, e.g. dynamic range and spread of excitation. However, generic models fail to provide insight into the detailed biophysics of and neural response to a specific user's implant. Only user-specific models are expected to shed light on, among others, variations in threshold level and pitch perception observed in users implanted with electrode arrays with the same design in similar intra-cochlear locations. The prediction of person-specific outcomes therefore necessitates the inclusion of model parameters that describe inter-personal variance. A recent study recognized this limitation of generic models and used four general human cochlear morphologies in an attempt to introduce inter-user variations in the model predictions (Kalkman et al., 2014a). While the approach simulates user variance, its objective is not to predict neural excitation for a specific user. To describe the cochlear environment and its response to electrical stimulation for a specific live human, it is necessary to represent the individual's cochlear morphology and electrode placement in a user-specific model.

A model that incorporates the morphology of a specific implanted guinea pig cochlea has been reported (Malherbe et al., 2013). The modelling technique used is, however, not suitable for constructing a model of a live human's implanted cochlea. This is mainly because the imaging technique used (micro-computed tomography (µ-CT)), which can only be used on non-living samples as a result of high levels of radiation for prolonged periods of time. Alternative imaging techniques are required for constructing a human model.

Clinically used CT is well suited to obtain the morphology of the cochlea of a living user, as it produces data on the bony structures of the cochlea and metal electrode contacts. However, standard CT data have low resolution relative to the dimensions of cochlear structures and do not show the fine internal structures of the cochlea. Augmenting the CT data with high-resolution photomicrograph data of the internal structures of a generic cochlea allows the dimensions of these structures to be approximated. Positioning the generic inner structure dimensions according to the user CT data still allows a level of user-specificity to be achieved. In general, construction of volume conduction models with a high level of irregular detail is a meticulous, time-consuming process, mainly because of the manual parameter extraction procedure. However, for user-specific models to be useful both in research and clinical applications, a rapid modelling technique is necessary, since user-specificity can only be studied if a statistically significant number of models are available to support analysis of model predictions based on user variability.

The aim of this article is to describe a method to construct user-specific models of the cochleae of living human CI users rapidly by extending the method used to create a subject-specific guinea pig model (Malherbe et al., 2013). Models that incorporate the cochlear morphology and electrode placement of specific CI users were constructed to assess the effect of variations in cochlear morphology and electrode location on modelled potential distributions and neural excitation profiles. It is also discussed whether such a more complicated modelling approach, compared to using generic morphology, is warranted.

3.2 PARTICIPANTS

Five models of implanted cochleae of three CI users, i.e. one unilateral and two bilateral implantees, were constructed. The participant were implanted in their own private capacity and invited to participate in this study. The ears were implanted with either contour or straight electrode arrays of the Nucleus 24 cochlear prosthesis from Cochlear Limited. This is summarized in Table 3.1. Four of the five user electrodes were inserted into the SV with

the electrode of S13R located inside the ST. The electrode array of user S25 intersected the SM near the base of the cochlea. The electrodes in all other models were located within their original scala.

Table 3.1. Summary of users of whom cochlear models were constructed. Two users have bilateral implants with different electrode arrays in both ears

User	Ear	Electrode Array
S3	L	Straight
S3	R	Contour
S13	L	Contour
S13	R	Straight
S25	R	Contour

3.3 COMPUTED TOMOGRAPHY

Computed tomography was used to obtain 3D images of the temporal bones of the participating CI users, showing the otic capsule and intra-scalar location of the electrode arrays.

A Siemens Sensation Cardiac 64 CT scanner was used with the following parameters: 120 kV tube voltage, 112 mA tube current and 0.6 mm slice thickness. No contrasting agent was administered. Reconstruction was carried out from the raw scan data using Syngo CT software. An oblique reconstruction parallel to the basal turn of each cochlea (Connor, Bell, O'Gorman and Fitzgerald-O'Connor, 2009) was made using a U90u reconstruction kernel (specified in the Syngo CT software) with 0.1 mm slice thickness. A 50 x 50 x 56 mm area around the inner ear was included in the reconstruction. This image set was then resliced radially from the centre of the modiolus at 1 degree increments of angle θ (measured from the centre of the round window (RW)) for 360 degrees using the same software. The result was a set of 360 mid-modiolar images from which the cochlear dimensions could be measured. Figure 3.1 shows the reconstruction parallel to the basal

plane, as well as three of the 360 radial slices made perpendicular to that plane through the modiolar axis.

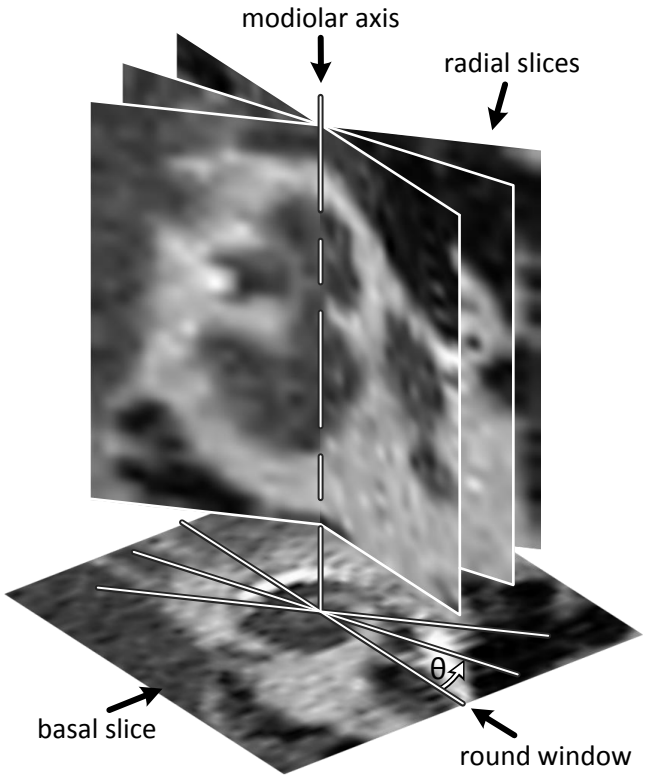

Figure 3.1. The cochleae were imaged using standard clinical CT. An oblique reconstruction through the basal turn was first obtained (basal slice). 360 radial slices were then made around the modiolar axis at 1˚ increments (of θ) measured from the round window. For clarity only three radial slices are shown

The quality of the cochlear images was relatively poor because of the fairly low resolution (0.6 mm voxel size) of the conventional CT scanner used to image the small human cochlea (scala tympani (ST) diameter ranging approximately between 1 and 2 mm (Wysocki, 1999)). The images were enhanced to improve the visibility of the cochlear wall (boundary between the otic capsule and inner ducts), since the cochlear wall was used as the primary landmark to measure the cochlear dimensions. This entailed applying a colour lookup table to make the boundary show up as dark lines and then increasing the image size using interpolation techniques. Interpolation, however, caused the boundaries to appear lighter and the window and level parameters (histogram) of the image were re-

adjusted to make the boundaries appear dark again. The following procedure was applied to achieve this. First, a single radially sliced CT image was imported into an image manipulation software package, ImageJ[1] (Figure 3.2a).

An ICA3 lookup table was then applied (Figure 3.2b) and the window and level parameters (histogram) of the image were adjusted until the boundaries of the cochlear wall were clearly visible (Figure 3.2c). The particular lookup table that was used ensured that the boundary at the cochlear wall was indicated by a thin dark line. Placeholder markers were placed on areas of the boundaries that were clearly visible (Figure 3.2d). The image was then scaled to four times its original size using bi-cubic interpolation. This resulted in a higher resolution image, but also caused the colour of the boundaries to lighten, making them less distinct. The window and level parameters of the image were then adjusted until the dark edge of the boundary intersected the placeholders again (Figure 3.2e). This ensured that the positional accuracy of the boundary was maintained. The same window and level parameters were then applied to all the radial images after interpolation. The same parameters could be used for all the images as their colour ranges are the same. This also implies that any radial image may be used in estimating the initial window and level parameters. After application of these parameters, he images contained a more clearly visible boundary of the cochlear wall from which measurements could be made. Although this procedure does not enhance the resolution of the scan, it does produce a thinner boundary from which the cochlear dimensions can be measured. Figure 3.2e shows the final enhanced image compared to a histological slice of a cochlea with similar shape to indicate the position of the cochlear wall and electrode array.

[1] Wayne Rasband, NIH, public domain software.

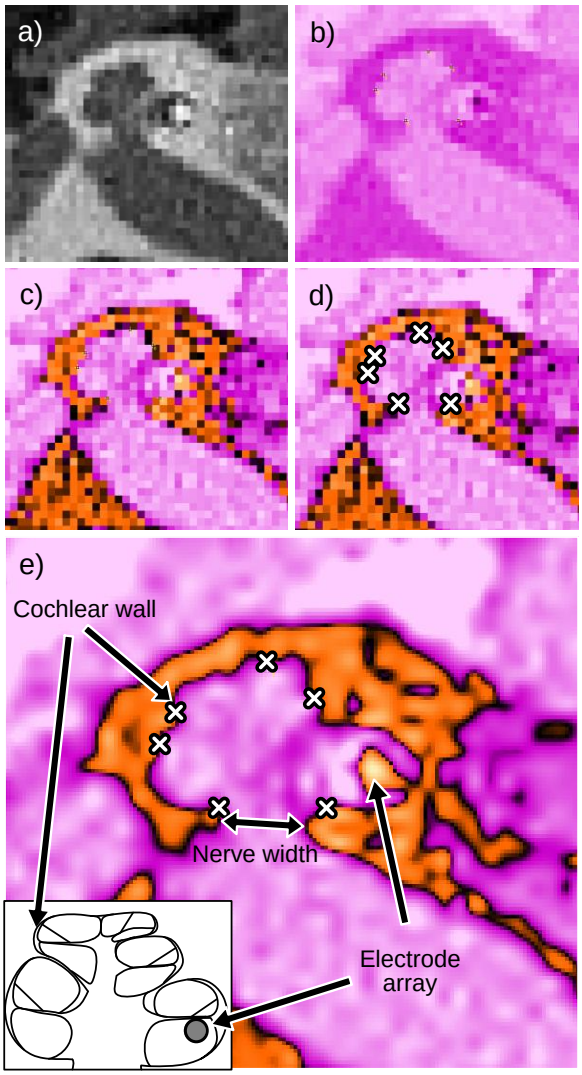

Figure 3.2. Steps taken to enhance the visibility of the cochlear wall in the CT images. The original CT slice (a) was enhanced using ImageJ by first applying a lookup table (b); the window and level parameters (histogram) were then adjusted until sections of the cochlear wall were clearly visible (c), placeholder markers were then placed on the clearly visible boundaries (d) and the image was resized using bi-cubic interpolation (e). The window and level parameters were then adjusted until the cochlear wall was indicated by a thin dark boundary that intersected the placeholders. This ensured that positional accuracy of the boundaries was maintained during interpolation. The final enhanced CT image with the dark cochlear wall clearly visible (e) is compared here to an outline of a cochlea to indicate the positions of the cochlear wall and the electrode array. The position where the width of the cochlear inlet, which was used as the width of the nerve in the model, is measured is also shown

3.4 MEASUREMENTS

Selected points were measured from the enhanced CT scan data and were used to construct the geometric structure of the model. Each point is described in terms of θ, ρ and z. Each radial CT slice corresponds to a certain θ value and each pixel on the slice has a corresponding ρ and z value. ρ is defined as the horizontal distance from the centre of the modiolus and z is defined as the distance from the lower edge of the CT slice (which is at an arbitrary level below the cochlea) (see Figure 3.3a).

Measurements were used to define the following parameters: the outer spiral shape as seen from a superior view of the cochlea (henceforth referred to as the *measured boundary spiral*), the height of the cochlear ducts and the position of the electrode array. To achieve this, four points were measured on each duct on each radial slice (indicated by capital letters in Figure 3.3a): the most lateral boundary of the cochlear wall (A), the inferior boundary of the cochlear duct (B), the superior boundary of the cochlear duct (C) and the centre of the electrode array (D). Points were measured on all 360 slices. If a point was not clearly distinguishable on a radial slice, it was omitted from the measurements.

The measured boundary spiral of the model was obtained from the θ and ρ values of point A. Figure 3.3b shows this spiral constructed from the measured markers. In this specific cochlear image, the boundaries of the individual apical turns were not clearly distinguishable and were thus omitted from the measured boundary spiral.

The remainder of the method relies on measurements taken parallel to the modiolus to ensure geometrical accuracy of the model. In some cases the z-axis around which the radial CT images were resliced did not align perfectly with the axis of the modiolus. This may be ascribed to human error in estimating the position of the modiolus from low resolution CT images and the imperfect estimation of a plane through the basal turn of the cochlea, which by its nature is not completely planar. To correct for this, the measured values were rotated to minimize the axis-modiolus alignment error.

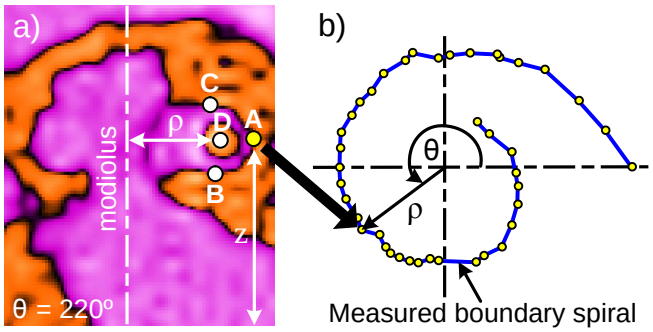

Figure 3.3. a) A radial slice through the cochlea at an angle of 220° (measured from the centre of the round window) is shown with white markers indicating the positions of the four points measured at each radial angle to construct the cochlear geometry: the most lateral boundary of the cochlear wall (A), the inferior boundary of the cochlear duct (B), the superior boundary of the cochlear duct (C) and the centre of the electrode array (D). b) The measured boundary spiral defining the outer edge of the cochlea was constructed from the combined measurements of marker A on each radial slice where the boundary was clearly distinguishable (circular markers)

3.5 ORIENTATION ADJUSTMENT

The following algorithm was applied in software written in Matlab[1] to minimize the alignment error of the measured modiolus:

1. The measured points, which are in cylindrical coordinates (θ, ρ, z), were converted to Cartesian coordinates (x, y, z).
2. The measured points were then rotated iteratively around the x and y-axis in 0.1˚ degree increments.
3. The degree to which each rotated point set was orientated parallel to the modiolus was then assessed (see explanation below).
4. The rotated set that was closest to parallel to the modiolar axis was then converted back to polar coordinates and used as the measurement points from which the rest of the model was constructed.

[1] MATLAB 2012b, The MathWorks Inc., Natick, MA, 2000

To assess the degree to which a rotated point set is orientated parallel to the modiolus, the *z*-values of the measured boundary spiral were examined. The outer boundary spiral was defined as having the θ and ρ values of marker A and the *z*-values of the centre of the duct (the average of the *z*-values of markers B and C). To simplify the approach, the *z*-values of a spiral that is orientated parallel to the *z*-axis are assumed to be monotonically increasing. In reality the cochlea does not represent a perfect spiral and has sections that decrease along its trajectory (Avci et al., 2014; Verbist, Ferrarini, Briaire, Zarowski, Dmiraal-Behloul, Olofsen, Reiber and Frijns, 2009), but to simplify the method it was assumed to be sufficiently represented by a perfect spiral (Ketten et al., 1998). If such a spiral is rotated around the *x* or *y* axis, its *z*-values will no longer increase monotonically, but also decrease at intervals, thus resembling an oscillation owing to its spiralling nature (solid line in Figure 3.4a). A measure to which a set of *z*-values increases monotonically was obtained by measuring its straightness by fitting a straight line (dashed line Figure 3.4b) to the *z*-values using least squares regression using the *polyfit* function in Matlab. The mean square error between this fitted line and the *z*-values given was used as an indication of its straightness. The rotation angles that resulted in the boundary spiral having *z*-values in the straightest line were thus assumed to orientate the spiral parallel to the modiolus. The coordinates of all the measured points were then rotated by these angles and used in the rest of the study. Figure 3.4b shows the same spiral that has been rotated to a position parallel to the modiolus using this method.

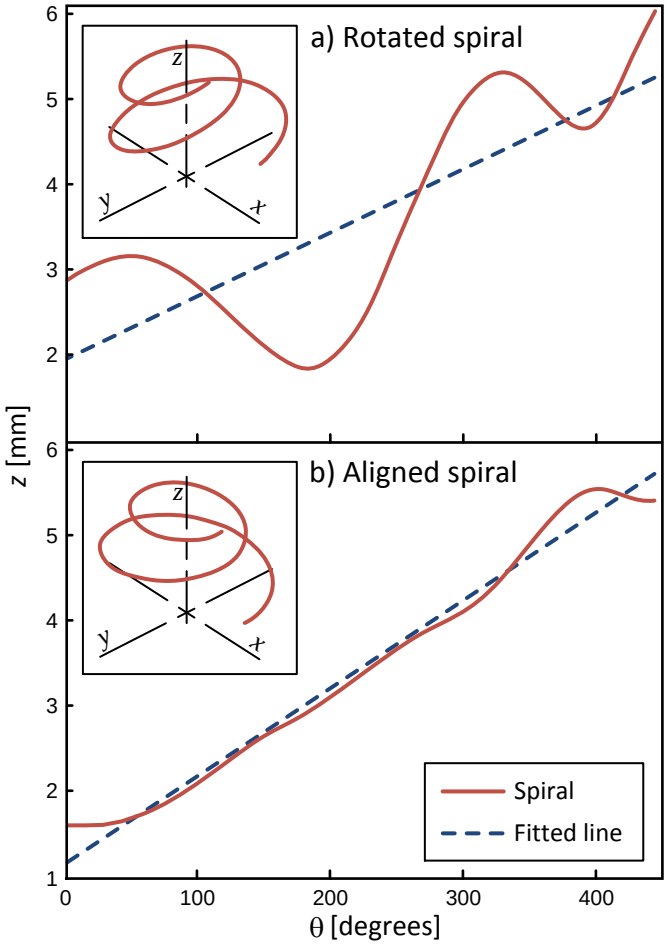

Figure 3.4. a) z-values of an example spiral that is not parallel to the centre line of the modiolus. A clear oscillation is visible in its z-values (solid line). A straight line was fitted to the z-values to determine its straightness (dashed line). The spiral was rotated around the x- and y-axis iteratively to minimize the error between the z-values and the fitted straight line. b) The rotated spiral with the smallest error was assumed to be parallel to the modiolus and used as the rotated boundary spiral around which the model was constructed

3.6 BOUNDARY TEMPLATE FITTING

To obtain an estimate of the points that were not clearly distinguishable in the CT scan data (this generally included the most apical turn of each of the cochleae modelled in this study and smooth out measurement inaccuracies, the measured boundary spiral (see previous section) was compared to 11 template spirals (six are shown in Figure 3.5) that were obtained from images of corrosion casts of human cochleae in literature (Erixon et al., 2009). Each template spiral was scaled, rotated and translated iteratively and in each iteration the ρ-values of the template were subtracted from the ρ-values (in terms of θ) of the measured boundary spiral to obtain the error between the two spirals (Procrustes superimposition). The scaled template spiral that matched the measured boundary spiral best was subsequently used as the spiral around which the rest of the model framework was constructed (henceforth referred to as the *new boundary spiral*). Only the θ and ρ values of the templates were available and thus the spiral matching was only carried out in two dimensions. The z-values of the measured boundary spiral were used as the z-values for the new boundary spiral. To extrapolate the z-values of the apex, which are indistinguishable on the CT images of some cochleae, the most superior point of the cochlear duct was estimated from the CT data and z-values were interpolated linearly between that point and the existing measurements for each value of θ.

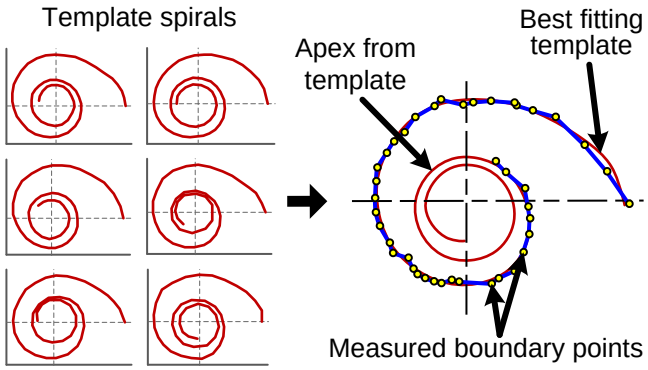

Figure 3.5. The histologically measured template from literature that best fit the measured boundary spiral from the CT data (after scaling) was used as the new boundary spiral around which the outer structures of the model were constructed. This was done to obtain a complete boundary spiral that included the apical dimensions that were not clearly distinguishable on the CT slices

3.7 INNER STRUCTURE TEMPLATE

The inner cochlear structures were not visible on the CT images because of the limitations of CT when imaging soft tissue, as well as the relatively small size of the inner bony structure of the spiral lamina (0.2 mm) compared to the scan resolution (0.6 mm voxels) . A 3D inner template model of a healthy human cochlea containing the inner cochlear structures was remapped so that its boundaries corresponded with the boundaries of the new boundary spiral obtained in the previous section. This inner template was constructed using the same techniques used to construct the inner template for the guinea pig model (Malherbe et al., 2013). In summary, the inner template was constructed by first segmenting a single photomicrograph of a mid-modiolar slice of a healthy human cochlea into the following cochlear structures: scala tympani, scala vestibuli, scala media, Reissner's membrane, basilar membrane, stria vascularis, organ of Cori, spiral ligament, peripheral nerve fibres and axonal nerve fibres (Figure 3.6a). These sections were then extruded in a spiralling fashion around the modiolus using interpolation techniques. This resulted in a 3D geometry of a cochlea containing the inner structures (Figure 3.6c). For full details on the construction of this inner template, the reader is referred to Malherbe et al. (2013).

Because of the morphological variations that exist among individual cochleae, the outer boundaries of the 3D inner template did not match the boundaries of the new boundary spiral obtained in the previous section. The inner template was thus adjusted to match the dimensions of the new boundary spiral. This was done by moving the cochlear duct of the 3D inner template model until its outer boundary intersected the new boundary spiral (Figure 3.6b and Figure 3.6c). The procedure was repeated at 1˚ angles around the full rotation of the cochlea.

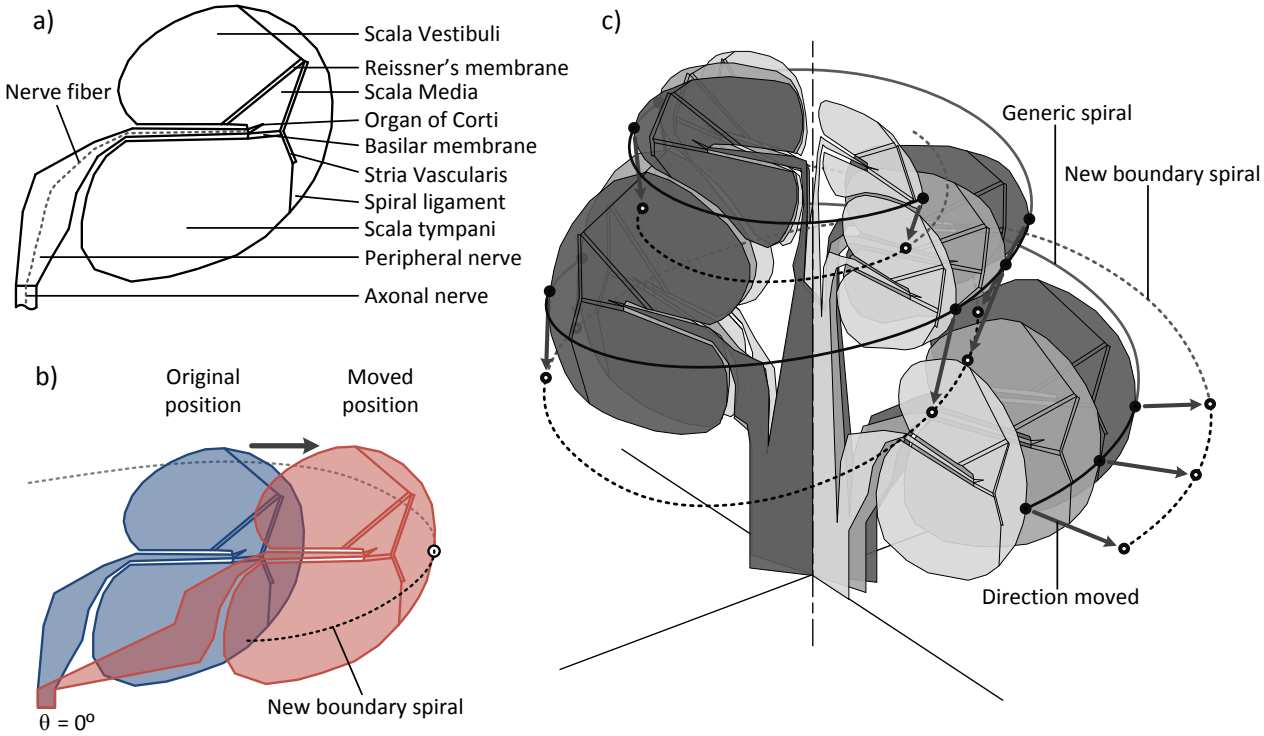

Figure 3.6. A 3D inner template model of a healthy human cochlea containing the cochlear structures that were not visible on the CT was remapped so that its boundaries corresponded with the boundaries of the new boundary spiral. a) A 2D slice of the model showing the inner cochlear structures. b) The cochlear duct was moved to the new boundary spiral at every value of θ. c) The 3D inner template (grey) is shown with the directions into which each duct was moved indicated by arrows. A limited number of slices are shown for clarity

For some users the measured boundary spiral was smaller than the 3D inner template at certain values of θ. Moving the duct of the inner template closer to the modiolus caused the inner structures that are proximal to the modiolus to intersect the modiolus. To correct for this intersection, all the ρ-values of the cochlear ducts were scaled smaller at the angles where the intersection occurred, resulting in a narrower duct that did not intersect the modiolus.

In some cases the template remapping caused two template ducts from adjacent cochlear turns to overlap vertically. At angles where this occurred, the ρ- and z-values of the

template spiral were adjusted until no overlap occurred. These adjustments were usually small and proved to be less complicated to implement than adjusting the shape of the template ducts at the point of intersection.

3.8 BONY CANAL FOR COCHLEAR NERVE WIDTH MEASUREMENTS

A study that investigates cochlear morphology among children showed that the width of the bony canal in which the cochlear nerve lies varies significantly among individuals (Teissier et al., 2009). Because of this variation, the cochlear inlet width was measured and incorporated into the model. The width of the cochlear inlet was measured from the radial CT slice at the angle of the round window ($\theta = 0^{\circ}$) at the narrowest part of the modiolus that is below the cochlear ducts (Figure 3.2e). It is assumed in this study that the width of the nerve stem equals the measured width of the cochlear inlet. The modelled template nerve stem was thus scaled independently from the cochlear ducts to match the width of the cochlear inlet. The width of the nerve stem was interpolated at all other angles to create a circular structure that intersects the $\theta = 0^{\circ}$ plane at the landmarks that specify the cochlear inlet.

3.9 ELECTRODE MODELLING

The modelled electrode array was positioned relative to the cochlear walls using the method described by Malherbe et al. (2013). The position of each electrode was measured relative to the cochlear walls by measuring the centre of the electrode array in each slice that clearly showed the electrode array and duct boundaries. The metal electrodes have a higher X-ray absorption rate than the surrounding biological tissue and thus have the brightest voxels on the CT images. The centre of the electrode array was determined by calculating the centroid of the pixels with the highest absorption rate (measured in Hounsfield Units) in each radial slice.

In the CT data sets of some users, the individual electrode contacts were not distinguishable from the wires inside the electrode array. This was usually the case in slightly blurred CT scans where adjacent electrode contacts showed up as a curved solid metal cylinder. In those cases a curved line was generated at the centroid of this cylinder. The apical end of this line represented the tip of the electrode array. Electrodes were then placed onto this line, starting at the apical end, at the distances that the electrodes were spaced from the tip of the specific implanted array (Nucleus 24 cochlear prosthesis from Cochlear Limited: contour or straight arrays) (Figure 3.7). The accuracy of the electrode contact location is limited by the resolution and blurring of the CT data. It was estimated that the error in electrode contact position did not exceed 0.2 mm. Figure 3.8 shows a 3D rendering of the cochlear model with the electrode array inserted.

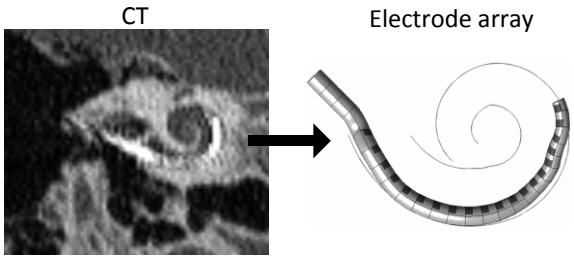

Figure 3.7. The position of the electrode array was determined from the CT images. Where individual electrode contacts were indistinguishable, the contacts were placed the appropriate distance from the array tip on a line representing the centre of the array

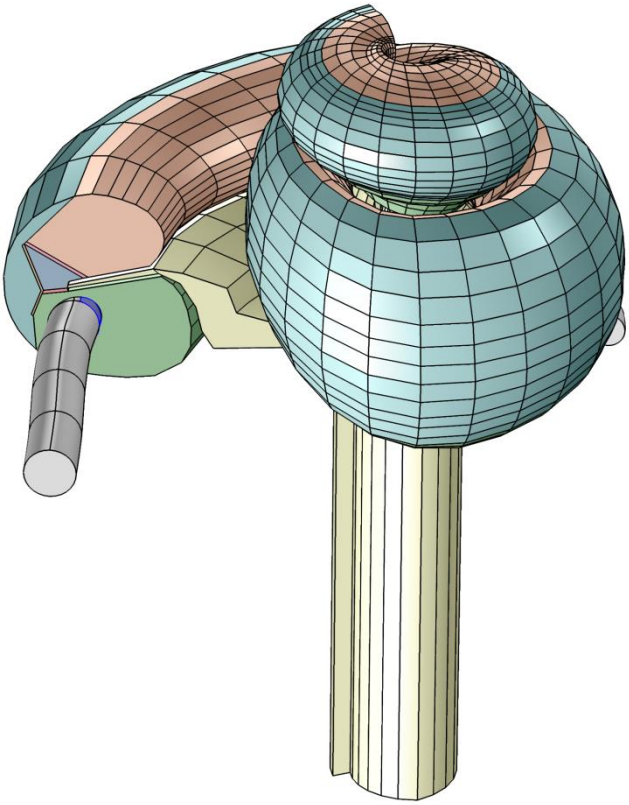

Figure 3.8. 3D view of a user-specific cochlear model with the electrode array in position

3.10 RETURN ELECTRODE AND HEAD MODELLING

The cochlea is encased in the petrous part of the temporal bone, which forms part of the skull. When using monopolar stimulation, current follows a path from an intra-cochlear electrode to one or two extra-cochlear electrodes located on the outer surface of the skull under the skin. The morphology of the structures surrounding the cochlea and the location of the extra-cochlear electrodes determine the path that current will follow through the cochlea. A previous study found that neural excitation patterns are affected by the implementation of the return electrode and structures surrounding the cochlea (Malherbe, Hanekom and Hanekom, 2015). The location of the extra-cochlear return electrodes was thus included as a model. The location of the return electrodes was determined by measuring the distances between the modiolus at the base of the cochlea and return electrodes in the x, y, and z-directions from the CT data of each user (Figure 3.9e). The

Nucleus implant has two extra-cochlear return electrodes: a spherical electrode and the casing of the implanted electronics. The spherical electrode was modelled with a diameter of 2 mm. The casing of the implanted electronics was modelled as an ellipsoid with semi-axes lengths of 2, 10 and 10 mm to have approximately the same surface area as the physical return electrode.

Contrary to the guinea pig cochlea that protrudes into an air-filled bulla, the human cochlea is embedded in dense bone. Previous human models have embedded the cochlea in a homogeneous bone volume (Hanekom, 2001b), while the guinea-pig model of Govindasamy (2012) provided a description of the air-filled bulla surrounding the otic capsule. A previous study (Malherbe et al., 2015) showed that modelled monopolar neural excitation patterns are dependent on the implementation of the structures surrounding the cochlea. Assuming that an accurate geometric representation of these structures will result in more accurate neural predictions than using a homogeneous bone volume, the cochlea was modelled inside an accurate description of the human head. A head was modelled that consists of skull, scalp and bone volumes that approximate the true geometry of these structures (Figure 3.9a-c). The skull was constructed from CT scan data of an adult skull by segmentation of CT slices using Osirix (Rosset, Spadola and Ratib, 2004). The brain volume was obtained by filling in the brain cavity of the skull and the scalp model was obtained from a Comsol Multiphysics template file[1] that was adapted to fit the shape of the skull.

[1] COMSOL Model Gallery: Absorbed Radiation (SAR) in the Human Brain, http://www.comsol.asia/model/absorbed-radiation-sar-in-the-human-brain-2190 (date last viewed 15/10/2014).

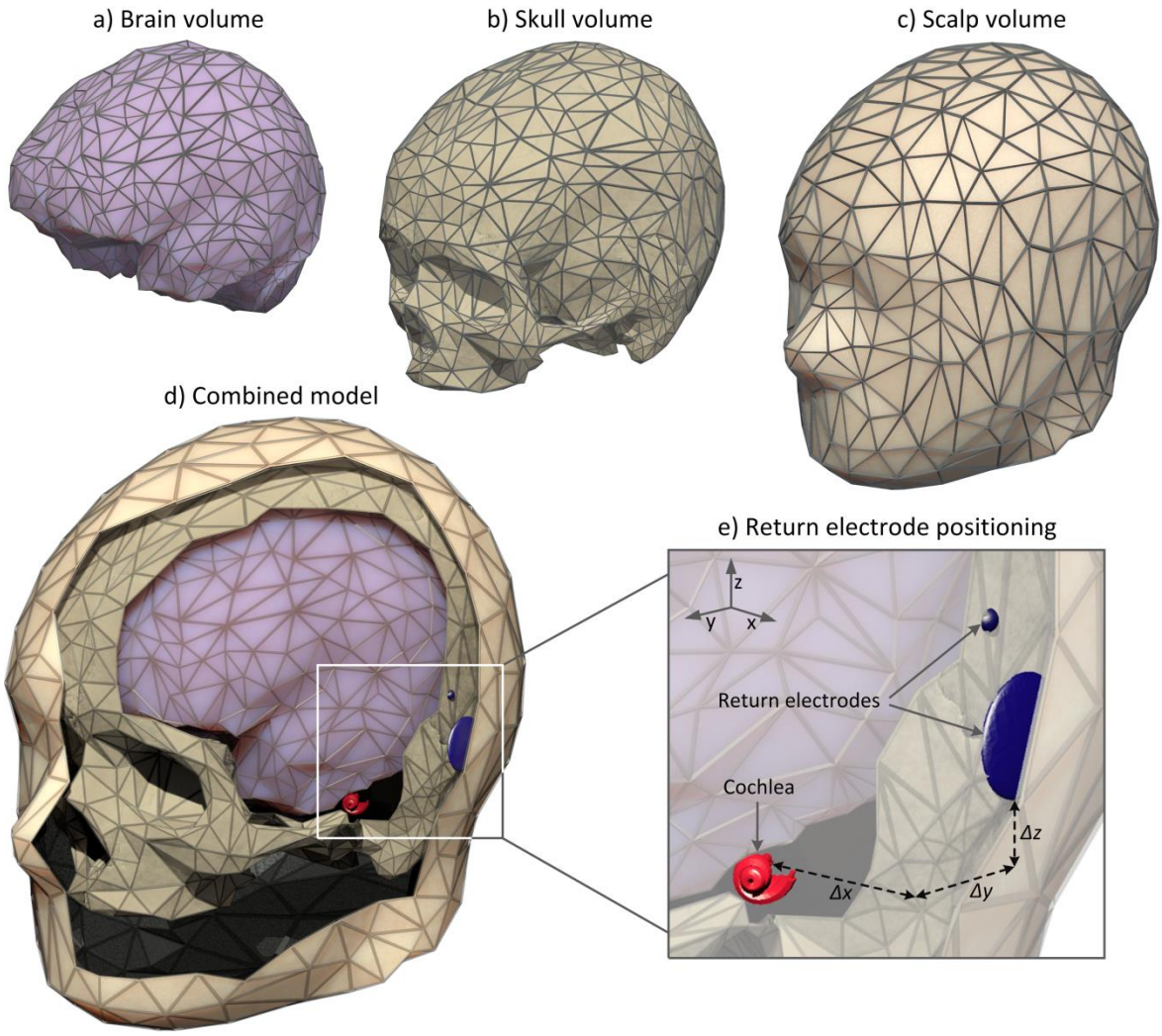

Figure 3.9. The cochlea was modelled inside a head model in an attempt to obtain an accurate estimation of the current path between a stimulating electrode and the return electrodes. The combined head model (d) consists of a brain volume (a), skull volume (b), scalp volume (c) and return electrodes that are placed in the positions in which they occur in the user. The positions of the return electrodes were determined by measuring the distance between each electrode and the modiolus at the base of the cochlea (Δx, Δy and Δz shown for the larger electrode) from the CT data of each user (e). The size of the ball electrode was increased in this figure for clarity

3.11 ELECTRIC POTENTIAL DISTRIBUTION

To simulate the electric potential distribution caused by a stimulating electrode inside the model, the finite element modelling software package Comsol Multiphysics 4.4[1] was used. The final cochlear geometry containing the electrode array was implemented in Matlab using the Comsol Multiphysics LiveLink for Matlab interface. This interface allowed the use of the Comsol Multiphysics geometry functions to be used to generate 3D solid structures of the geometry from within Matlab. Comsol Multiphysics was set up to use the *stationary electric currents* physics toolset in the *AC/DC* toolbox.

A free tetrahedral mesh was applied in Comsol Multiphysics using the predefined *normal* mesh size. Some structures, such as the thin Reissner's membrane, required finer meshing and were meshed using finer mesh parameters. The meshes of all the models consisted of approximately 2 000 000 tetrahedra (1 300 000 for the cochlea, 700 000 for the head model).

3.12 MATERIAL PROPERTIES

The material properties of each cochlear structure were defined in Comsol Multiphysics and are listed in Table 3.2. Because electrical fields are modelled, only the relative permittivity and electrical resistivity of each structure were defined. The relative permittivity of all the structures was set to 1 as the capacitive effects of the structures on potentials were assumed to be negligible for the frequencies typically applied to an implant (Briaire and Frijns, 2000a) (derived from Spelman, Clopton and Pfingst (1981)). The resistivity of the brain volume was set to the average resistivity of grey and white matter (500 Ω.cm) (Haueisen, Ramon, Eiselt, Brauer and Nowak, 1997). The other values are those reported to be used by similar modelling studies and were mainly derived from

[1] COMSOL Multiphysics modelling and simulation, http://www.comsol.com (date last viewed 23/10/2014).

guinea pig data (Hanekom, 2001b; Frijns et al., 2000; Finley et al., 1990; Misrahy et al., 1958; Strelioff, 1973; Rush and Driscoll, 1968).

Table 3.2. Conductivities of cochlear structures used in model. *For the simulations reported in this study a value of 100 Ω.cm was used for silicone rubber. This value (from [1]) is lower than reported by other studies (approaching 1^{10} Ω.cm). Analysis has shown that the results of the specific model setups in this study are not affected significantly by using a higher resistivity for silicone rubber

Cochlear Structure	**Resistivity [Ω.cm]**
Basilar Membrane	8000
Bone	10000
Brain	500
Metal electrodes	0.1
Organ of Corti	8333
Peripheral axons - axial	303
Peripheral axons - transverse	1492
Reissner's Membrane	1020408
Scala Media	59
Scala Tympani	69
Scala Vestibuli	69
Scalp	303
Silicone Rubber	10^{10} (100*)
Spiral Ganglion	303
Spiral Ligament	60
Stria Vascularis	18868

3.13 STIMULI

The electrical voltage distribution resulting from a stimulating electrode was investigated for monopolar stimulation modes. When using monopolar stimulation, the outer surfaces of the two return electrode geometries were set to ground and the active intra-cochlear electrode was configured as a current source.

When applying a current source to the model, a voltage distribution was induced throughout the model (Figure 3.10). Because the material properties of the model are purely resistive (i.e. no capacitive effects are present), the voltage at any point in the model (V_{point}) is linearly related to the stimulating current (I_{stim}) according to Ohm's law: $V_{point} = I_{stim}.R_{trans}$ with R_{trans} being the transfer resistance caused by the geometry and its material properties between the stimulating electrode and the point. To obtain the value of R_{trans}, the voltage at the point was divided by the stimulating current. A time-varying voltage at any point in the model, as is caused by a bi-phasic current source ($I_{stim}(t)$), can then be obtained by: $V_{point}(t) = I_{stim}(t).R_{trans}$. Simulating a constant current also has the advantage of setting up Comsol Multiphysics to run in a steady state mode, which takes considerably less time to solve than a time domain simulation. A solution was computed in approximately 24 minutes on a computer with a 2.6 GHz AMD 64 processor with eight cores and 16 GB of RAM.

Voltages were extracted from the modelled results at points corresponding to the locations of the nodes of Ranvier on a set of neurons that covered the length of the cochlea along the basilar membrane, i.e. in a radial pattern around the modiolus, each spaced 1˚ apart. The neurons were placed in the centre of the modelled peripheral and axonal nerve fibre regions with the tip of the peripheral process located just medial to the organ of Corti (dashed line in Figure 3.6a). Refer to Malherbe et al. (2013) for additional details.

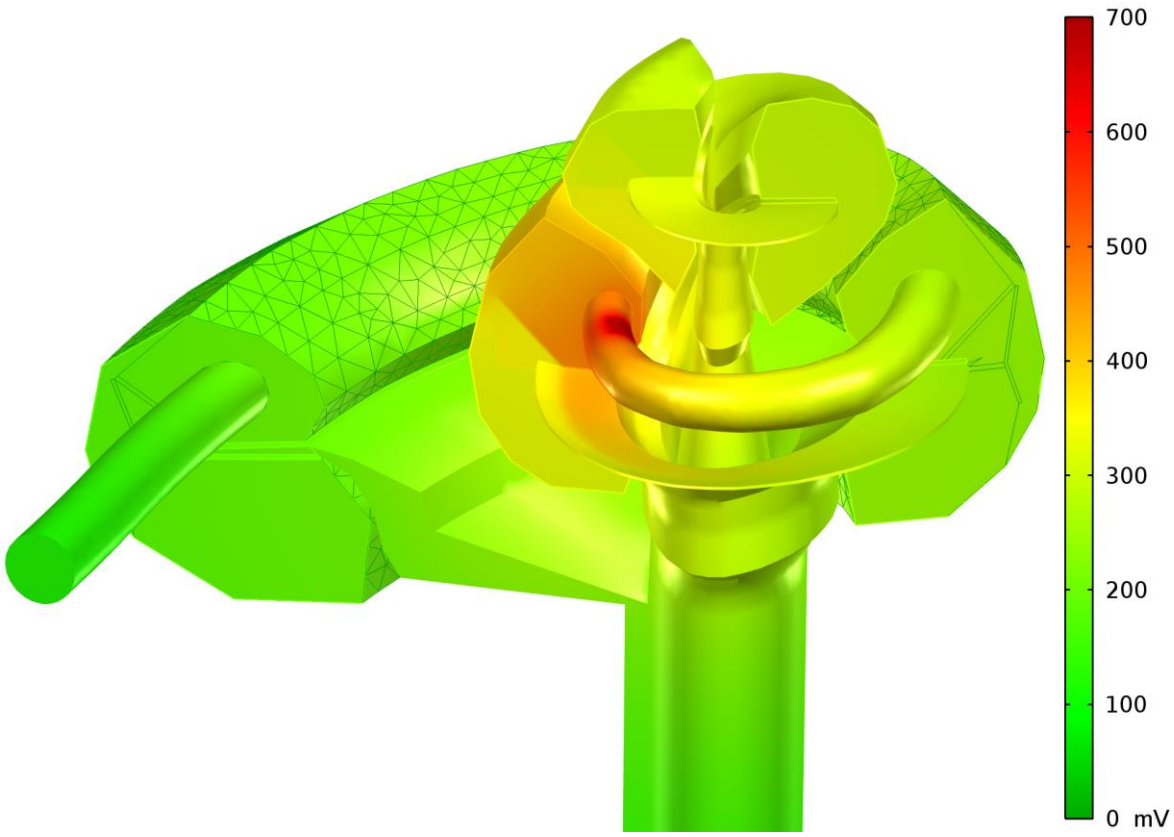

Figure 3.10. Comsol Multiphysics prediction of the electric potential (in mV) in the cochlear model induced by stimulating an electrode at the apical end of the electrode array with a current of 1 mA using monopolar stimulation

3.14 NEURON MODEL

The electric potential at the nodes of Ranvier were extracted and used as input to a cochlear neuron model. The generalised Schwartz-Eikhof-Frijns (GSEF) model (Frijns et al., 1995), was used with the internodal distances modelled as defined in this reference. This model is a cable model that incorporates non-linear mammalian nerve fibre properties and predicts the membrane potential at each node as a function of time. The minimum current (threshold current) at which each neuron produces a propagating action potential along the axon was iteratively determined and used to create a threshold profile. Threshold profiles were predicted by stimulating electrodes located in the same radial position,

around 90˚ from the RW, in the five modelled cochleae. Each model contained around 160 neurons each spaced 5 degrees apart with each neuron having 27 nodes of Ranvier.

3.15 INFLUENCE OF COCHLEAR MORPHOLOGY ON NEURAL THRESHOLD PROFILES

User-specificity may be included in a volume conduction (VC) model by, among others, user-specific electrode location and user-specific cochlear morphology. A model that incorporates both these factors shows the combined effect of these factors on the predicted electrical and neural responses to electric stimulation, but it does not show the relative importance of each factor to produce user-specific outcomes. The question thus remains whether it is sufficient to model user-specific outcomes through user-specific electrode location alone using a generic morphology, or whether the morphology also affects the predicted outcomes. To assess the extent to which variations in cochlear morphology influences electrical potential distribution and neural excitation profiles, its effect on excitation profiles was isolated by replacing the modelled user-specific electrode arrays with two versions of a modelled generic array: one located medially in the ST and one located laterally. The two generic locations of the array in each model allowed an assessment of the influence of the cochlear morphology on predicted outcomes, e.g. thresholds, relative to the effect of electrode location, which is known to be significant (Parkinson, Arcaroli, Staller, Arndt, Cosgriff and Ebinger, 2002). The generic medial array was placed in the vertical centre of the ST and one third of the width of the ST from the modiolus horizontally while the lateral array was placed one third of the width of the ST from the lateral cochlear wall. Individual electrode contacts were modelled onto the arrays at 30˚ increments around the modiolus measured from the RW. This allowed a stimulus to be generated from an electrode in the same spatial position in all the models regardless of the model's size and shape. The same return electrode positions were also used in all five models. Electrode 4, located at 90˚ from the RW on the generic arrays, was stimulated and the resulting potentials at the nodes of Ranvier and neural excitation profiles were compared.

By (i) isolating the effect of user-specific morphology from that of user-specific electrode location by the use of generic arrays and (ii) re-introducing electrode location as a controlled parameter into the models by the use of two generic electrode locations, it is possible to interpret the results in terms of the potential benefit that a user-specific model that includes both electrode location and morphology could have compared to a model based on a generic morphology.

3.16 RESULTS

3.16.1 Generic arrays

There is a noticeable difference among the neural excitation profiles produced by each model containing the generic arrays. Figure 3.11 shows part of the neural excitation profiles produced by the modelled cochleae and electrodes proximal to the stimulating electrode. The positions of the minima of the neural excitation profiles (referred to as the thresholds) are indicated with symbols. The threshold levels (in dB re 1 μA), characteristic frequencies (CFs) of these thresholds and excitation spread in terms of bandwidth were used as the basis of comparison and are summarized in Table 3.3. Where changes in CFs are compared, the distance (in mm) along the organ of Corti between the threshold locations is given to make values comparable as the CF is a function of the cochlear length which varies between users.

The threshold levels, CFs and excitation spread predicted using the generic medial arrays show variability among cochleae with the maximum difference in threshold level being 4 dB, the maximum difference in CF location being 2.1 mm and the maximum differences in 3 dB and 10 dB bandwidths being 1.9 mm (0.4 octaves) and 3.2 mm (0.7 octaves) respectively. The same effect of cochlear morphology on predictions is observed for the lateral arrays.

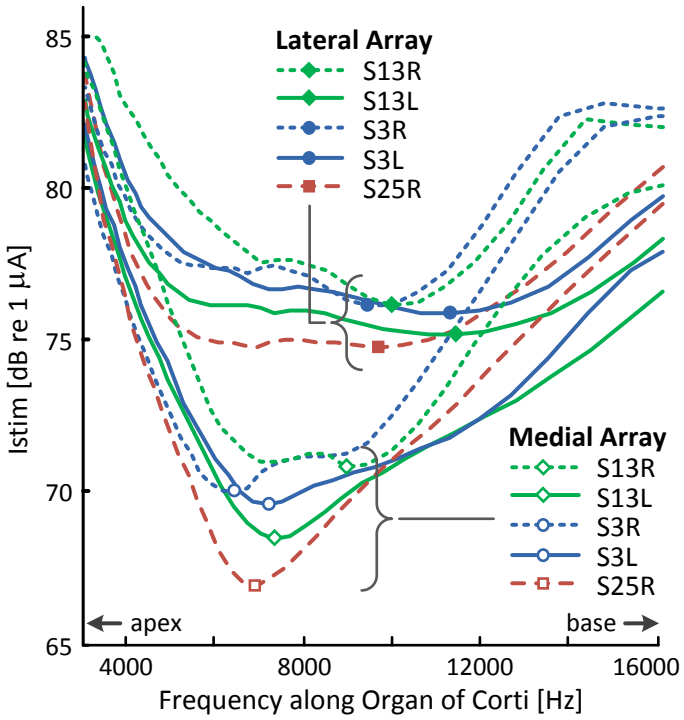

Figure 3.11. Neural threshold profiles of five cochlear models inserted with identical medial and lateral electrode arrays when stimulating with electrode 4 inserted at the same angle in all the models. It is evident that the neural excitation profiles differ for each model, specifically as described by the CFs and thresholds (indicated by symbols). This is due to the morphological variations of the cochleae causing model-specific current paths and thus threshold profiles

Table 3.3. Summary of the threshold levels (in dB re 1 µA), characteristic frequencies (CFs) and bandwidth of the predicted threshold profiles in this study

	Threshold	**CF**		**Bandwidths**			
Medial	**dB**	**mm**	**Hz**	**3dB mm**	**3dB Oct**	**10dB mm**	**10dB Oct**
S13R – Medial	70.8	5.6	8944	4.7	1.0	11.2	2.5
S13L – Medial	68.4	6.4	7318	4.0	0.9	10.1	2.4
S3R – Medial	70.1	7.7	6408	4.9	1.1	9.5	2.1
S3L – Medial	69.6	6.3	7153	4.7	1.2	10.4	2.6
S25R – Medial	66.9	6.8	6888	3.0	0.7	8.0	1.9
Average	69.2	6.5	7342	4.3	1.0	9.8	2.3
Max-Min	3.9	2.1	2535	1.9	0.4	3.2	0.7

Lateral							
S13R – Lateral	76.1	4.8	9954	5.3	1.2	14.9	3.3
S13L – Lateral	75.2	3.7	11413	8.2	1.9	13.1	3.1
S3R – Lateral	76.1	5.2	9421	7.0	1.6	16.4	3.7
S3L – Lateral	75.8	3.6	11255	7.0	1.7	14.3	3.6
S25R - Lateral	74.7	4.7	9661	7.4	1.7	12.1	2.9
Average	75.6	4.4	10341	7.0	1.6	14.2	3.3
Max-Min	1.4	1.6	1992	2.9	0.8	4.3	0.8
Lateral-Medial							
S13R	5.3	0.7	1011	0.5	0.1	3.7	0.8
S13L	6.7	2.7	4095	4.2	1.0	3.1	0.7
S3R	6.1	2.5	3013	2.1	0.5	6.9	1.6
S3L	6.3	2.7	4103	2.3	0.6	3.9	1.0
S25R	7.9	2.1	2773	4.4	1.0	4.2	1.0
Average	6.4	2.1	2999	2.7	0.6	4.4	1.0
Right-Left Ears							
S13 Medial	2.4	0.9	1625	0.8	0.1	1.1	0.1
S3 Medial	0.5	1.4	745	0.2	0.1	0.9	0.5
Average	1.4	1.1	1185	0.5	0.1	1.0	0.3
S13 Lateral	0.9	1.2	1459	2.9	0.8	1.8	0.2
S3 Lateral	0.3	1.6	1835	0.0	0.2	2.1	0.1
Average	0.6	1.4	1647	1.5	0.5	1.9	0.1
User electrode arrays							
S13R	76.5	3.3	12583	3.6	0.8	12.9	2.8
S13L	71.2	5.3	8834	3.0	0.7	6.2	1.5
S3R	75.1	6.5	7682	3.6	0.8	9.8	2.2
S3L	74.2	6.0	7487	3.1	0.8	6.6	1.6
S25R	70.9	6.2	7538	2.9	0.7	5.8	1.4
Average	73.6	5.5	8825	3.2	0.7	8.3	1.9
Max-Min	5.5	3.2	5095	0.7	0.1	7.1	1.5

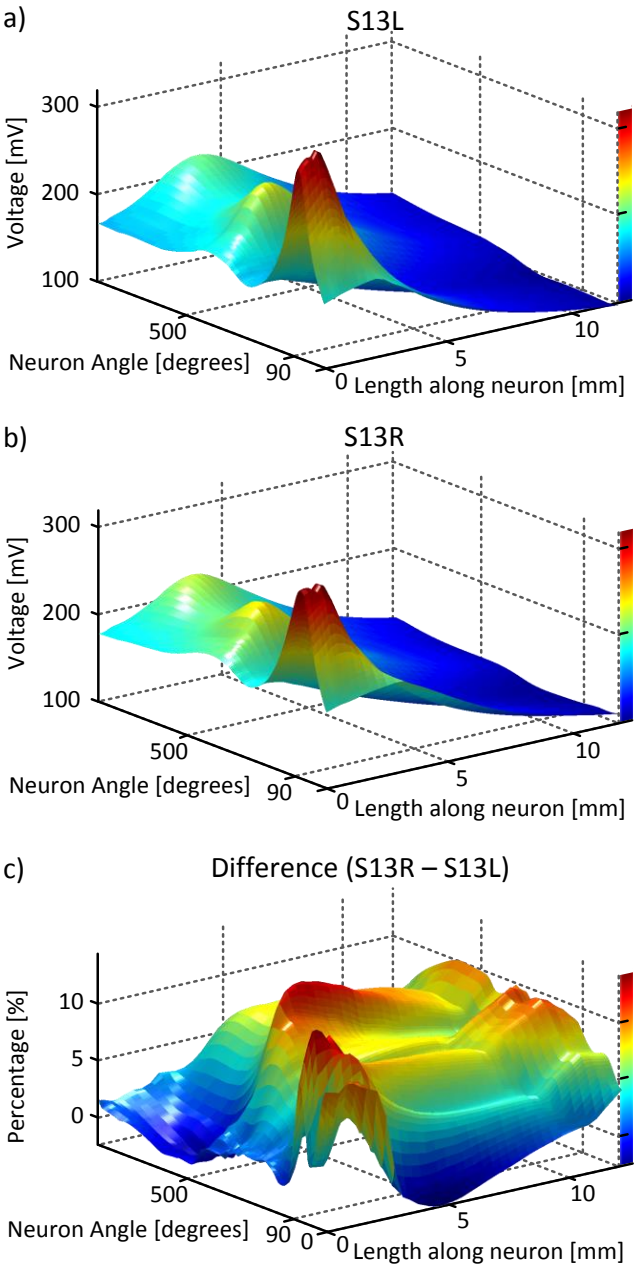

Figure 3.12. Potential profiles produced at the nodes of Ranvier by stimulating electrode 4 (inserted at 90˚ from the RW) on a generic medial array inserted into the left and right modelled cochleae of the same user (S13) with a current of 1 mA. A generic array with electrodes in the same spatial positions in all models was used to assess the effect that user morphology has on predicted potential profiles. It is evident that the potential profile predicted by the model of the left cochlea (a) differs from that of the right cochlea (b). The percentage difference between the two potential profiles is shown in (c). Neuron angle is measured from the RW around the modiolus. Length along the neuron is measured from the neuron tip

Also worth noting is the difference in neural excitation profiles between the left and right cochleae of the same users (S3 and S13). The threshold level, CF locations and 3dB and 10 dB bandwidths for the two ears differ on average by 1.4 dB, 1.1 mm, 0.5 mm (0.1 octaves) and 1 mm (0.3 octaves) for the medial array and 0.6 dB, 1.4 mm, 1.5 mm (0.5 octaves) and 1.9 mm (0.1 octaves) for the lateral array. The neural threshold profiles are determined by the neuron models' response to the potential profiles (measured in mV) in the cochlea induced by electrode stimulation. Figure 3.12 shows the potential profiles, obtained on the nodes of Ranvier, produced by the left (Figure 3.12a) and right (Figure 3.12b) cochlear models of user S13 stimulating electrode 4 on the generic medial array with 1 mA. When the two potential profiles are subtracted from each other, it is evident that they differ in shape (Figure 3.12c) up to 14.3% at the angle of the electrode (90˚). This difference is ascribed to morphological differences between the two cochleae of the user.

To quantify the effect of morphology on neural excitation, it was compared to the effect of intra-scalar electrode location, which is known to be significant (Parkinson et al., 2002). The mean difference between the threshold levels of the medial and lateral arrays is 6.4 dB this is only slightly more than the effect of morphology (max. 4 dB). When the CF locations are considered, the shift from medial to lateral electrode array for the specific electrode contact is on average 2.1 mm. The inter-user variability in CF location for the medial and lateral electrodes is 2.1 mm and 1.6 mm respectively, showing that the effect of morphology approaches that of electrode location. The difference in 3dB and 10dB bandwidths between the medial and lateral electrode placements are on average 2.7 mm (0.6 octaves) and 4.4 mm (1 octave) respectively. This is comparable to the maximum variation in the bandwidths due to morphologic variations. Threshold, CF and bandwidth values thus demonstrate that variations observed as a result of morphology are almost as large as variations observed as a result of electrode placement, suggesting that user-specific morphology is an important determinant of CI performance.

The generally observed shift of the CF towards the base when moving the electrode from a medial to a lateral location in the ST is demonstrated in Figure 3.13. The figure shows basal sections through models containing each of the electrode arrays indicating (i) the region of neurons activated (blue line) when stimulating at a current that is 2 dB above the threshold level (which is unique in each model) and (ii) equipotential lines representing the potential fields induced by the stimulating electrodes in red. The lines for the medial and lateral electrodes are at the same potential relative to the potential of the stimulating electrode, showing the less focused potential field of the lateral electrode relative to that of the medial electrode. For both electrode locations the equipotential lines are relatively symmetrical on the apical and basal sides of the electrode, but the active neurons are located more basally relative to the electrode's position. This effect is more pronounced for the lateral electrode than for the medial electrode, as can be seen from the wide basal extension of neural activity for the lateral electrode. The dissimilarity between the symmetric equipotential region around the electrode and the non-symmetric neural excitation region also suggests that a direct relation between current spread and neural excitation cannot be inferred. In other words, neural excitation is dependent on complex current paths in the cochlea related to the trajectories of the individual neurons (as neuron excitation is governed by a non-linear response to the voltages along the trajectories of the neurons) and does not directly translate to potential decay in the ST.

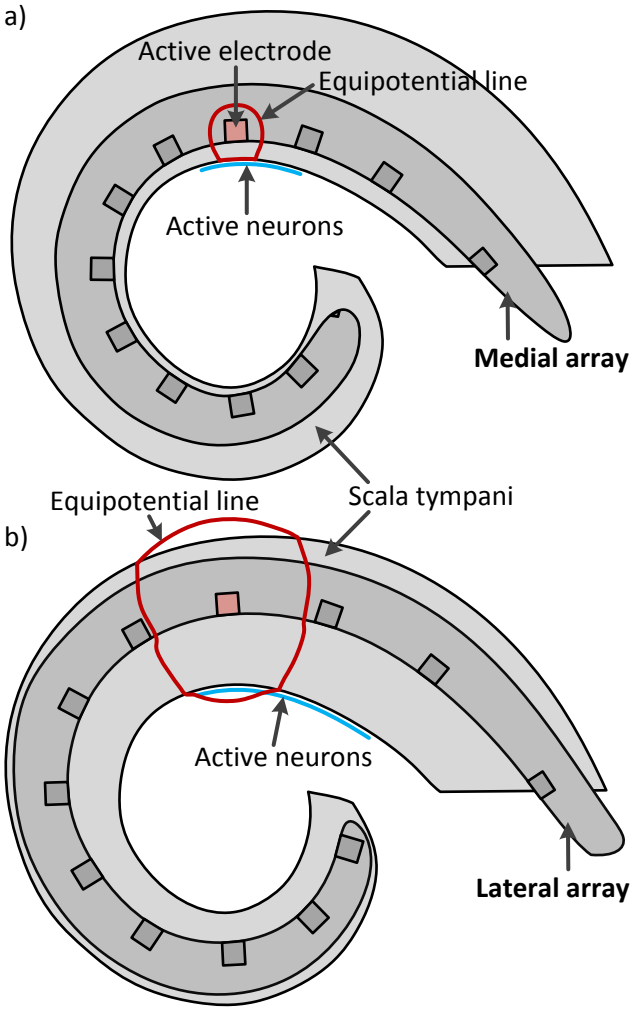

Figure 3.13. Medial (a) vs. lateral (b) generic arrays of cochlea S13L. Electrode 4 was stimulated at a level of 2 dB above threshold level for both arrays and the resulting regions of active neurons are indicated in blue. The equipotential lines indicating the same voltage level relative to the stimulus shows the wider potential field associated with the lateral array. Electrode contacts were placed at the same angular positions (30 degree increments) around the modiolus in all the generic array models to make the results comparable. This caused the lateral array to be longer than the medial array

3.16.2 User arrays

The effect of user-specific neural excitation becomes even more distinct when the user-specific electrode location is re-introduced into the models. Figure 3.14a shows the threshold profiles predicted when stimulating electrodes located at approximately 90˚ insertion angle (i.e. approximately the same insertion angle as the generic electrodes) indicated by crosses in Figure 3.14b. The geometries of the cochlear walls and locations of the user electrode contacts are also shown in Figure 3.14b. The left and right cochleae of the same users (S3 and S13) are superimposed on top of each other for comparison. The type of electrode (contour or straight) is indicated in brackets (C or S). Interestingly, the left cochlea of user S3 is smaller than the right cochlea. This is not the case for user S13 where the cochlear geometries only differ near the base. The predicted excitation profiles for both ears of user S3 are similar in shape, while the excitation profiles of user S13 differ in threshold levels by 3.9 dB, CF locations by 1.96 mm and 3 dB bandwidth by 0.7 mm (0.1 octaves). Among all the models, the maximum difference in threshold levels, CF location and 3 dB bandwidth is 5.5 dB, 3.2 mm and 0.7 mm (0.1 octaves) respectively. The 5.5 dB variation in thresholds reflects both the user-specific geometry (up to 4 dB for the generic arrays depending on the location of the electrode) and the user-specific location of the electrode relative to the modiolus (6.4 dB for medial vs. lateral placement of the generic array). The shift in CF produced by user-specific electrode location is larger than the CF shift observed on average between lateral and medial electrodes using generic arrays. This is expected, as the user-specific electrodes are not perfectly aligned at 90˚as is the case for the generic arrays.

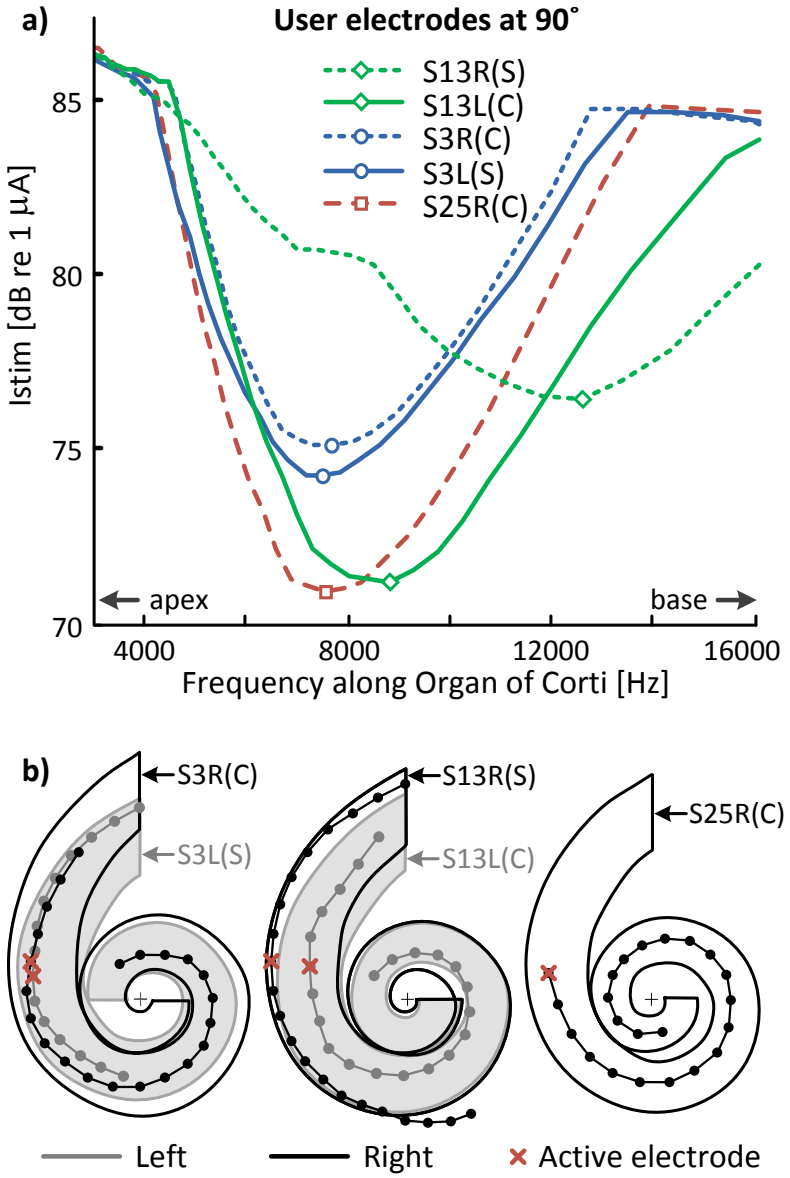

Figure 3.14. a) Threshold profiles of the modelled user electrode arrays when stimulating electrodes located approximately 90˚ from the RW. b) The cochlear geometries of the users are shown with the left and right cochleae of the same users superimposed. Users were fitted with a combination of contour (C) and straight (S) electrode arrays

3.16.3 Models as visualization tool

The 3D models of the individual users' cochleae can also be used as a tool to visualise the electrode array relative to cochlear structures. Models of the implanted user cochleae of two users are shown in Figure 3.15. Such high resolution visualisations may be of assistance in a clinical setting during model based diagnosis (MBD) where a clinician is given a clear indication of the electrode array relative to other structures.

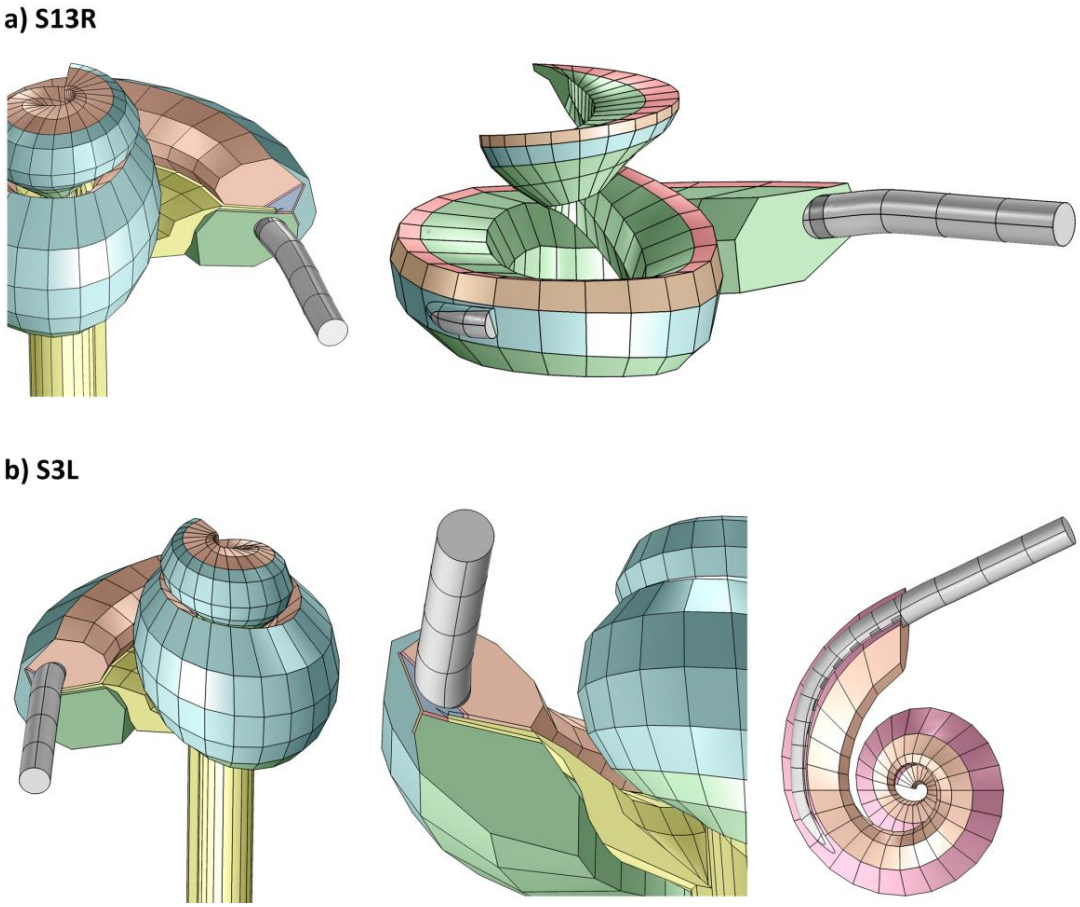

Figure 3.15. The constructed 3D models of the user cochleae may be used as a high resolution visualisation tool to assess electrode placement. Here the models of two user cochleae are shown. a) S13R. This user has a straight array located in the lateral portion of the ST. The tip of the electrode is seen protruding slightly from the ST. This may be an indication as to why the array was only inserted around half a turn. b) S3L. A fairly deep SV insertion is shown. The array is seen intersecting the SM at the basal end of the SV. This indicates that the SM was either damaged or pushed aside during insertion

3.17 DISCUSSION

In this study it has been shown how the implanted cochlea of a specific living human user can be modelled from CT data. This is an improvement over cochlear models based on a generic cochlear morphology, as it was shown that cochlea-specific outcomes such as potential distribution and neural activation profiles are dependent on cochlear morphology. Integration of the morphology of a specific CI user's cochlea into a model is thus recommended if such user-specific outcomes are to be predicted from a model. This has application both in basic and applied CI research. In basic CI research the mechanisms that underlie perception with a CI are studied, including the factors that cause inter-user performance to vary so greatly (Firszt et al., 2004). User-specific models provide an instrument to probe the peripheral contributors to these differences at a physiological level that is not accessible in live humans, i.e. at the single nerve fibre level. In applied research the effect of new technological innovations are being investigated, such as the use of current focusing and beam steering to improve frequency resolution in CIs. In this case the potential distribution in a specific cochlea, due to multiple current sources, has to be determined (Bonham and Litvak, 2008; Van Den Honert and Kelsall, 2007; Saba, Elliott and Wang, 2014) and its effectivity to increase spatial and thus frequency resolution needs to be evaluated. User-specific implementation of cochlear morphology in a model could, for example, inform the design criteria for beam-steering electrode arrays that need to function over a morphologically diverse implant population.

The added complexity of the modelling method was intentionally limited to enable user-specific models to be created rapidly. To ensure this, a number of assumptions and simplifications were made that could affect the accuracy of model predictions. The first of these include the description of the head volume with only three types of homogeneous materials (scalp, bone and brain), whereas a real head volume consists of more intricate structures of varying densities. Although it was assumed that the three structures that were modelled are the main determinants of return current paths because of their large size, including different bone densities (e.g. denser bone in the otic capsule) and areas of different bone type (e.g. cancellous bone that is found between the tables of the skull) as

well as cerebrospinal fluid in the brain volume may improve the accuracy of the model predictions.

Further assumptions were made concerning the inner cochlear structures of a specific user (which are currently not obtainable *in vivo* using existing imaging techniques) by augmenting these details in each model using a generic photomicrograph. Here the assumption is made that the dimensions of the inner structures are the same for all cochleae. This is, however, not the case as variability in the size and shape of the inner cochlear structures have been shown to exist (Avci et al., 2014; Rebscher, Hetherington, Bonham, Wardrop, Whinney and Leake, 2008). An example is the 9-14% variance in the cross-sectional diameter of the ST of 16 cochleae as measured by Avci et al. (2014). A method to estimate the inner structures of an individual more accurately might prove to enhance the predictive ability of the model. A third assumption was necessary regarding neural survival in a modelled ear. For these models all the neurons were assumed to be present. In reality it is known that neural survival comprises both total neural loss in some areas and loss of dendrites in areas where the neurons are still alive (Kujawa and Liberman, 2009). Neural survival in terms of regions where limited or no neurons occur may be estimated from masking experiments (Earl and Chertoff, 2012), but the present study did not take this into account. Finally, resistivity values of intra and extra-cochlear structures are currently based mostly on non-human data, i.e. resistivity values for human tissues may differ from these values, which may also affect the predicted potential spread and neural excitation spread. This was observed in another study (Malherbe et al., 2015) where neural excitation width was shown to be dependent on the resistivity value of the bone surrounding the cochlea. This suggests that material conductivities that represent human structures more accurately may influence the predictions of the models.

Another important assumption is that the neuron model that was used and its implementation describe the workings of a human cochlear neuron accurately. The neurons were modelled as fibres emanating radially from the modiolus to the OC, whereas in reality only neurons near the base of the cochlea emanate radially and start to follow a

'bicycle spoke' pattern along the cochlea towards the apex (Stakhovskaya et al., 2007). As neural excitation patterns were predicted for basal electrodes, CFs of the present results are assumed not to be affected by using such a simplified radial neuron pattern. When predicting CFs of more apical electrodes or when stimulation with a larger current affects neurons located more apically, implementation of an accurate neuron trajectory may be necessary. Another limitation of the present model is its inability to predict absolute threshold levels accurately. Although the effects of morphological differences can be observed in the relative differences in predicted threshold levels, absolute threshold levels in the range of the perceptual T-levels of the users are not predicted. The relationship between neural threshold levels and perceptual T-levels is not known precisely. Snel-Bongers, Briaire, Van Der Veen, Kalkman and Frijns (2013) used a 1 mm region of excitation as an indication of perceptual threshold levels and based on their findings, single-fibre threshold levels may be expected to be lower than mapped T-levels. However, the present model predicts these to be around 25 dB higher than the T-levels in the maps of the specific users whose cochleae were modelled. Over-estimation of threshold levels may have different sources. While inaccurate resistivity values in the volume conduction model will influence threshold predictions, the ability of the selected neural model to predict threshold levels of human auditory nerve fibres correctly has not been established. For comparison, the neuron model of Rattay et al. (2001a) was also implemented and yielded threshold levels of the same order as those predicted using the GSEF model. The same dependence of neural excitation on cochlear morphology was also observed. The assumption is also made that user perception is directly related to the excitation of the peripheral auditory neurons. This is, however, not the case as perception also relies on more central processes. Incorporating aspects that model more central processes into the models may also increase their predictive ability of measured T-levels.

The dependence of neural thresholds and CF locations on cochlear morphology was found to be relatively large when compared to a known effect such as lateral vs. medial electrode placement. The maximum difference in threshold levels observed between the cochlear geometries is about two-thirds of the mean difference in threshold levels between the

medial and lateral arrays. Similarly, the maximum difference in CF locations observed between the cochlear geometries was found to be the same as the mean difference in CF locations observed between the medial and lateral arrays. The observation that the effect of cochlear morphology is comparable to the effect of medial vs. lateral electrode placement suggests that the large variations in performance that are observed among CI users (Firszt et al., 2004) could at least partially be ascribed to variations in cochlear morphology. In general the model predicts that substantial variations in peripheral neural excitation characteristics may be expected among individual CI users. Another interesting observation is the large difference in bandwidths predicted for the lateral and medial arrays. This confirms experimental results where a modiolus-hugging electrode was found to reduce the spread of excitation (Rubinstein, 1993).

An important observation is that the cochlear morphologies between the left and right ears of the two bilateral users in the study differ sufficiently to elicit different neural threshold levels and CFs. While it has been suggested that matching insertion depths of bilateral implantees may lead to better speech perception (Van Besouw, Forrester, Crowe and Rowan, 2013), model results suggest that similar placement of arrays in both ears will most likely not result in similar neural excitation characteristics. Model predictions suggest that variations in threshold levels and CFs as a result of morphological differences between the right and left cochleae may also be as large as two-thirds of the variation that may be observed in these variables as a result of medial or lateral placement of the electrode array. Pre-operative user-specific modelling could provide a means of predicting the optimal placement of a second electrode array if similar outcomes to those of the first implant are desired. The results also suggest that appropriate mapping of a second implant may be a means to match or integrate the perceptions from the two implants in an attempt to create binaural fusion in the system. After isolating the effect of morphology on neural excitation by modelling generic electrode arrays in the cochleae, the user-specific electrodes were modelled. Neural excitation profiles of stimulated electrode contacts at approximately the same angle around the modiolus (90˚) were predicted. These profiles contain the effects on neural excitation of both morphology and electrode placement. The variations in threshold

level and CFs are in the same order as when the electrode location and geometric effects were isolated, suggesting that the effects of morphology and electrode placement on neural excitation are not independent. Accurate prediction of cochlear neural excitation therefore necessitates the incorporation of the cochlear morphology as well as electrode placement into a model.

The study also allowed an assessment of the applicability of current or voltage decay models to predict spread of neural excitation. This method is commonly used when a simple model of spread of neural excitation as a function of stimulation intensity is required. One such application is within acoustic models of CIs (Bingabr, Espinoza-Varas and Loizou, 2008), where noise bands are used to represent the acoustic equivalent of an electrically evoked sound. The bandwidth of the noise signal is determined by the current or voltage spread predicted at a certain stimulus intensity. Model predictions from the present study have shown that the spread of neural excitation cannot directly be represented by the spread of the potential along the length of the cochlea. This has implications for the study of, for example, pitch-related phenomena in models that employ a direct relation between potential decay and spread of neural excitation. Furthermore, a current decay-based prediction of spread of excitation cannot reflect user-specific neural excitation characteristics. If a model thus intends to reflect user specificity, current or voltage decay models of spread of excitation are not appropriate.

The models developed of the individual cochleae also afforded a high resolution view into the structure of a user's cochlea as well as the placement of the electrode array. Such information may be used by a clinician during diagnostics of a specific implant that is functioning abnormally (MBD).

This study demonstrated the feasibility of rapidly constructing user-specific cochlear models from low-resolution clinical CT image data. Previous studies (Hanekom, 2001b; Malherbe et al., 2013) showed that a model of a cochlea based on a single generic morphology will only allow the prediction of general trends in electrophysiological

variables and that these trends will rely on the model's specific morphology. In contrast, the present study demonstrated an important effect of user-specific cochlear morphology on neural excitation characteristics. This suggests that user-specific models may allow investigation of variance in neural excitation characteristics among different users as a function of their individual cochlear morphologies. The pronounced differences in neural excitation profiles between the left and right ear of bilateral implantees under ideal conditions (i.e. the same electrode inserted in exactly the same location in both cochleae) were also demonstrated. This suggests that optimization of the maps of the two implants is critically important to reduce the effects of offsets in CF and threshold between the two implants. The study also showed the importance of a morphologically detailed description of the volume conductor to translate current or voltage distributions to spread of neural excitation. All of these factors support the inclusion of an individual's cochlear morphology into a model when investigating user-specific neural excitation differences in spite of the added complexity of the modelling process.

3.18 CONCLUSIONS

1. Low-resolution CT scans may be used to construct a model of the implanted cochlea of a specific living human user.
2. Such a model may serve as a high resolution visual aid to clinicians that indicates the position of the electrode array relative to other cochlear structures during MBD.
3. Modelled potential distributions and neural excitation profiles (threshold amplitudes, centre frequencies and bandwidths) are significantly affected by user-specific cochlear morphology.
4. Representation of a CI user's cochlear morphology in a model is recommended to predict user-specific neural threshold profiles.
5. The use of a more complex modelling method opposed to a model based on the morphology of a generic human cochlea is warranted, given that outcomes that are affected by cochlear morphology may be predicted.
6. A model of a living user's cochlea may facilitate the investigation of user-specific factors that affect implant performance.

CHAPTER 4 BONE RESISTIVITY ESTIMATION

The contents of this chapter is included in the following article:

Malherbe, T. K., Hanekom, T. and Hanekom, J. J. "The effect of the resistive properties of bone on neural excitation in cochlear implants" Hearing Research 2015; 327:126-35.

Having a method to create multiple user-specific models allows for predictions that include inter-user variability. Predictions form a population of models may then be compared to data from literature from a number of ears. This chapter explains the methodology followed to derive a bone resistivity value for use in volume conduction models of a cochlear implant by comparing the outputs of five user-specific models to measured data from five ears from literature.

4.1 INTRODUCTION

Geddes and Baker reported in 1967 that the resistivity of bone is the most variable of all the tissues of the body because of the variation in its composition throughout the body (Geddes and Baker, 1967). This is supported by numerous studies over the years that reported values from 312 Ω.cm (Gabriel, Lau and Gabriel, 1996) to 84 745 Ω.cm (Akhtari, Bryant, Mamelak, Flynn, Heller, Shih, Mandelkem, Matlachov, Ranken, Best, Dimauro, Lee and Sutherling, 2002), depending on the type of bone (cancellous vs. cortical), orientation of the bone sample during measurement, measurement frequency, species, state of the bone (e.g. live vs. dried and rehydrated) and the specific site, e.g. skull vs. tibial bone.

Volume conduction (VC) modelling studies of the distribution of currents as a result of intra-cochlear stimulation with cochlear implant electrodes have conventionally used a homogeneous, isotropic, purely resistive value to represent the electrical characteristics of bone. However, since the compact bone that envelops the human cochlea is mainly responsible for directing current through the cochlear structures instead of allowing dispersion of the currents throughout the surrounding head tissues, it is hypothesised that its electrical properties will have a significant effect on the excitation profiles of the

auditory neurons. This effect is especially significant using monopolar stimulation where the return electrode is located outside the cochlea in the surrounding bone. The human cochlea is enveloped in what is regarded as some of the densest bone in the human body. Although bone density is not a good indicator of the absolute resistivity of cortical bone, it is reported to be less conducting than cancellous bone. Bone density is affected by many factors including age, chemical composition, gender and disease, e.g. otosclerosis (Bozorg Grayeli, Saint Yrieix, Imauchi, Cyna-Gorse, Ferrary and Sterkers, 2004), and varies among individuals (Marshall, Johnell and Wedel, 1996).

Some VC models of the cochlea have thus far used a value of 641 Ω.cm for the resistivity of the bone surrounding the vestibular duct (Frijns et al., 1995; Finley et al., 1990; Hanekom, 2001b; Malherbe et al., 2013). This value originated from a value reported in 1987 by Spelman and Clopton (cited in Finley et al. (1990)) and was derived from guinea pig experiments. However, absolute thresholds predicted for humans using this value are greatly overestimated (Hanekom, 2001a; Briaire and Frijns, 2006), while some animal models predict relatively accurate thresholds using this value, e.g. the guinea pig model of Govindasamy (2012), 7143 Ω.cm (Kalkman et al., 2014a), 6250 Ω.cm (Frijns et al., 2009a) and a 100:1 bone to scalar fluid conductivity ratio (Mens et al., 1999; Whiten, 2007) which equates to around 7042 Ω.cm in the present study. These values were mainly derived by comparing modelled results to objective data. These values are an order larger than the value used in the other studies mentioned. Such large variability of values complicates the selection of the resistivity value to use in a VC model.

The objective of this communication is to report the effect of bone resistivity variations on neural excitation spread and intra-cochlear potential spread predictions that use VC models as their premise and to propose a range of values that provide realistic predictions when all other tissue resistivities that are used in present VC models of the cochlea are assumed to be sufficiently accurate. The report also deals with various levels of complexity of the implementation of the head volume surrounding the cochlea to assist modellers in making an appropriate choice for the bone resistivity value based on the structure of their model.

Forward-masked spatial tuning curve (fmSTC) widths and slopes and electric field profile length constants are compared to measured data found in literature to assess the validity of a predicted result for a bone resistivity value.

4.2 METHODS

Volume conduction models of the implanted cochlea in different configurations were used to assess the effect that the value of bone resistivity has on the spread of neural excitation and intra-cochlear electric fields. In all model configurations the bone resistivity value was varied while neural and electric spread was calculated using monopolar stimulation. Monopolar stimulation was used as current has to pass through large areas of bone between the intra-cochlear electrodes and return electrode. Changes in bone-resistivity should thus influence spread more that using a stimulation mode that only employs intra-cochlear electrodes. Spread was measured in the form of width (mm) and slope (dB/mm) of the neural excitation curves and in the form of length constant of the intra-cochlear electric field profiles. These neural and electric spread predictions were then compared to data from literature to determine appropriate bone resistivity values to be used in cochlear models.

The model predicted neural excitation spread from the present study was compared to data in a study from Nelson, Donaldson and Kreft (2008) in the form of fmSTCs. The average monopolar spread for six implanted Clarion (two HiFocus, four HiFocus with positioner) users was estimated. The fmSTC slope of 1.2 mm/dB which they obtained was used as the benchmark for the predictions in the present study. Their study also measured the average fmSTC width at 1 dB above threshold as 4.6 mm, which was used as the benchmark to which the results in the present study were compared to. Care was taken to mimic the methodology of the Nelson et al. experiments to ensure that the data is comparable.

The electric field data from literature came from a study by Tang, Benítez and Zeng (2011) where electrical field imaging (EFI) data of five implanted cochleae are presented. An EFI

curve represents the voltages measured on all the electrodes of an implanted array when a stimulus is presented through a single electrode. In that study EFI profiles were obtained for a basal, middle and apical stimulus electrode in each of five implanted ears. The averaged EFI profiles of these electrodes in all the ears were compared to the modelled data in the present study. All the ears in the Tang et al. (2011) study were implanted with Clarion HiFocus electrode arrays; subsequently the volume conduction models in the present study were also implemented with Clarion HiFocus electrode arrays.

4.2.1 Volume conduction models

Five finite element (FE) volume conduction (VC) models based on the morphologies of five individual implanted cochleae of live human implantees were used. All ears of the users have been implanted with the Nucleus 24 cochlear prosthesis from Cochlear Limited: four with contour electrode arrays and one with a straight electrode array. However, although the Nucleus device allows the recording of electrode potentials, a floating reference ground causes difficulties in obtaining absolute potential levels and thus electric field profiles cannot be measured for Nucleus users. To compare modelled results to the Nelson et al. data in the neural domain (fmSTCs) and to the Tang et al. (2011) data in the electrical domain (electric field profiles), it was thus necessary to convert the Nucleus electrode arrays in the VC models to Clarion HiFocus electrode arrays. This was done by changing the size and spacing of the modelled electrode contacts to those of a HiFocus array while maintaining the intra scalar location of the electrode carrier of each user. This conversion resulted in the electrode contacts having a slightly curved surface as opposed to a flat surface of a HiFocus array. The effect of this slight curvature on results was assumed to be minimal as the surface area of the HiFocus electrodes was maintained.

The geometry of each model was constructed from computed tomography (CT) data of each implanted ear using similar methodology as described for the construction of our guinea pig model (Malherbe et al., 2013). In that study, the bony geometry of the cochlea and location of the electrode contacts were estimated from µ-CT data and augmented with

a model containing the finer inner structures of the cochlea. The same approach was followed in the present models, with the exception being that the bony cochlear geometry was estimated from relatively low resolution standard clinical CT images of which the image sharpness was increased using bicubic interpolation and application of a colour lookup table. Figure 4.1 shows a mid-modiolar section through a single duct of a user's cochlear model with regions that have different material properties (electrical resistivity) indicated. The material that envelops the structures is bone and is indicated in grey. The spiral lamina is also represented by the same material property as that of the enveloping bone volume (see Figure 4.1). This assumption is based on the observation that the spiral lamina is an extension of the bone that envelops the cochlear canals. The material properties are the same as those used in the guinea pig model with the exception of the bone value that is being varied.

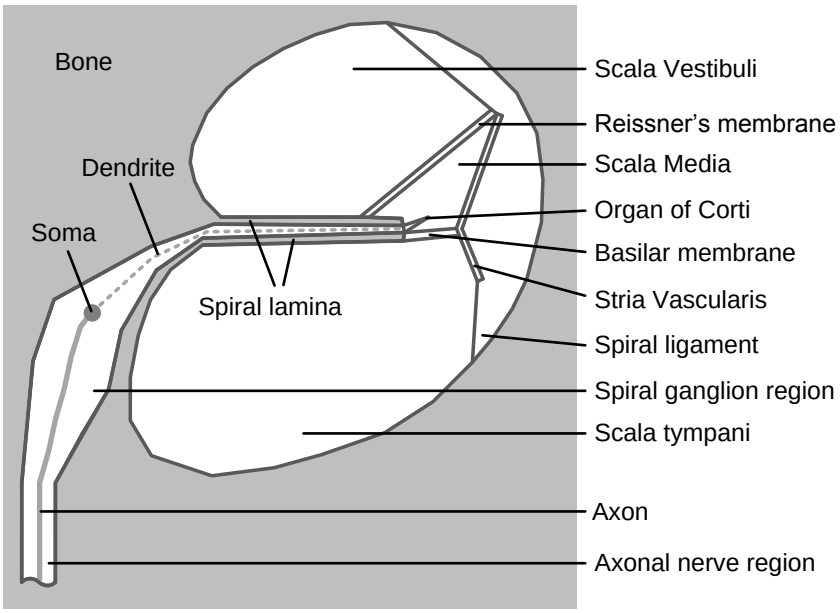

Figure 4.1. Mid-modiolar section through a single duct of the cochlear part of the VC model indicating modelled structures that were assigned different material properties. Modelled structures are entirely encased in bone (grey area). The spiral lamina is also modelled with the same material as the surrounding bone. The position of the neuron is indicated with the soma in the spiral ganglion region

Three levels of complexity of the description of the head volume enveloping the cochlea were implemented in conjunction with the user-specific cochlear models described in the previous paragraph. This is important since the structure and materials comprising the head volume affect the current paths, especially in the case of monopolar stimulation. The first type of head model, called the infinite bone model (Figure 4.2a), contained a rudimentary description of the head consisting of an infinitely large homogeneous bone volume with the user-specific cochlear model at the origin. A sphere with finite dimensions was modelled with its boundaries moved to a virtual distance of infinity using the FEM software package Comsol Multiphysics 4.4. For monopolar stimulation, the return electrode was defined as the entire outer surface of the infinite sphere. This configuration represents the simplest implementation of the head volume and is typically used by modellers for its ease of implementation.

The second type of head model, called the elliptical return electrode model (Figure 4.2b), aimed to implement an accurate return electrode. This was done by embedding the cochlear structures into an elliptical homogeneous purely resistive bone volume approximately the shape and size of a full human head (measured crown to chin, ear to ear and nose to back of head from CT data). The position of the return electrode (casing) was estimated from the CT data and placed in the model in the position in which it occurs relative to the cochlea in each user close to the exterior boundary of the bone volume. The accurate return electrode implementation allows for a more realistic representation of the current paths from the cochlea than the infinite bone model whilst being relatively simple to implement.

The third type of head model, which is the most complex implementation of the tissues enveloping the cochlea, was represented by a detailed skull containing a brain volume and scalp. The skull was constructed from CT scan data of a human head with the return electrode placed in a location specific to each user. This type of model, called the skull model (Figure 4.2c), did not reflect any cancellous bone volumes that might be present in the temporal bone in the vicinity of the cochlea. The brain volume was assigned a

resistivity equal to the average of grey and white matter (500 Ω.cm) (Haueisen et al., 1997) and the scalp a resistivity of 300 Ω.cm (Rush and Driscoll, 1968). The outer surfaces of the skull model and the elliptical return electrode model were set up as insulators to resemble the models being in a highly non-conductive medium such as air.

In total 15 models were generated, i.e. the five user-specific cochlear models were embedded into the infinite bone, elliptical return electrode and skull models. In each model the resistivity of the bone volumes was adjusted from 641 Ω.cm (the value that is traditionally used in VC models) to 26 546 Ω.cm (which approximates the value reported by Akhtari in 2002 for compact live skull bone) at intervals as reported in Table 4.1.

A value of 2000 Ω.cm was included to allow for continuity across the resistivity range. The VC model was solved for a direct current injected through an electrode to produce a potential distribution throughout the 3D model. This was done for each electrode with each bone resistivity value for each user-specific cochlear model in each of the three head models. Electrode and neural node voltages were then extracted from these potentials and processed further to obtain fmSTCs and electric field profiles.

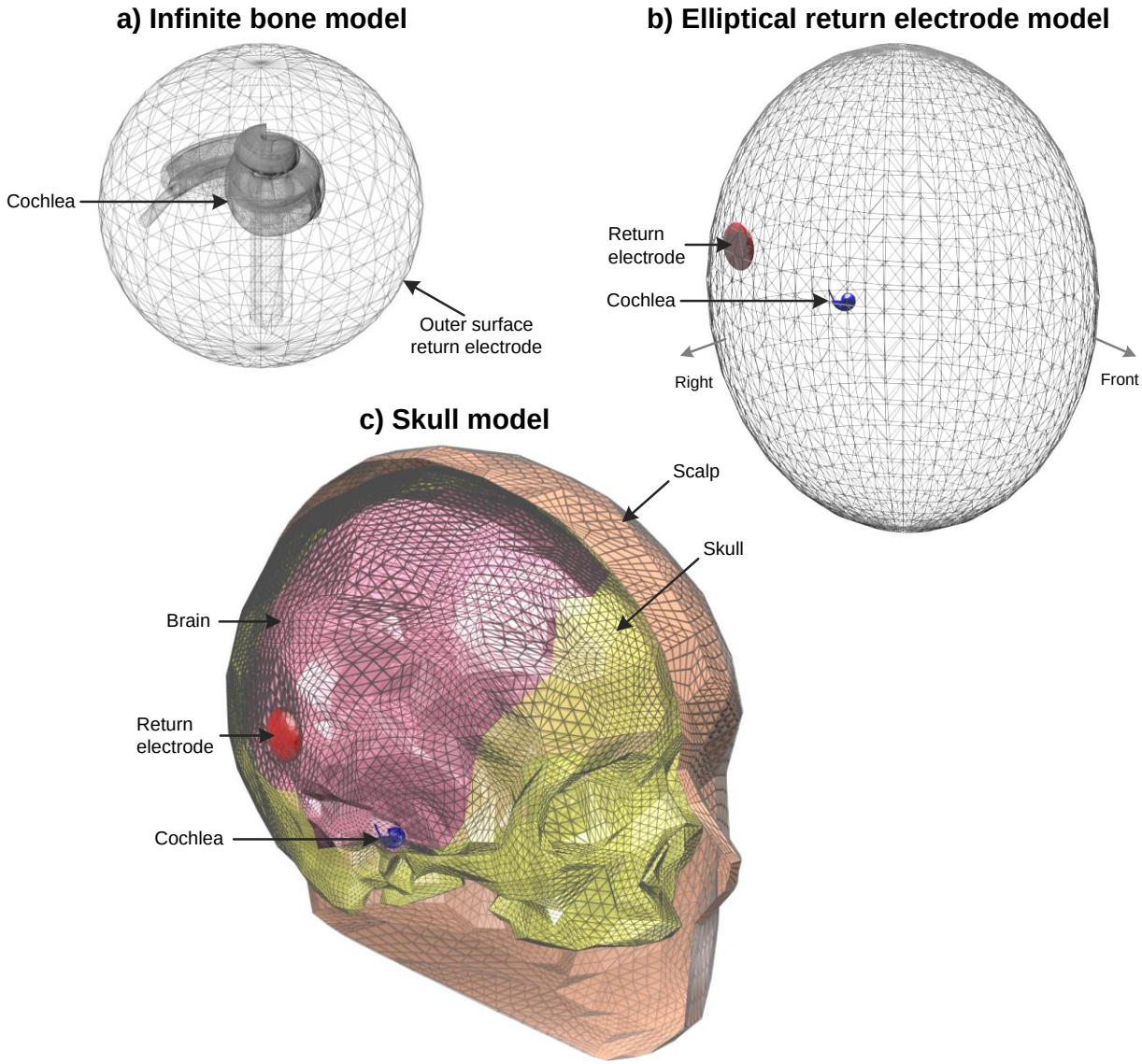

Figure 4.2. Three levels of complexity of the description of the head volume enveloping the cochlea were implemented to investigate the effect of model structure on the bone resistivity. a) Infinite bone model: The cochlea is modelled in an infinitely large bone sphere (see text) with the entire outer surface as the return electrode. b) Elliptical return electrode model: An accurate return electrode position relative to the cochlea is implemented and modelled inside a bone ellipse roughly the size of a human head. c) Skull model: A detailed skull containing a brain volume and scalp with accurate return electrode position relative to the cochlea. The image shows the different layers of the model (sections of the scalp and skull removed to show the brain volume) with the return electrode located on the external surface of the skull

Table 4.1. Bone resistivity values used in the simulations. The values represent human skull resistivities that were reported in literature (citations provided)

Bone resistivity (Ω.cm)	Reference	Skull sample details
641	1987 by Spelman and Clopton (cited in Finley et al. (1990))	
2 000	Chosen for continuity	
3 125	Hoekema, Wieneke, Leijten, Van Veelen, Van Rijen, Huiskamp, Ansems and Van Huffelen (2003)	Live skull (reported values) 1 248 - 3 125 Ω.cm)
4 673	Akhtari et al. (2002)	Spongy part of live skull
5 782	Tang, You, Cheng, Gao, Fu, Yang and Dong (2008)	Dentate suture of live skull
6 667	Oostendorp, Delbeke and Stegeman (2000)	Skull few days after excision
7 943	Tang et al. (2008)	Standard tri-layer
16 207	Akhtari et al. (2002)	Top compact bone of skull
26 546	Akhtari et al. (2002)	Low compact bone of skull

4.2.2 Neuron models

Approximately 160 neurons (depending on the basilar length of the specific cochlea) were placed in each cochlear model from the base to the apex at 5 degree intervals around the modiolus (Figure 4.3a). Each neuron represents a cluster of neurons of the 30 000 neurons in the human cochlea. Here the assumption is made that the threshold of a single neuron represents the threshold of all the neurons in the cluster. The node corresponding to the soma of each neuron was placed in the spiral ganglion region of the cochlea (Figure 4.1). Non-degenerate and degenerate neurons were modelled to represent the extreme cases of a healthy implanted cochlea with no neural degeneration as well as a cochlea that is assumed to have a large degree of neural degeneration. Degenerate neurons were modelled by excluding the dendritic part of the neuron and including only the somatic and axonal regions (Figure 4.2 and Figure 4.3a) (Briaire and Frijns, 2006). The potentials at these nodes were extracted from each voltage distribution profile.

To translate the potential distributions to neural excitation profiles, the resistivity matrix that describes the relationship between the injected current at the chosen electrode and the potential values at the nodes of Ranvier of the neurons was obtained. The location of the neurons along the length of the organ of Corti is represented on the x-axis of the resistivity map in Figure 4.3b and the location of the nodes of Ranvier along the nerve fibres is represented on the y-axis. The transfer resistances were obtained by dividing the potential distribution values produced by the FE solution at the neural nodes by the injected stimulating current. These transfer resistances were then used to calculate the voltage at every node given an input current and used as inputs to a neuron model.

The responses of two physiologically based, single-fibre neuron models that are commonly employed to predict neural excitation in models of cochlear implants were compared: the Hodgkin-Huxley-based compartmental model of Rattay (Rattay et al., 2001b) and the generalised Schwartz-Eikhof-Frijns (GSEF) model (Frijns et al., 1995). The positions of the nodes of Ranvier differ slightly according to the internodal distances associated with each model. A biphasic cathodic-first monopolar stimulus with phase duration of 77 μs and an interphase gap of 0 μs was used to excite the neuron model (as used in Nelson et al.). A search algorithm was employed to find the lowest current level (accurate within 1 μA) for which a neuron generates an action potential (the threshold). The thresholds of all the modelled neurons were calculated and this yielded a threshold profile.

Threshold profiles were computed for all combinations of neuron models, state of degeneration, electrode contacts, user cochlear models, head configurations and bone resistivity values. For the results reported in this study around 1 000 000 individual neuron thresholds were calculated.

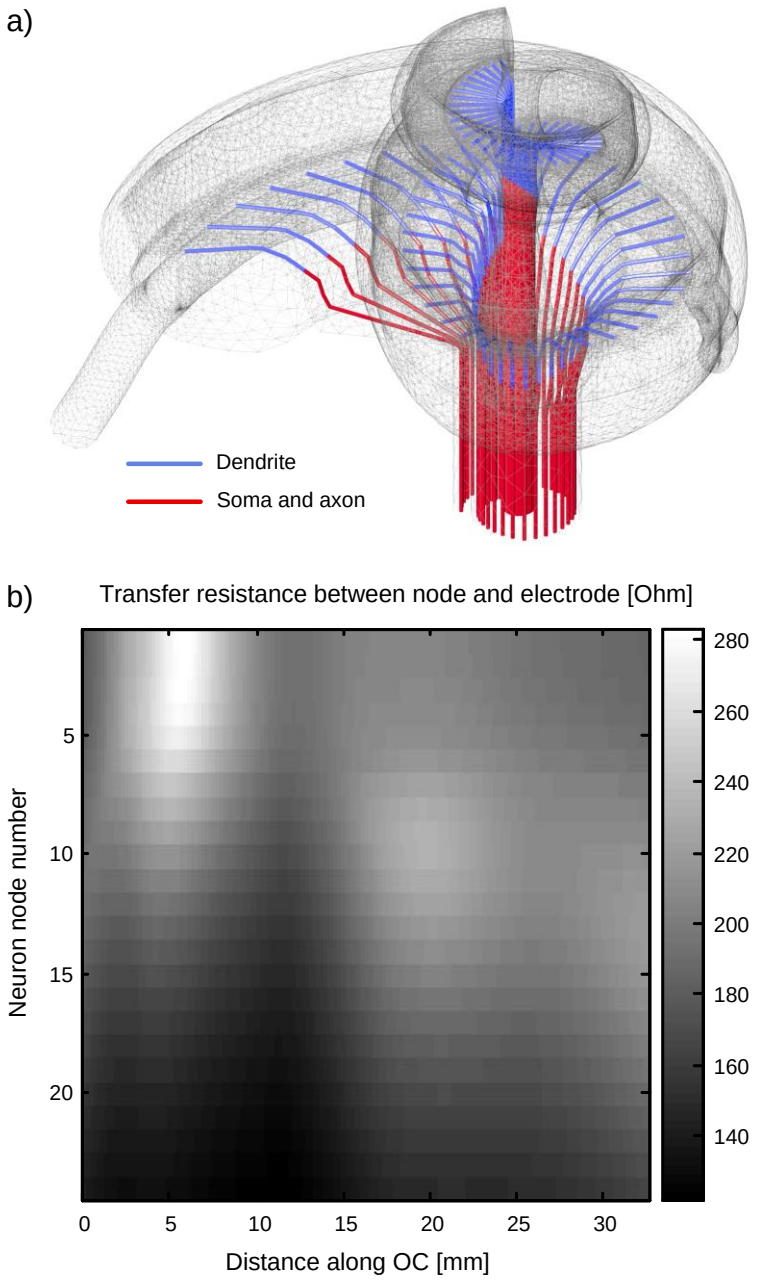

Figure 4.3. The transfer resistance between each stimulating electrode and neuron node is determined and used to calculate the input node potentials to the neural models. a) The positions of the neuron trajectories are shown here for the model of user S13R. Neurons were placed 5 degrees apart around the modiolus. Nodes were placed on these trajectories according to the nodal spacing of the neuron model used. The dendritic parts of the neurons were omitted when modelling degenerate neurons. b) The calculated transfer resistances between electrode 16 and each of the neural nodes in Ohm at a bone resistivity of 641 Ω.cm

4.2.3 Bone resistivity derived from fmSTC

Predictions of excitation spread in the present study estimates neural excitation spread directly from modelled cochlear neurons and does not consider central processing. In order to validate a model of this nature, neural excitation spread data measured at the peripheral auditory neuron level is required. This data, however, is not available and estimates from forward masking presently remains one of the only non-invasive indications of excitation spread in the live human ear.

Nelson et al. used a forward masking experiment to estimate neural excitation spread. Their forward masking paradigm was implemented on the modelled neural threshold profiles using a simplified masking model where the following assumptions were made.

1. A probe pulse is "heard" or unmasked when enough neurons are stimulated to produce a psychoacoustic threshold. The stimulus level at which this occurs is referred to as the probe threshold and was defined as the level at which a neuron population over a width of 1 mm along the length of the basilar membrane is stimulated (Snel-Bongers et al., 2013). For the probe to be heard above the masker, a section of at least 1 mm of neural excitation needs to extend beyond the masker's neural response.
2. Conversely, the probe pulse is masked when the non-overlapped portion of the probe response is less than 1 mm wide.

The same parameters as those used by Nelson et al. were used to facilitate comparison of predicted results with the measured data. The probe level was chosen as 30% of the dynamic range above threshold where the maximum comfort level was calculated as the current at which a region of 4 mm along the basilar membrane is stimulated (Snel-Bongers et al., 2013). A single probe electrode was used, this electrode was chosen as an electrode situated around the first half turn of every cochlea. All the electrodes were used as maskers and the level at which the probe becomes masked was determined for each masker resulting in an fmSTC from which the slope and width were measured.

The slope of each fmSTC curve was calculated by first converting the fmSTC to dB and then fitting two straight lines to the steepest parts of the fmSTC directly adjacent to the position of the minimum masking level, as was done by Nelson et al. Effectively this resulted in two exponential curves being fitted to the fmSTC curves measured in mA (Figure 4.4). The average slope of the two lines (in dB/mm) was used as the slope of the modelled fmSTC. The fmSTC width was calculated as the distance (in millimetres) between the two fitted slopes at a level of 1 dB above the minimum masker level (Figure 4.4). The widths and slopes of all the computed configurations were averaged for each bone resistivity value in each of the model configurations. The averages of the different configurations were then calculated and are summarised and compared against the Nelson et al. data (slope: 1.2 dB/mm, 1 dB width: 4.6 mm) in Figure 4.6 and Table 4.2 (discussed in the results section).

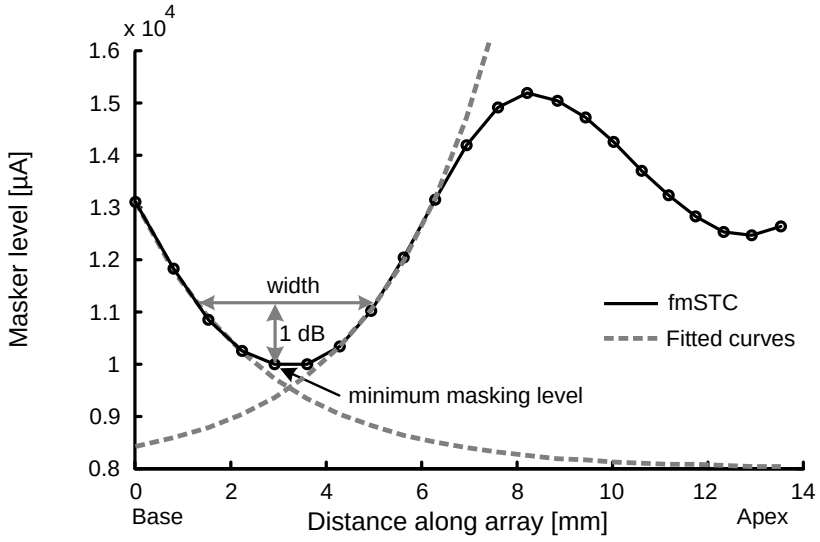

Figure 4.4. Following the methodology of Nelson et al. (2008) the slope of a fmSTC was determined by fitting two exponential curves (dashed lines) to the fmSTC adjacent to the minimum masking level. The mean of the two slopes (in dB/mm) was used as the slope of the profile. The 1 dB width was determined as the length along the electrode array between the fitted slopes at a level of 1 dB above the minimum masking level

4.2.4 Modelling electric field profiles

In Tang et al. (2011), the EFI profiles (averaged over five ears) of three stimulating electrodes (numbers 1, 9 and 15) are presented. Electrodes in the same angular positions as these electrodes were chosen for stimulation in the present models to make data comparable. Electric field profiles were generated using the five user models in each of the three head configurations using each of the specified bone resistivity values. The average electric field profile of the five user models in each configuration was used to compare to the averaged EFI profiles from literature. As the models in the present study only represent the resistive properties of the cochlear tissues and not that of the electrode tissue interface, predictions were only compared to the measurements made on the non-stimulating electrodes where there is negligible current through the electrode-tissue interface.

The electric field spread of each of these profiles was characterized in terms of its length constant λ. This was done by fitting the following exponential function (4.1) to each profile:

$$V_{stim\_elec}(x) = Ae^{-\frac{x}{\lambda}} + C \tag{4.1}$$

where A represents the amplitude, x the distance from the stimulating electrode, λ the length constant and C the DC offset of the profile of a single stimulating electrode (V_{stim_elec}). The function was only fit to the first six electrodes adjacent to the stimulating electrode as cross-turn stimulation effects distort the exponential profile further along the electrode array especially at low bone resistivity values. An electrode spacing of 1.1 mm (Clarion HiFocus) was used when calculating the length constants. Figure 4.5 shows an example of the average electric field profile of a basal stimulus electrode of all the user models implemented in the skull model. The fitted exponential curve is indicated with a dashed line.

Only the length constant was used as the basis of comparison and not the absolute voltages (as was done by Kalkman et al. (2014a)) or the 1 dB width as was used for the fmSTC

data. The reason for this is that the three head configurations have different ground implementations (the infinite ground model resembles a true monopole and the other models dipoles). As all modelled potentials are calculated relative to ground, the data from each modelled head configuration will have a different DC offset. This in turn makes values calculated in dB incomparable. This issue is not present in the predicted neural results as the neural models use the relative potential differences between neural nodes as inputs. Different DC offsets between models do thus not affect neural model outputs.

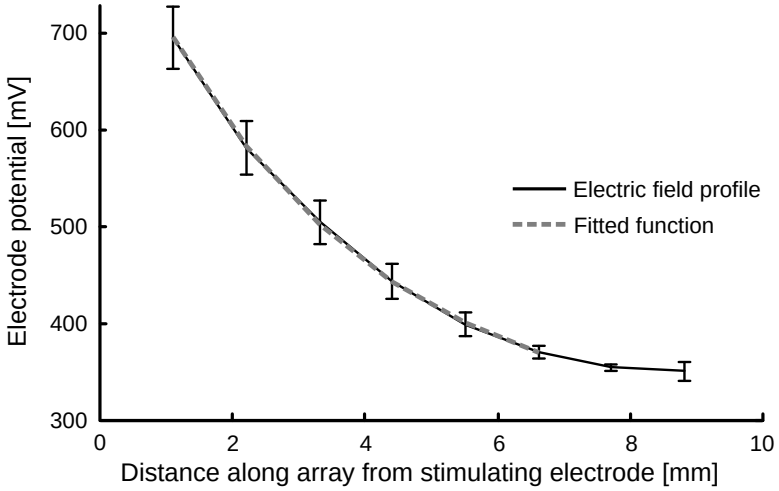

Figure 4.5. The length constant was determined by fitting the exponential function $V_{stim\_elec}(x) = A.\exp(-\lambda/x) + C$ to an electric field profile. Here an example is shown where the function was fit to the average electric field profile produced by stimulating the most basal electrode in all the user models. The skull head model was implemented with a bone value of 6 667 Ω.cm. The function was fit to the six electrodes adjacent to the stimulating electrode to exclude cross-turn stimulation effects that occur far from the stimulating electrode

The average length constant of the EFI profiles of the three stimulating electrodes presented in Tang et al. (2011) was calculated as 3.15 mm. This was used as the benchmark against which the length constants of the modelled electric field profiles were compared. The predicted length constants of the three modelled head configurations are displayed as a function of bone resistivity in Figure 4.8 and discussed in the results section.

4.3 RESULTS

4.3.1 Bone resistivity derived from fmSTCs

The 1 dB fmSTC width increases as the bone resistivity increases (Figure 4.6). This indicates that neural excitation becomes less focussed as bone resistivity increases. The results indicate that the 1 dB width varies between 0.7 and 12.6 mm for the infinite bone model (a), between 0.6 and 15.0 mm for the elliptical return electrode model (b) and between 0.6 and 15.2 mm for the skull model (c) as the bone resistivity increases. Nelson et al. reported an average measured 1 dB width value of 4.6 mm for monopolar stimulation. The bone resistivity values that produce a 1 dB fmSTC width of 4.6 mm for the various model configurations are summarised in Table 4.2. It shows that, except for the degenerate Rattay neural models in the elliptical return electrode model, the resistivity values required by the GSEF and Rattay models are very similar for the three levels of complexity of the head model, i.e. a ratio of 91% on average between the resistivity values derived from the Rattay model to those derived for the GSEF model. The exception is for the degenerate fibres in the elliptical return electrode model where the Rattay model requires only about 31% of the resistivity value for the GSEF model to produce predictions that match the Nelson et al. data.

The average predicted fmSTC slopes also decrease as the bone resistivity increases (Figure 4.6). The bone resistivity values derived from the Rattay model versus the values derived from the GSEF model once again agreed to within 83% of one another for all the models but the degenerate nerve fibre models in the elliptical return electrode model. For this case the Rattay model once again only required 39% of the resistivity value required by the GSEF model to predict slopes that match the 1.2 dB/mm slope of the measured Nelson et al. data.

If the two outlier values in the head model are ignored, the average bone resistivity value predicted over all the models is 10 176 Ω.cm with a standard deviation of 1 635 Ω.cm.

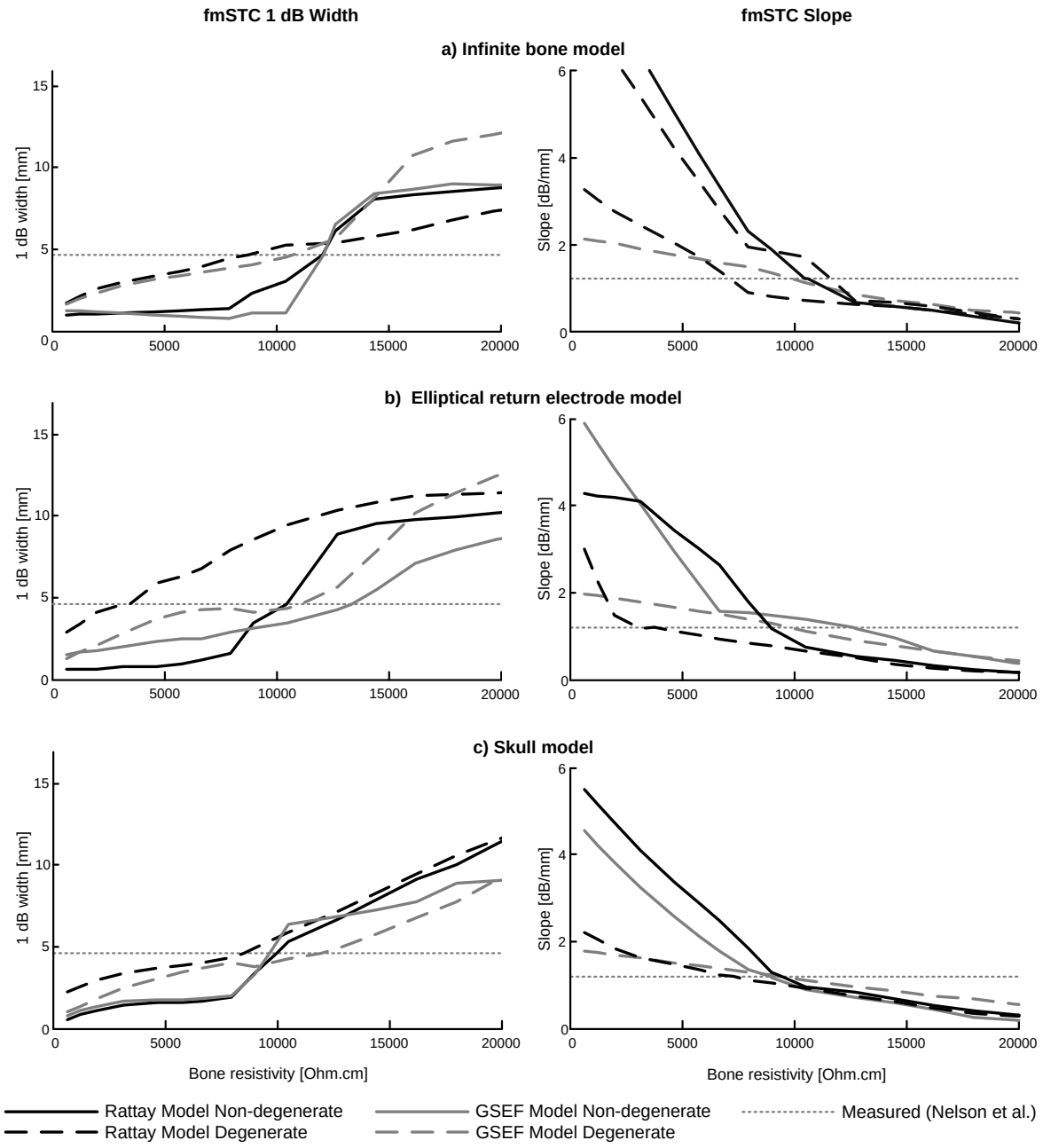

Figure 4.6. The average predicted 1 dB widths (mm) and slopes (dB/mm) of the forward masked spatial tuning curves (fmSTCs) of the three head model configurations namely the spherical model (a), elliptical model (b) and skull model (c). It is evident in all configurations that the neural excitation spread becomes wider when the bone resistivity is increased

Table 4.2. Bone resistivity values (Ω.cm) at which 1 dB widths and slopes from predicted fmSTCs from the three head models match measured data from Nelson et al. Two neuron models (Rattay and GSEF) were implemented with neurons in non-degenerated and degenerated states.). The average and standard deviation of the five user cochlear models are shown in each configuration

		Infinite bone		**Elliptical return electrode**		**Skull**	
		Rattay	**GSEF**	**Rattay**	**GSEF**	**Rattay**	**GSEF**
Non-degenerate	**Width**	12 016 ±1 043	12 222 ±1 697	10 475 ±1 591	13 342 ±2 508	9 988 ±1 554	9 649 ±4 504
	Slope	10 628 ±1 527	11 669 ± 1 069	8 940 ±1 095	12 608 ±4 290	9 425 ±1 181	8 932 ±1 382
Degenerate	**Width**	8 830 ±2 506	10 808 ±1 982	3 450 ±2 411	11 067 ±1 882	8 485 ±2 032	11 254 ±2 270
	Slope	7 160 ±1 325	9 927 ±2 637	3 772 ±1 717	9 741 ±2 611	7 273 ±2 472	9 292 ±2 560
Average		**10 426 ±1 730**		**9 174 ±3 718**		**9 287 ±1 155**	

4.3.2 Bone resistivity derived from electrode field profiles

Figure 4.7 shows the cochlear part of the elliptical return electrode head model of a single user when stimulating an electrode when three different bone resistivities are used. The green surfaces are equipotential surfaces all at 0.5 dB (chosen for visual clarity) below the electrode potential and visually indicate that there is a considerable change in potential field when the bone resistivity is increased.

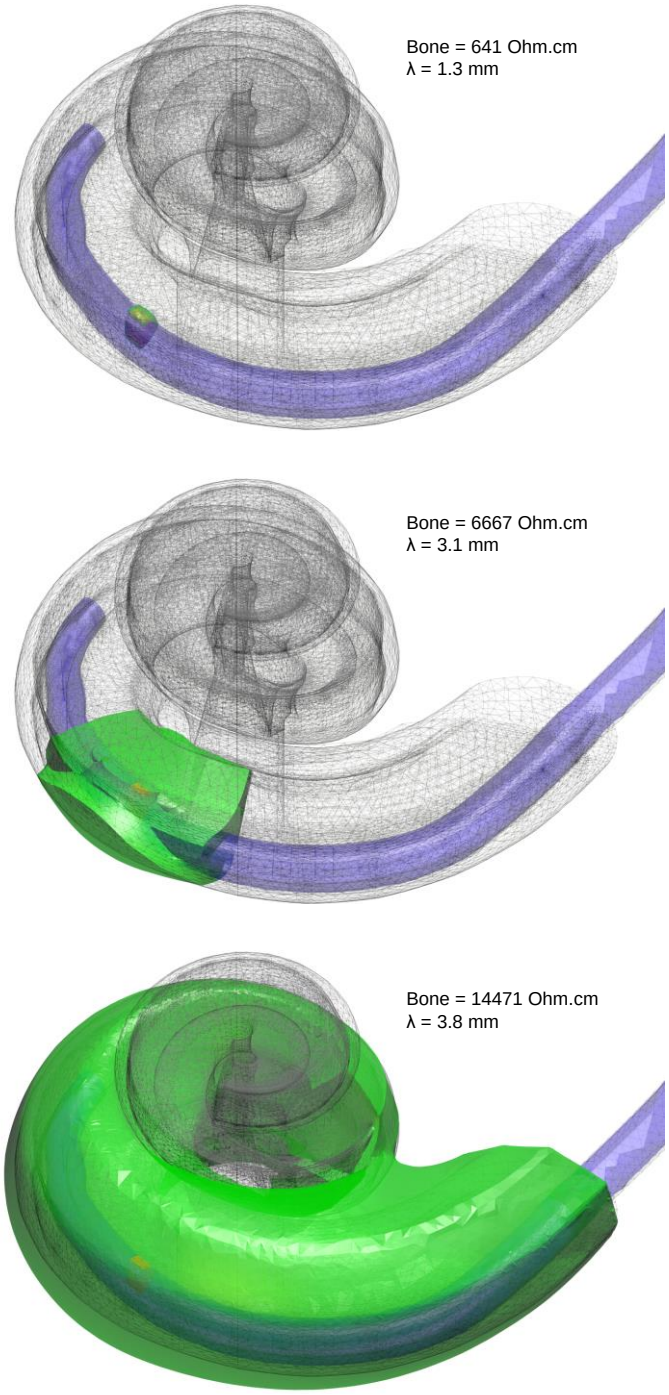

Figure 4.7. The cochlear part of an elliptical head model when stimulating a single electrode using three different bone resistivities. The green surfaces are equipotential surfaces at 0.5 dB below the electrode potential and indicate the widening potential field when the bone resistivity is increased. The length constant λ, approximated using the assumption of exponential decay of the potential field from the electrode ($y = Ae^{-x/\lambda} + C$), is also presented for comparison

The measured data presented by Tang et al. (2011) exhibits an average length constant of 3.15 mm (dashed line in Figure 4.8) when fitted with the exponential function (1). The bone resistivity values (interpolated from predicted data points shown in Figure 4.8 and summarized in Table 4.3) that produce these values for the various head configurations are 6 217 Ω.cm for the infinite bone model, 6 694 Ω.cm for the elliptical return electrode model and 6 567 Ω.cm for the skull model. The average of the three head configurations being 6493 Ω.cm with a standard deviation of 2161 Ω.cm when including the individual values of each of the 15 models (five user models in three head configurations) in the calculations.

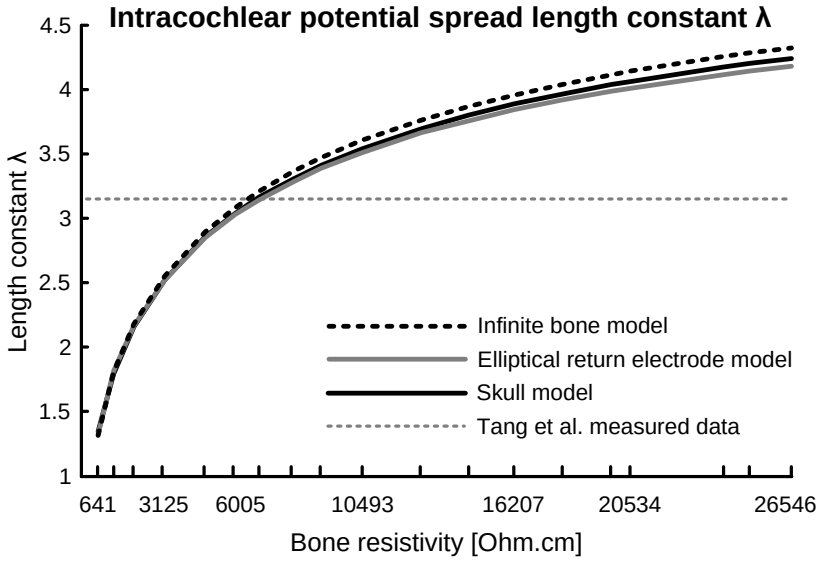

Figure 4.8. The average predicted intra-cochlear potential length constants, λ, of each modelled head configuration. Predicted data is compared to the length constant (3.15 mm) calculated from EFI measurements by Tang et al. (2011). The bone resistivity value required to match data from literature is around 6500 Ohm.cm for all three head configurations indicating that potential decay inside the scala is largely unaffected by current paths to the return electrode

Table 4.3. Bone resistivity values (Ω.cm) at which length constants (λ) from predicted electric field profiles match the length constants of EFI measurements obtained by Tang et al. (2011). The average and standard deviation of the five user cochlear models in each head configuration are shown

Head configuration	**Bone resistivity (Ω.cm)**
Infinite bone	6 217 ±2 139
Elliptical return electrode	6 694 ±2 462
Skull	6 567 ±2 507
Average	**6 493 ±2 161**

4.4 DISCUSSION

The present study set out to investigate if bone resistivity and implementation of the head structures surrounding the cochlea have a significant effect on neural excitation and intra-cochlear potential spread and to find a range of bone resistivity values that will allow a VC model to produce neural excitation spread predictions comparable to data measured in human implantees.

This study complements existing cochlear VC models by including various descriptions of the head volume surrounding the cochlea. It was demonstrated that the type of head model and implementation of the return electrode affects the bone resistivity value that produces predictions that match measured data. This is an important finding for modellers who wish to implement a specific level of detail into their models.

Because of the variation in human cochlear geometry (Erixon et al., 2009), cochlear models based on the geometry of five user-specific cochleae were constructed. This was done to take the effect of individual geometry variations and electrode insertions into account when predicting the average spread. The predictions from the models were averaged among the five user models to enable comparison to data from Nelson et al. and

Tang et al. that were reported as the averages of multiple users. The predicted results were compared to measured fmSTC and EFI data to estimate bone resistivity values that may be used in cochlear models. Nelson et al. used a forward masking experiment to estimate neural excitation spread. These results may be compared to the predictions of the present model, but with specific reservations. Estimation of spread of excitation from forward masking data relies on feedback given by the implanted user in a behavioural experiment. The results are thus not only a function of the neural excitation spread at the level of the cochlear neurons, but are also influenced by more central processing.

The five cochlear models were then combined with three different VC models of varying complexity of the head structure surrounding the cochlea that includes the implementation of the return electrode. In each of these 15 VC models the resistivity of the bone structures was varied and the potential spread induced by each electrode in the electrode array for each of these bone values was obtained. The voltage potentials on the electrode contacts were subsequently used to calculate electric field profiles. The voltage potentials at the locations of the neuron nodes were also applied as inputs to two physiologically based neuron models. Each of these models was used in two states of neural degeneration (degenerate and non-degenerate) to obtain threshold profiles for all the VC model configurations. Finally, a simple model was implemented to obtain fmSTCs from these threshold profiles.

The results of the present study indicate that the neural excitation and electric field spreads predicted by the models are significantly affected by the resistivity of the surrounding bone tissue. Wider spread (neural excitation and electric field profiles) is evident for all model configurations in both an increase in profile widths and length constants and a decrease in profile slopes as the bone resistivity increases (Figure 4.6 and Figure 4.8). The reason for this is that a higher resistivity of the bone structures shields a larger component of the stimulating current into the lower resistivity cochlear structures causing wider spread. Conversely, lower bone resistivity allows more current to leak from the cochlear structures

thereby causing narrower spread of currents and thus narrower electric field and neural excitation profiles.

The bone resistivity values that predict measurements from literature differ among the three types of head models. This alludes to the fact that the potential distributions and current paths to the return electrode are dependent on the structures external to the cochlea as well as the shape and position of the return electrode. In the skull model the bone resistivity parameter represents the resistivity value of the skull, but in the infinite bone and elliptical return electrode models, the bone resistivity parameter represents a number of other structures as well. The predicted bone resistivity values for the infinite bone and elliptical return electrode models are thus single values that represent the resistivity of the compound head structure best. The variation in bone resistivity values is more pronounced in the predicted neural excitation spread than in the electric field spread. This may be an indication that the neural node potentials (which are mainly in the modiolus) are more affected by the current paths to the return electrode than the electrode potentials in the scala. It is worth noting when comparing results, that the widths and slopes of the predicted fmSTCs (Figure 4.6) and length constants from electric field profiles (Figure 4.8) are not directly comparable with each other since they represent different measures. The bone resistivity values at which these model predictions match the data from literature are, however, directly comparable.

The predicted bone resistivity values when implementing different neuron models (Rattay and GSEF) and different levels of neural degeneration have an average value of around 10 000 Ω.cm, with the exception of the degenerate Rattay model in the elliptical return electrode model. The mechanism underlying this discrepancy is speculative, but is probably related to the current path between the stimulating and return electrodes. Since the elliptical return electrode model's head structure comprises a homogeneous bone volume, the current follows a fairly direct path between the stimulating and return electrodes causing high current densities in the modiolus where the sensitive, truncated neural terminals are located. Lower neural thresholds in turn cause wider spread of

excitation thereby requiring lower bone resistivity values to restrict the spread of excitation to measured values. What is evident is that truncation of the Rattay model in this head model markedly increased its sensitivity to excitation. This observation suggests that care needs to be taken when selecting a neuron model and particularly when changing the structure of a neural model, e.g. representing degeneration via truncation of the model.

Another observation is that as the bone resistivity increases, the shape of the neural excitation profile represents less of a classical threshold profile shape, which has a parabolic shape with a local minimum near the stimulating electrode, and approaches a shallower profile that has many local minima in positions not related to the stimulating electrode position nor any other obvious structures in the cochlea such as non-stimulated electrode contacts. At high resistivity values the threshold profiles from all electrodes approached a common "flat" shape. This is ascribed to the current spread in the cochlear duct being more uniform irrespective of the location of the active electrode as the insulating effects of the surrounding bone increases and forces current more longitudinally along the cochlear duct. Even though fmSTC widths and slopes could be obtained from these threshold profiles, they do not necessarily represent an accurate description of the environment in a real cochlea. Caution thus needs to be exercised when interpreting widths and slopes predicted using high bone resistivity values. It also has implications for diseases where bone density and with that possibly bone resistivity increase, e.g. in cases of osteopetrosis (Milroy and Michaels, 1990). The model predictions suggest that electrode discrimination and thus pitch perception may be decreased in such cases.

The bone resistivities predicted by modelling the electric field profiles are similar (average: 6492 Ω.cm) for all three head configurations (Table 4.3). This indicates that the electric fields near the electrodes in the cochlear duct are not greatly affected by structures external to the cochlea. This is intuitively correct as the perilymph in which the electrode array is located has a low resistivity compared to other cochlear structures. The cochlear duct is thus the default path for the bulk of the current to travel through before entering other cochlear structures where it is dispersed according to these structures of higher resistivity.

It was, however, found that this current path is highly dependent on the shape of the cochlear duct of the individual ear it was based on. This is clear from the high standard deviations (around 2300 Ω.cm) of the predicted bone resistivity values that match measured data for the five user models within each head configuration (Table 4.3). This highlights the importance of incorporating user-specific cochlear geometries into cochlear models when user-specific modelling results are sought.

In light of the variation on predicted electric field profile results, variations in neural excitation results from the different neural models and implementations as well as the fact that bone resistivity varies among individuals (Marshall et al., 1996), the following bone values are proposed for use in modelling studies. It is proposed that a bone resistivity value in the order of 10 000 Ω.cm be used in volume conduction models of the implanted cochlea using monopolar stimulation when neural excitation spreads are predicted in models that incorporate any of the modelled head configurations presented here. This value does not hold where a degenerate version of the Rattay neuron model is used inside the elliptical return electrode model and a value of 3500 Ω.cm is proposed. When predicting electric fields in the scala of the cochlea (such as electric field profiles), a single value of 6500 Ω.cm is proposed for all head configurations as head configuration has a small effect on inter scalar potentials. These values are an order higher than the bone resistivity value of 641 Ω.cm used in some volume conduction studies of the cochlea (Frijns et al., 1995; Finley et al., 1990; Hanekom, 2001b; Malherbe et al., 2013), whereas the values derived from the intra-cochlear spread is comparable to the bone resistivity values used in the studies of Rattay et al. (2001a) (6 400 Ω.cm), Kalkman et al. (2014) (7143 Ω.cm), Frijns et al. (2009) (6250 Ω.cm) and Mens et al. (1999) and Whiten (2007) (7042 Ω.cm from 100:1 bone to scalar fluid conductivity ratio).

4.5 CONCLUSIONS

1. Neural excitation and intra-cochlear electric field spread are dependent on the resistivity value of the bone surrounding the cochlea with wider spread observed with an increase in bone resistivity.
2. Neural excitation spread is highly dependent on the detail of the description of the head volume surrounding the cochlea as different bone resistivities are required in VC models to match measured spread reported in literature. The description of the head model does not considerably affect intra-cochlear electric fields in the highly conductive cochlear duct.
3. A general bone resistivity of 6500 Ω.cm is proposed when predicting intra-cochlear electric field spread. When predicting neural excitation spread a default bone resistivity value of 10 000 Ω.cm is proposed for all head implementations and neural models.

However, given the sensitivity of the predicted bone resistivity values on the type of neuron model and implementation thereof as well as the geometry of a specific cochlea it is advisable to specifically optimize the bone resistivity for models that implement features that are not described in this article.

CHAPTER 5
MODEL APPLICATION I:
MODELLING MONOPOLAR DECAY

Having a model based on an accurate cochlear geometry with an accurate bone resistivity allows the investigation of other parameters that are of importance to the field of cochlear implant research. This chapter describes how multiple models are used to develop a model that estimates the potential decay in the cochlea, measured at the neuron nodes, if the position of an electrode is known.

5.1 INTRODUCTION

The potential decay rate is often used to describe the magnitude of the electrical potential inside the scala of a cochlea when an electrode is stimulated. Monopolar electrical decay rates of around 3 dB/mm have been measured in physical models containing electrodes in salt solutions (Kral et al., 1998) as well as in animal models (Kral et al., 1998; O'Leary et al., 1985). Interestingly, it was found that neural excitation spread measured in animal models also exhibit a similar monopolar decay rate of around 3 dB/mm (Hartmann and Klinke, 1990; Kral et al., 1998). This led to the establishment of the monopolar electrical stimulus resolution in cochlear implants according to which many implant processor analysis filter slopes are chosen.

This decay rate does, however, characterise the decay of potential in the cochlea with a single value. This value is based on the decay rate at which the current from a current source in an isotropic, infinitely large, medium will decay. In reality, the cochlea with its intricate structure is far from an infinite isotropic medium with the neural elements contained in different cochlear structures than the scala where the electrodes are located. Thus the assumption that the decay rate of an isotropic medium applies to the implanted cochlea may not hold. Also the use of a single value to describe the potential decay in all human cochleae and everywhere in a stimulated cochlea may also not be valid as it was found in Chapter 4 that the potential spread in the cochlea is dependent on cochlear geometry as well as the location of the stimulating electrode.

This section investigates the effect that electrode location has on potential decay as measured from the neural elements. The tips of the neural elements (terminals) were chosen as reference points where the potential spread was measured. A simple model to predict decay rate based on the position of an electrode is also developed and proposed for use instead of the standard 3 dB/mm monopolar decay rate.

5.2 METHODS

5.2.1 Obtaining potentials for different point sources

The five detailed cochlear models developed in Chapter 2 were used in this study. The modelled user electrode arrays were removed and current injection was instead applied as point sources at different positions in the scala tympani (ST) of each model. The resulting potential decay for each source was obtained.

Stimuli were applied as individual point sources spaced on a regular grid in the scala tympani (Figure 5.1). Point sources were used instead of sources resembling the geometry of clinical electrode contacts, which have a larger area, to investigate the effect of a generic current source independent of specific manufacturer dimensions as well as to simplify the modelling approach. The dimensions of the source have the largest effect on predicted current spread very close to the source (near field). The predicted current spread becomes less dependent on source dimensions further from the source. To avoid these near field artefacts, a buffer area (dashed line Figure 5.1) was placed between the source positions and the walls of the ST. This also avoids very small mesh elements being created when a source is very close to a cochlear wall which could potentially give rise to FEM meshing problems. A regular grid containing the point source positions was duplicated along the entire length of the ST at 15 degree increments. Figure 5.2 shows the ST with the source positions indicated in different colours for clarity.

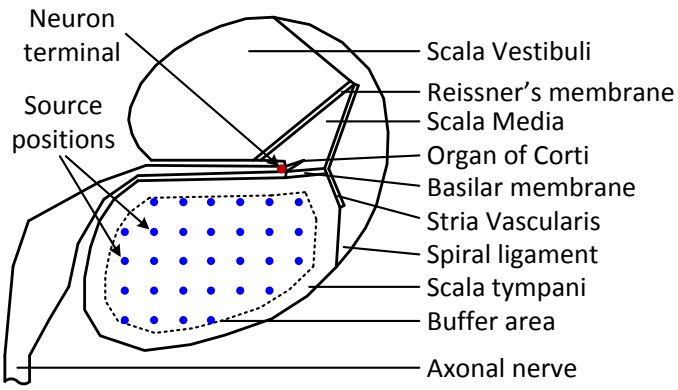

Figure 5.1. 2D mid-modiolar slice through a single duct of the model indicating the positions of the cochlear structures as well as the positions at which stimulus sources were applied. The potential spread was calculated at the positions of the neuron terminals near the organ of Corti

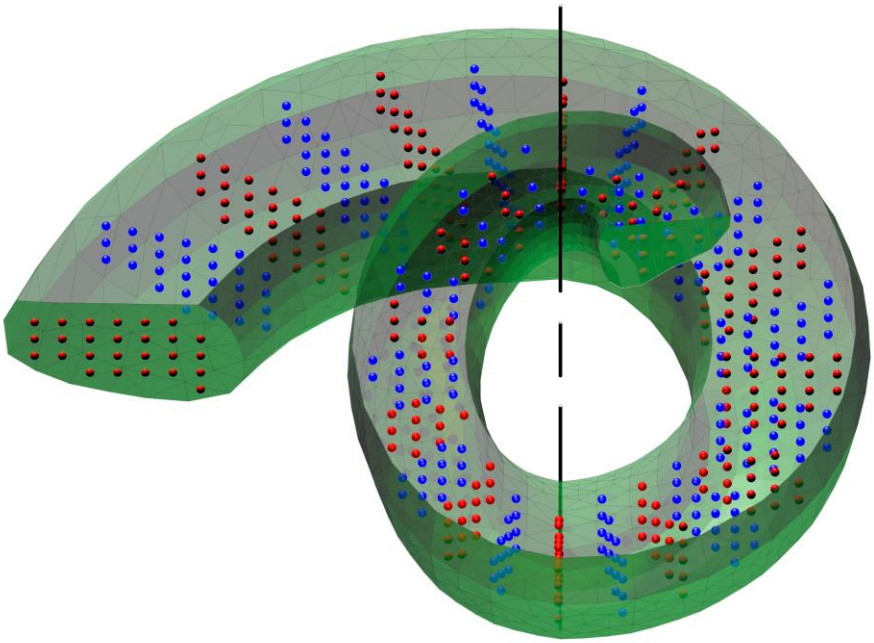

Figure 5.2. Positions of individual sources placed along the length of the scala tympani (green). Source positions are indicated in different colours (red and blue) for clarity

A voltage source was applied to a point located at each source position and the resulting potential distribution on the neural terminals was determined. The following operations were done iteratively to accomplish this:

- a single voltage point source was modelled in Comsol Multiphysics in a source position.
- The model was meshed.
- The model was solved.
- The resulting potential distribution was exported to a file for post-processing.

The process was automated by using the parametric solver in Comsol Multiphysics and repeated for each of the 5 cochlear models. All potentials were measured relative to the voltage at a point at a virtual infinite distance from the cochlea. This was done to eliminate any DC offset in values that may occur if potentials were measured relative to the modelled ground electrode which approximates a dipole. Voltage sources were used instead of current sources (as is used in CI's) as an accurate source voltage was required for subsequent calculations. Stimulating with a current source caused inaccurate source voltages to be measured in the FEM software as the source was modelled as an infinitely small point that approaches a theoretical voltage of infinity.

The resulting potential distribution file of each source position included the potentials obtained at the neural terminals (section 3.14). These nodes are positioned in the neuron region in the spiral lamina just medial to the organ of Corti (Figure 5.1). The neuron terminals were chosen as this point of reference is commonly used by other modellers in modelling potential spread. The potential of the stimulating source was also exported along with the nodal potentials. Only these potentials were extracted and exported to reduce the simulation time as interpolation of potentials in the solved 3D volume is a computationally intensive process.

An example of the node voltages produced by applying potential to a source is shown in Figure 5.3. Only the voltages between the source and half a turn to each side (apical and

basal) from the source were used for estimating the decay rate to avoid cross turn stimulation effects. Practically, an electrode does not stimulate an area larger than half a cochlear turn, thus not including voltages beyond half a turn will not reduce the applicability of the developed model.

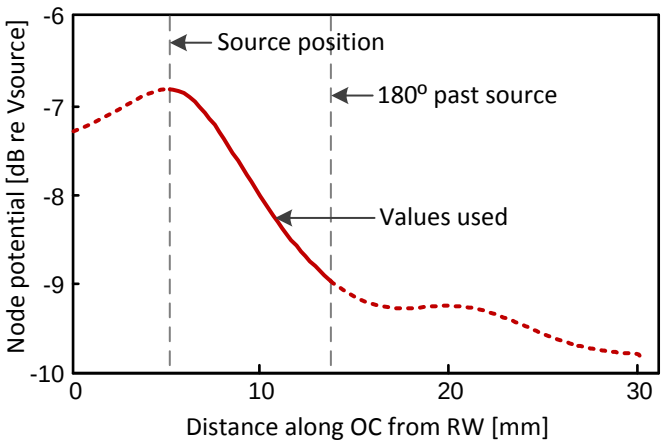

Figure 5.3. Node potentials exported from stimulation from a point source. The values between the source and half a turn to each side from the source were used for estimating the decay rate. Here the values used on the apical side are shown

To determine the decay rate, the distance from the current source (*s*) and each node (*n*) along the OC was determined using the approximation of an unrolled cochlea with the following equation.

$$distance_{s,n} = \sqrt{(source\ dist.from\ OC)^2 + (node\ dist\ along\ OC)^2} \quad (5.1)$$

Here *source dist. from OC* refers to the distance from the source to the nearest neural terminal directly below the OC and *node dist. along OC* refers to the distance between the node in question and the node nearest to the source measured along the trajectory of the OC (Figure 5.4).

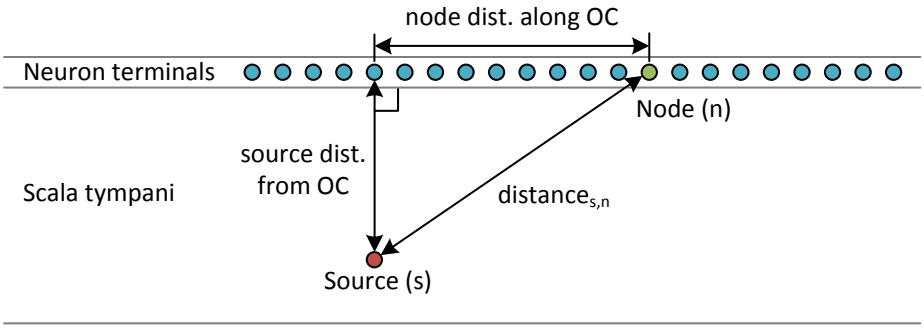

Figure 5.4. Calculation of the distance between a source and a neuron terminal (node)

The decay rate was calculated as the ratio of the difference in dB between the source (v_s) and a node (v_n) potentials to the distance between the source and node ($distance_{s,n}$):

$$DecayRate_{s,n} = \frac{20\log(V_s - V_n)}{distance_{s,n}} \tag{5.2}$$

Figure 5.5 shows the decay rate (in dB/mm) calculated from the node potentials apical to the source shown in Figure 5.3. Interestingly the decay rate is not a constant value across the cochlea, but changes as the distance between the source and measurement point increases. This is counter intuitive as an exponential potential decay (constant decay rate in dB/mm) is observed in the scala where the electrodes are located. Upon further investigation it was found that this change in decay rate was due to a constant offset between the source and the measured voltages of the neural terminals. This constant offset is due to the attenuation caused by the different structures in which the electrode (in the ST) and neuron nodes (spiral ganglion) are located which is separated by a layer of bone. When converted to dB, this offset causes the decay rate to vary with distance from the stimulating electrode.

This leads to the conclusion that potential decay as measured at the location of the neural terminals cannot be described by a single decay rate value (such as 3 dB/mm).

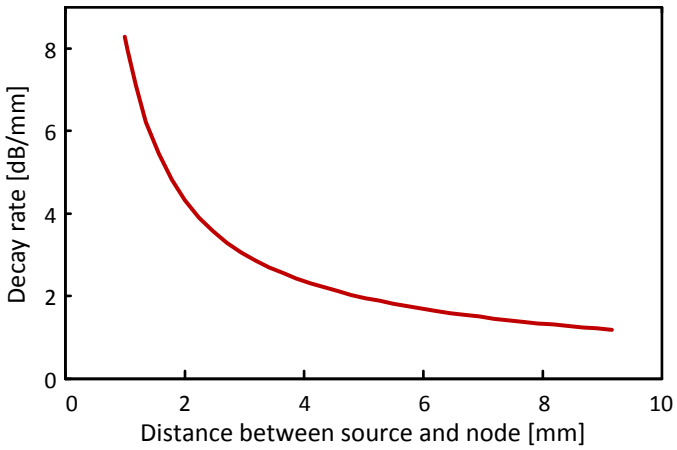

Figure 5.5. The decay rate (dB/mm) calculated for the source in Figure 5.3. Interestingly the decay rate is not a constant value across the cochlea, but changes as the distance between the source and measurement point increases along the OC

The name 'decay rate' implies that there is a constant decay per distance unit in the medium. As this is not the case, describing the potential decay (dB) in the cochlea as a function of distance between source and measurement position (node), instead of a constant rate, is more applicable.

Figure 5.6 shows this potential decay as a function of the distance between the source and the measurement node. This decay is fairly well approximated by fitting a linear function to the values. The offset of this function is presumed to be due to the attenuation between the source and the nodes and the slope of the line is due to the exponential decay inside the cochlear duct. Linear functions were fitted to all the node potentials induced by each of the source positions and served as an approximation of the decay associated with a source.

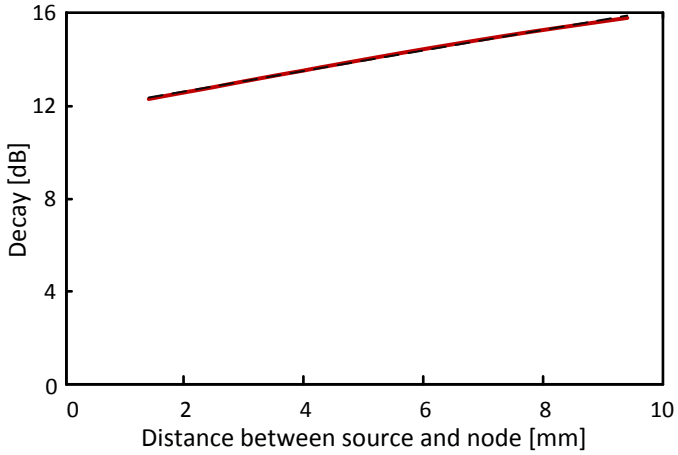

Figure 5.6. The potential decay calculated for the source in Figure 5.3. Decay (dB) is plotted as a function of the node position along the OC (red line). A straight line fitted to the data is a good approximation of the decay (dashed line). This line has an offset caused by the attenuation between the source (in the ST) and the neuron terminals (in the spiral lamina) where the voltages are measured

5.2.2 Obtaining a function for potential decay

The potential decay in dB to one side (apical or basal) of the stimulating source in the cochlea due to a stimulating source *s* can be approximated by a linear function in the form of:

$$decay_s = m_s x_{s,n} + c_s \tag{5.3}$$

where m_s is the slope, c_s is the offset of the function (Figure 5.6) and $x_{s,n}$ is the distance of the source to the measurement node. m_s and c_s are themselves functions of the location of the source. In order to derive a general function that describes $decay_s$, two functions were derived to describe m_s and c_s. As the decay slope differs between the basal and apical sides of the stimulating electrode, a different decay function was derived for each side. These functions were designated as $decay_s^{apical}$ and $decay_s^{basal}$. The inputs to these functions were parameters that describe the location of the source.

To make the function derived here clinically applicable, the position of the source has to be described in terms of clinically measurable parameters. Initially the following parameters were used to describe each of the source positions: ST duct height, ST duct width, distance from modiolus, distance from medial wall, distance from lateral wall, distance from top wall, distance from bottom wall, theta, distance from OC, model number, medial/lateral placement, ST duct area, vertical percentage from OC, horizontal percentage from OC and the base width of the cochlea. m_s is plotted as a function of each of these parameters in Figure 5.7.

In order to assess if there is correlation between these parameters and the decay in the cochlea, a neural network was trained using these parameters as inputs and m_s^{apical} and c_s^{apical} as outputs. The neural network fitting tool included in the Matlab Neural Network Toolbox 8.2 was used for this purpose. 70% of the data was used as the training set, 15% as the validation set and the remaining 15% used as a testing set. A single hidden layer with 1000 neurons and a single output layer with 17 neurons were used. Training was done using the Levenberg-Marquardt method. The output of the trained network produced relatively small errors (R=0.813 for c_s and R=0.806 for m_s) to the validation data set indicating that there is sufficient information contained in the input parameter set to estimate the output.

To be applicable for use in a clinical setting, a reduced set of input parameters that are easily obtainable from standard clinically available data have to be used. The parameter set describing an electrode was reduced to only four parameters: theta (angle from RW in radians), distance from the modiolus and cochlear base width. These parameters were deemed easily obtainable from standard radiographic data such as CT or radiographs. These parameters were used to obtain functions that describe m_s and c_s. Simple functions were used instead of a neural network to simplify the use of this method.

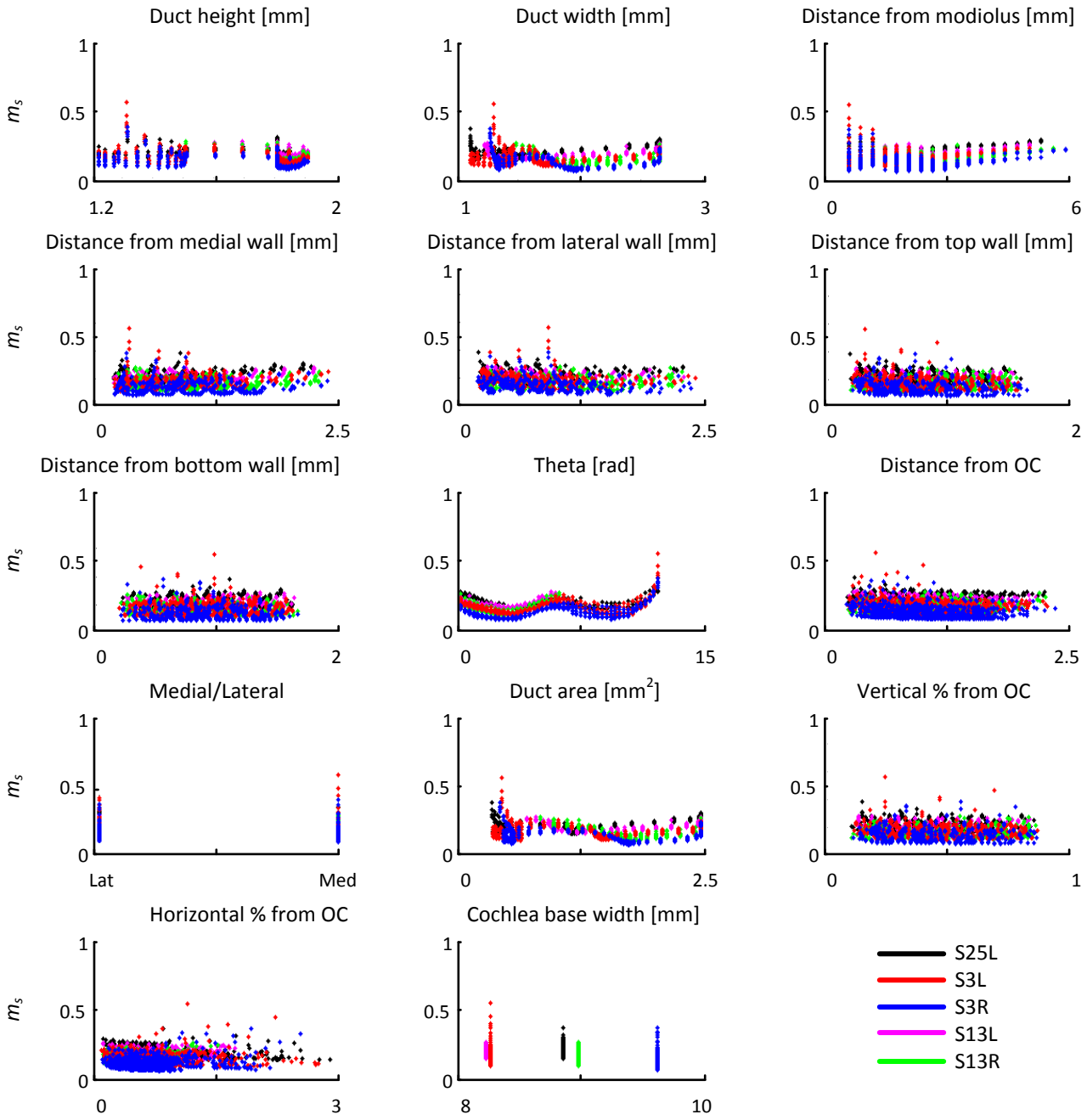

Figure 5.7. m_s as a function of the parameters describing the source locations. Each colour represents the predictions from a different user-specific cochlear model

Functions for m_s and c_s were derived using non-linear regression using the *NonLinearModel* class in the Matlab Statistics Toolbox. The resulting function for m_s^{apical} has a mean error of 0.025 (9.87%) and c_s^{apical} a mean error of 0.97 (13.7%). The resulting function for m_s^{apical} has a mean error of 0.025 (9.87%) and c_s^{apical} a mean error of 0.97 (13.7%). The function for m_s^{basal} has a mean error of 0.021 (11.9%) and c_s^{basal} a mean error of 0.99 (14.7%). The following functions were derived:

$$m_s = (a_1 p_1 + a_2).sin(a_3 p_1 + a_4) + a_5 p_2 + a_6 {p_3}^2 + a_7 p_3 + a_8 \tag{5.4}$$

$$c_s = a_9 {p_1}^2 + + a_{10} p_1 + a_{11} {p_2}^2 + a_{12} p_2 + a_{13} p_3 + a_{14} {p_4}^2 + a_{15} p_4 + a_{16} \tag{5.5}$$

with the following values:
a^{apical} = [0.0038 0.0510 0.7847 2.5302 0.0192 -0.0120 0.1768 -0.3973 -0.0020 0.3074 -1.5362 1.4956 -27.2338 1.7968 -5.1178 135.1325], a^{basal} =[-0.2020 -0.0736 0.3351 1.5938 -28.9375 1.2163 -3.4951 139.6396 0.0190 -0.0851 0.9015 0.7522 0.0112 0.0129 -0.2445 1.3367], p_1 = theta (angle measured from RW in radians), p_2 = distance from the centre of the modiolus and p_3 = cochlear base width and p_4 = distance from the OC of the stimulating electrode.

Thus, to determine the decay (dB) that a neuron node will experience due to a stimulating electrode (s) at a distance of x mm apical to the stimulus source, the following equation may be used (from equations 5.3, 5.4 and 5.5) by substituting in the values of a^{apical}, p and x:

$$\begin{aligned} decay_s(x) = &\left[(a_1 p_1 + a_2).sin(a_3 p_1 + a_4) + a_5 p_2 + a_6 {p_3}^2 + a_7 p_3 + a_8\right] \times x_{s,n} \\ &+ \left[a_9 p_1 + a_{10} {p_2}^2 + a_{11} p_2 + a_{12} {p_3}^2 + a_{13} p_3 + a_{14} {p_4}^2 + a_{15} p_4 + a_{16}\right] \end{aligned} \tag{5.6}$$

When determining the decay basal to the stimulating electrode, a^{basal}, p and x should be substituted.

5.3 RESULTS

To assess the performance of the derived formula, the decay of each source was firstly determined for half a turn apical to the source from the FEM models. Secondly, this decay was modelled using equation in 5.6. The absolute difference in decay predicted by the equation and the 3D models on each measured node was used to assess the accuracy of the formula. The mean absolute error was found to be 1.4 dB. The mean decay from the FEM models is 8.2 dB, making the mean error of the results of the derived formula 17.06%.

When calculating the decay using the standard decay rate of 3 dB/mm, the average error between the predicted values and the decay values of the FEM model is 6.35 dB or 79.02%.

5.4 DISCUSSION

Using only four clinically measurable parameters, the function fitted here is capable of predicting decay in a cochlea with an average error of around 1.4 dB (17%). Although this error may seem substantial, it is still an improvement over using a standard value of 3 dB/mm which produces an average error of 6.35 dB (79%) on the modelled data.

A linear function indicating the change in decay is produced for each source position. This function has a large offset and a shallow slope. This may have implications in the design of cochlear implant analysis filters where filters may have to have different characteristics for each electrode based on its location. The filter responses should also have a different shape to a purely 3 dB/mm cut-off rate to take the linear decay curve of each electrode into account. The cut-off rate should then be related to the shallow slope (m_s) of the predicted linear decay curve which was found to generally be around 0.26 dB/mm (apical) and 0.19 dB/mm (basal). This implies that current synthesis filters assuming a 3 dB/mm cut-off rate are delivering stimuli to a wider area of the cochlea than is thought. This may in part explain why speech perception is worse than expected in some users. This is based on the

finding by Bingabr et al. (2008) where speech perception performance was found to be negatively affected when using very narrow synthesis filters.

5.5 CONCLUSION

1. The potential decay rate inside the cochlea is a function of the position of the electrode inside the scala.
2. A model for the decay as a function of the distance along the OC was derived in equation 5.6. The model describes decay as a linear function with a large offset and a shallow slope. The slope is in the order of 0.26 dB/mm (apical) and 0.19 dB/mm (basal) and the offset is in the order of 7.07 dB (apical) and 6.2 dB (basal).

This indicates that the decay rate at the neural elements in the spiral lamina cannot be described using the assumed monopolar decay rate of 3 dB/mm as voltages are affected by the shape and resistive properties of the structures surrounding the neural terminals.

CHAPTER 6
MODEL APPLICATION II:
ESTIMATING USER PITCH MISMATCH

One of the objectives of user-specific models is to translate them to the clinical domain (Figure 1.1). This is a step towards the development of the model predicted mapping instrument where models provide assistance during the mapping of a user. The work described in this section shows an example where models are used to estimate the mismatch between a user's map and perceived pitch.

6.1 INTRODUCTION

A cochlear implant maps audible frequency bands to individual electrodes in the cochlea. When current is injected through an electrode, neurons in the vicinity of the electrode are stimulated. As the neurons in the cochlea are arranged tonotopically, an indication of the pitch that the user perceives can be calculated using Greenwood's equation (Greenwood, 1990).

The procedure described above is a simplified method to calculate the perceived frequency of a stimulating electrode and relies on two basic assumptions. First, that current injected by an electrode follows a predictable path (usually assumed to be decaying exponentially through the cochlear duct) and stimulates the neurons closest to the stimulating electrodes. Secondly, as Greenwood's equation relates the position on the basilar membrane to perceived frequency, it is assumed that the tip of the dendrite near the Organ of Corti is stimulated electrically. As cochlear neurons degenerate from the dendrites, dendritic stimulation is not guaranteed and stimulation may occur in the spiral ganglia or neuron axons. And as cochlear neurons do not emanate radially from the modiolus, but rather in a 'bicycle wheel spoke' pattern from the spiral ganglion (SG) to the OC, a frequency mismatch will occur when applying the Greenwood equation directly to calculate the excitation frequency as described by Stakhovskaya et al. (2007).

The aim of this study is to investigate what the perceived frequencies are of implant users where these assumptions do not hold. I.e. where current follows a complex path through he cochlea and where the site of neural excitation does not occur at the neuron terminals or dendrites but rather in the axons or somas. Such stimulation is common where perimodiolar electrode arrays are used that target axons for stimulation. Non-dentritic stimulation may also occur when there is a large degree of neural degeneration caused by certain etiologies. In this study the etiologies of the subjects were not known and a large degree of neural degeneration was assumed. Comments are also made on the frequency maps that have been programmed in the processors of these users.

6.2 METHODS

In order to investigate the perceived frequencies of individual users, the 3D finite element models developed in Chapter 3 of the cochleae of 5 individual implanted users were used. To simulate the case where excitation does not occur near the OC, degenerate neurons were modelled. This was achieved by including only the axonal and somatic regions in the modelled neurons with the somas located in the SG region of the cochlea. The cochlear neuron model of Rattay et al. (2001b) was used to predict the threshold current at which each neuron in the cochlea fires due to a stimulus from a specific electrode. The position of the neuron with the lowest threshold was used as the site of neural excitation and used to calculate the perceived frequency when stimulating with that electrode.

To estimate the perceived frequencies from activated neurons, the site of excitation, that is located in the SG due to the degenerate nature of the neurons, was mapped to a position along the organ of Corti using the SG frequency position function derived by Stakhovskaya et al. (2007) (Figure 6.1). Greenwood's equation (Greenwood, 1990) was then applied to obtain the frequency that the user perceives when stimulating that electrode (referred to as predicted frequency). This frequency is assumed to be the pitch that the user perceives and assumes that more central processes do not change that pitch.

Five cochleae belonging to three individual living implant users were modelled. Two of these users have bilateral implants and allows the assessment of frequency mismatch between the two ears. All the users were fitted with nucleus electrode arrays from cochlear Ltd. The users with bilateral implants both have different electrode arrays in both ears (contour and straight arrays) as summarized in Table 3.1.

The frequency bands assigned to each electrode was obtained from each user's latest programming map. In the maps a frequency band is defined in terms of the upper and lower frequencies of the filter assigned to that electrode.

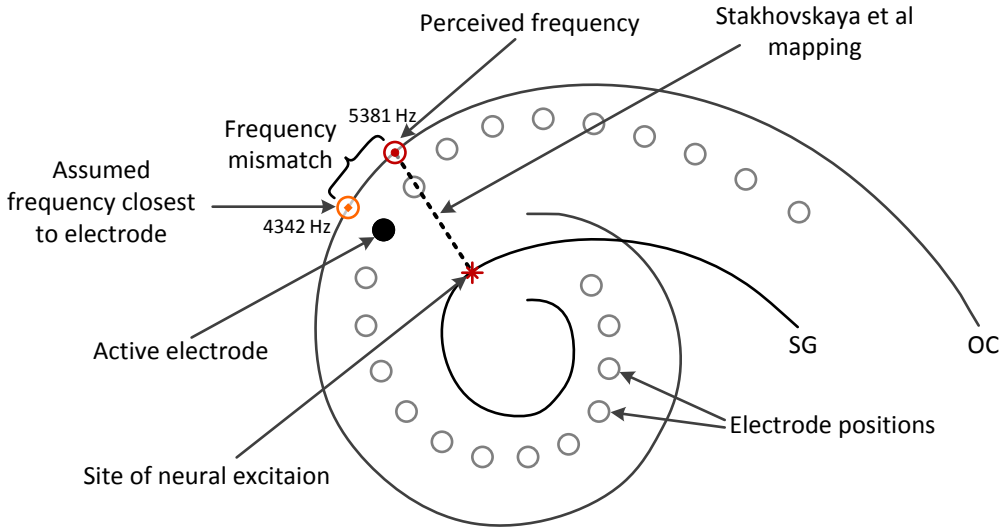

Figure 6.1. Predicting the perceived frequency of a stimulating electrode. It is generally assumed that the perceived frequency will be the frequency mapped to the position of the OC closest to the active electrode (4342 Hz). If the neurons are degenerate in nature (no dendrites) this assumption does not hold as the site of excitation is then in the SG (red). Due to the non-radial trajectory of neurons from the SG to the OC (Sridhar et al., 2006; Stakhovskaya et al., 2007), the perceived frequency will be at a different value (5357 Hz) and cause a frequency mismatch of 0.3 octaves from what is assumed

6.3 RESULTS

The site of stimulation of each electrode in each cochlea was determined using the models. The perceived frequencies as well as the frequencies that one would assume a user will hear due to the electrode being closest to the active electrode were determined. Figure 6.2 shows the effect on the five cochleae when stimulating with electrode 10 (black dot). The assumed frequency (orange dot) in each case is defined as the Greenwood frequency at the location of the OC closest to the electrode. The position of the soma of the neuron that fires at the lowest current when stimulating with the active electrode (threshold position) is indicated in the SG region as a red star. As no dendrites were modelled, the site of excitation occurred in the SG or the axonal regions of each neuron. To calculate the perceived frequency, the location of the dendritic tip along the OC where the dendrite was is determined and used as input to Greenwood's equation. This non-radial trajectory of the dendrite is indicated as a dashed line and its intersection with the OC is indicated as a red dot. The positions along the OC of the upper and lower frequencies of the filter assigned to the electrode are also shown (light and dark blue dots respectively). The results of all the electrodes are summarized in Figure 6.3.

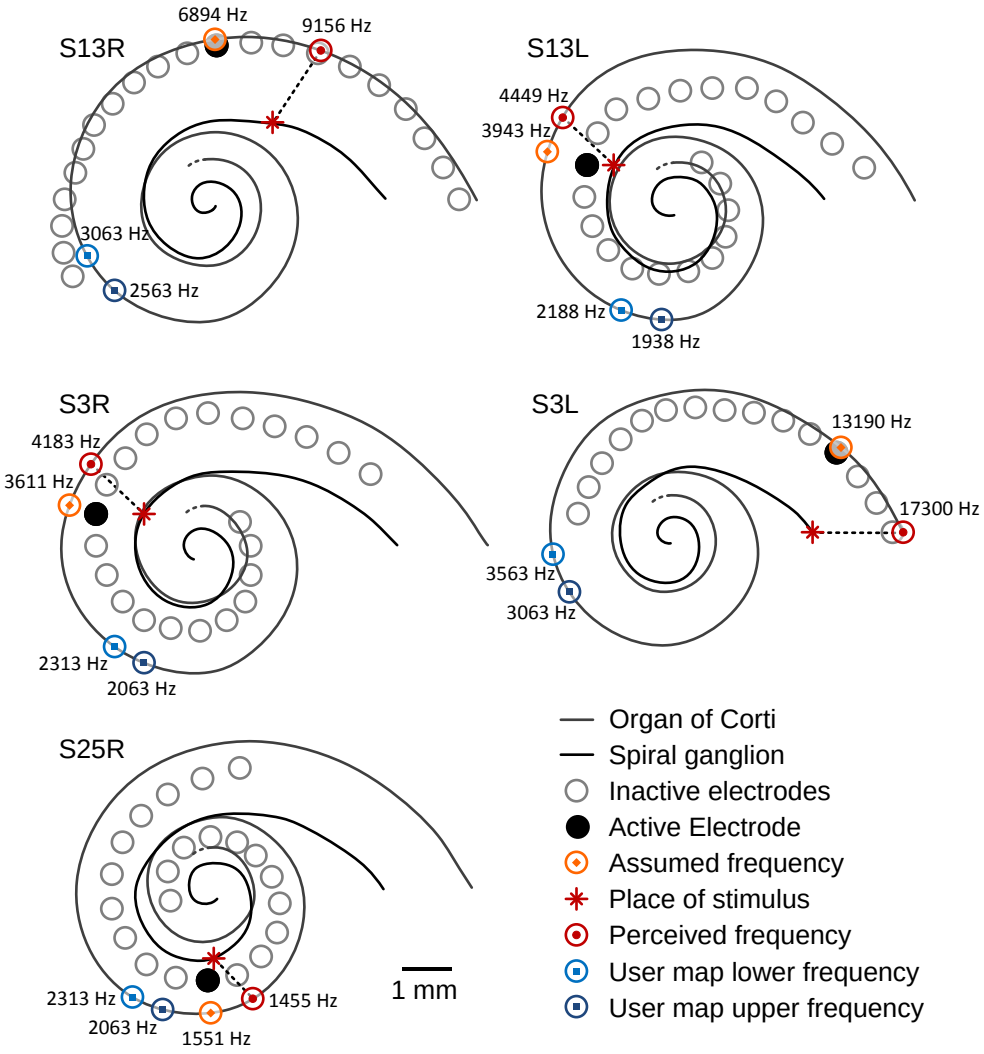

Figure 6.2. Stimulating with electrode number 10 in all five models

From Figure 6.3 it is evident that there is a large mismatch between map frequencies and perceived frequencies for all the ears except S25R. As mapping is generally done to spread the frequency spectrum across the implanted array, this is not unusual. In the case of ear S25R, where a very deep electrode insertion is present, the perceived frequencies are close to the map frequencies.

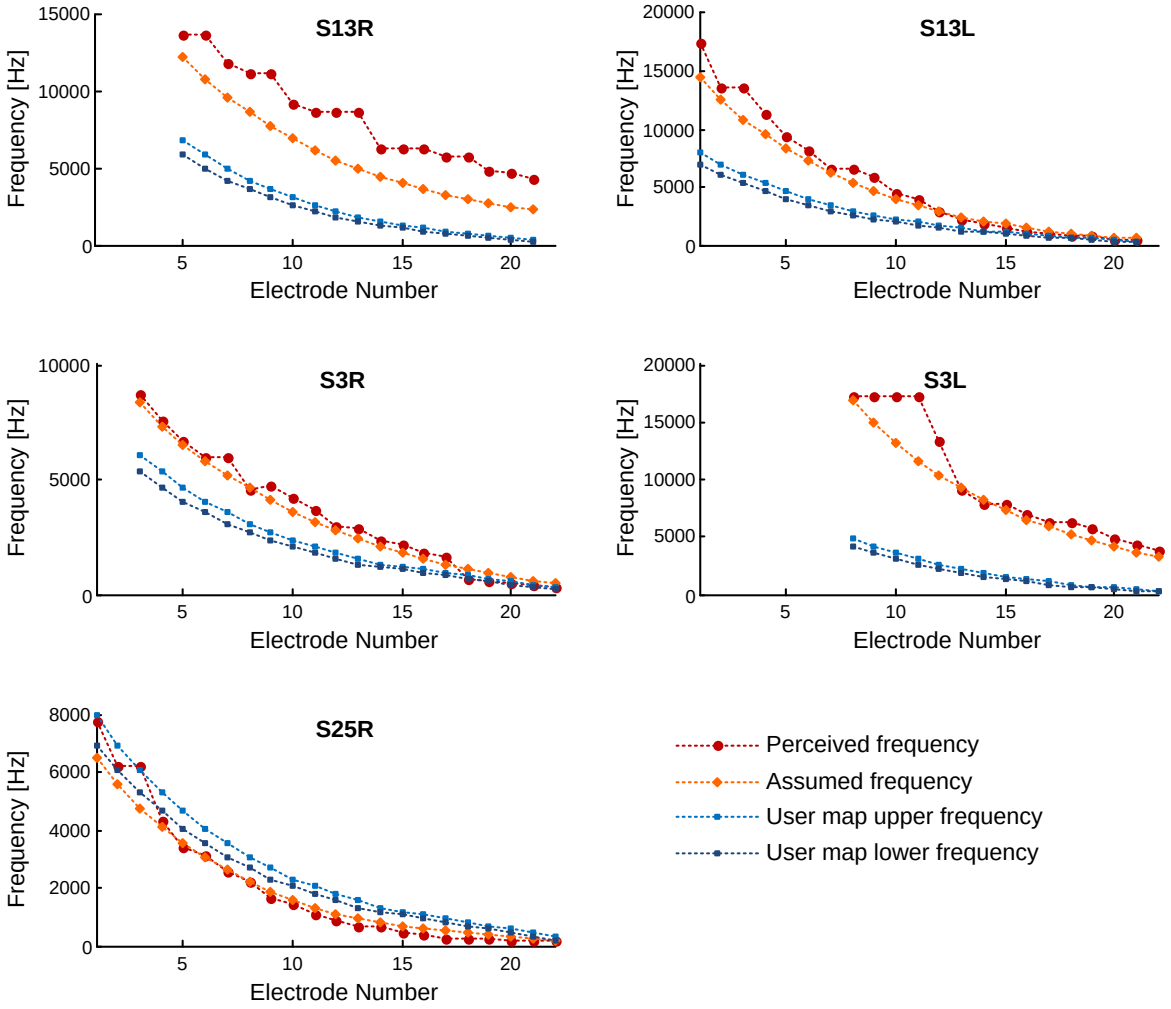

Figure 6.3. Summary of the frequencies of all the electrodes

In ear S13R there is a large difference between the perceived frequencies and the frequencies the user is assumed to be hearing based on the electrode locations. When examining the neural excitation patterns, it was found that the threshold locations are not at the neurons closest to the stimulating electrodes, but generally offset towards the base of the cochlea. This may be ascribed to the geometry of the cochlea as well as the very lateral placement of the electrode array that causes less focussed current spread. A similar mismatch is observed in the basal four electrodes of ear S3L that also has a more lateral array placement. In this case the perceived frequencies are all at the basal tip of the cochlea as the model indicated neural thresholds at the most basal neuron. This may be an artefact

of the model, as the basal end of the cochlea was modelled as a flat wall. This may cause current reflections and a concentration of current near the model edge giving the most basal modelled neuron a higher chance of firing.

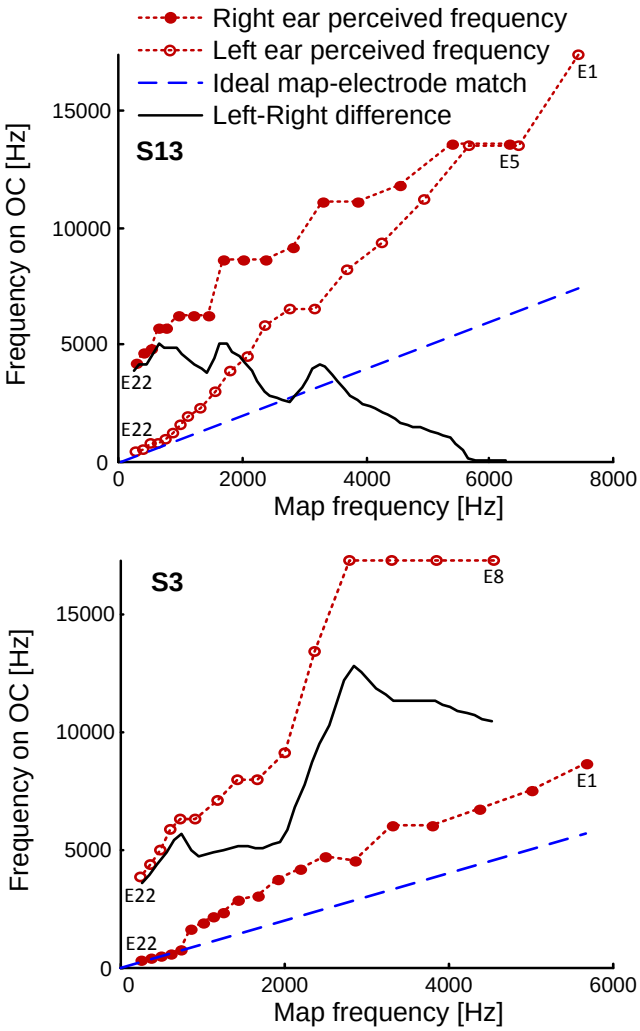

Figure 6.4. Comparison between the mapped frequencies of the left and right ears of the bilateral implantees S13 and S3. The horizontal axis indicates the mapped frequency of an electrode (from the user's programming map) and the vertical axis indicates the perceived frequency of that electrode determined by the model. In both users there is a considerable difference between the two ears (solid black line). Under ideal circumstances an electrode should stimulate a frequency that corresponds to the frequency of the electrode map. This ideal case is indicated by the blue dashed line

It is evident from Figure 6.3 that the electrodes of the left and right ears of the bilateral implantees (S13 and S3) are not mapped to the same frequencies in both ears. Figure 6.4 shows a direct comparison of the electrodes of both ears of each of these users. The horizontal axis represents the frequency that an electrode is mapped to (the average of the lower and upper frequencies of an electrode taken from the user's programming map) and the vertical axis represents the frequency that is perceived when that electrode is stimulated. Under ideal circumstances an electrode should stimulate a frequency that corresponds to the frequency that the electrode was mapped to in order to represent the sound the most realistically. This ideal case is indicated by the blue dashed line. There is a considerable mismatch between the perceived frequencies in the left and right ears of these two users. This implies that when an audible sound is presented to the user, they will perceive sounds of differing frequencies in their left and right ears. This difference is indicated by the solid black line in Figure 6.4 and is calculated by subtracting the perceived frequencies of both ears from each other. The most basal and apical electrode numbers are also shown for clarity.

6.4 DISCUSSION

The perceived frequencies of individual cochlear implant users were modelled and compared to their map frequencies and large differences were generally found. The models assume fully degenerate neurons to model the case of complete loss of dendrites. If a cochlea has residual dendrites and is incorporated into the model as was done by Carlyon et al. (2010), the frequency mismatch between the expected frequency and perceived frequencies will be less. If a cochlea, however, has more severe neural loss in terms of axonal damage and regions of dead neurons, the frequency mismatch will be larger.To keep the modelling method simple, the threshold frequency was selected as the frequency of the neuron with the lowest threshold. In reality, the threshold will occur when a population of neurons around 1 mm wide is excited (Snel-Bongers et al., 2013). This may also cause a shift in the perceived frequency as the region of activated neurons are not always symmetrical around the threshold frequency as seen in Figure 3.11 and Figure 3.13.

Of the five cochleae modelled, a large mismatch between perceived and mapped frequencies was found in four of them. For both bilaterally implanted users a large mismatch between the perceived frequencies of left and right ears were also observed. This can be expected as the strategy followed by the clinician in the mapping of the users was to map the frequencies in the speech band across the entire electrode array.

Studies have, however, indicated that distortion of a frequency map leads to a decrease in speech perception performance (Shannon, Zeng and Wygonski, 1998; Baskent and Shannon, 2003; Başkent and Shannon, 2004). Other studies have, however, found that speech performance of users with distorted frequency maps may improve with time and training (Faulkner, 2006; Rosen, Faulkner and Wilkinson, 1999; Faulkner, Rosen and Green, 2012; Nogaki, Fu and Galvin Iii, 2007; Li, Galvin Iii and Fu, 2009). A study by Faulkner (2006) found that a basal frequency shift of 6 mm between binaurally implanted ears caused listeners to ignore the mismatched information rather than integrating the information. In light of this, having a map that more accurately maps frequencies to perceived frequencies should give users either a better chance at adapting to the incoming sound as well as lead to proper integration of signals from bilateral implants. A tool that allows the accurate determination of the perceived frequencies in a specific cochlea is a useful tool in the endeavour to optimize a user's mapping parameters.

A large predicted mismatch exists between the perceived frequencies of the left and right ears of users S13 and S3 (Figure 6.3). Given the information above, one could speculate that by remapping some of the electrodes to achieve a better left-right frequency match between ears will result in better bilateral speech perception. This may be especially true for user S3 where basal shifts in frequency larger than 6 mm occurs, causing the user to possibly ignore the information instead of integrating it. Further psychoacoustic testing should reveal if the matching of ears causes any improvement in listening experience for the user. As the users in this study have had implants for many years, their central

processes may have already compensated for this mismatch and changing their maps at this stage may have a detrimental effect to their hearing. An incremental change in the user map over time towards a matched map may possibly aid in better adaptation to the new map. Matching ears will, however, cause some of the frequencies in one ear not to be mapped to the ear if the electrodes have different insertion lengths. This may have a more negative effect on overall hearing performance than the mismatch between ears is causing. This is speculative, and should be tested. Also, user preferences may also play a role in the applied mapping strategy, where a specific user may prefer to have more environmental frequencies applied to an ear in order to have a more rich listening experience rather than have a matched map that increases speech perception but reduces the frequency channels presented to one ear. Mismatched ears also has a detrimental effect to sound localization (Kan, Litovsky and Goupell, 2015), having an indication of the extent of this mismatch using model predictions may aid in better binaural hearing.

Having an idea of the frequencies that a user should perceive when stimulating an electrode, may give researchers a tool to estimate neural degeneration. By designing an experiment that measures relative frequency discrimination using psychoacoustics and comparing that to relative frequency discrimination inferred from predicted results, a measure of regions of neural degeneration in the cochlea may be obtained.

6.5 CONCLUSION

1. User-specific models can be used to estimate the perceived frequencies elicited by a stimulating electrode.
2. Mismatch between users' maps and perceived frequencies were found.
3. Mismatches were found between the perceived frequencies in the left and right ears of bilaterally implanted users.
4. User-specific models show potential for use during model predicted mapping and model-based diagnostics.

CHAPTER 7 GENERAL DISCUSSION

7.1 RESEARCH OVERVIEW

This study aimed to develop a tool for researchers to probe the cochlea of a specific living implanted user non-invasively. A method was developed whereby a 3D FE model of a specific implanted cochlea could be modelled from standard CT data (Chapter 3). Using this method, five models were constructed and used to probe the implanted cochleae of the specific users in a computational environment. It was found that potential fields and neural excitation profiles are dependent on cochlear morphology. This indicates the use of user-specific models in predicting user-specific outcomes.

During the course of model development, aspects that influence modelled results were also investigated. These include the effects that bone resistivity, head volume shape, return electrode implementation and return electrode position have on modelled results (Chapter 4). The findings contributed to higher detailed cochlear models being produced than what is currently described in literature.

Two practical uses of these detailed, user-specific models were then demonstrated. The first was in the quantification of potential decay in the cochlea where a simple model was derived to predict decay based on the location of an electrode. The second was in the prediction of the mismatch between the perceived pitch and mapped frequencies of specific implanted individuals.

Details of these findings are summarized on the following pages.

7.2 SUMMARY OF RESULTS AND RESEARCH CONTRIBUTIONS

7.2.1 Method development

In Chapter 3 a method was developed to construct a 3D VC model of a specific implanted cochlea in order to predict parameters that cannot be measured non-invasively from a living implant user.

Standard CT was identified as a suitable method to obtain the dimensions of a cochlea. This non-invasive method requires only that the user lies still for a few seconds. The resolution produced by these scans is also high enough to obtain cochlea-specific dimensions from.

Five individual cochlear models were constructed based on the CT measurements taken from five implanted cochleae. Electrode arrays and monopolar return electrodes were also modelled in the positions that they occur in the cochleae. The cochlear models were also modelled within a head model containing a detailed description of the skull, brain and scalp. This allowed the extra-cochlear current pathways to the monopolar return electrode to be accurately represented.

From the models it was found that intra-cochlear potentials as well as neural excitation spread are dependent on cochlear morphometry. This was done by modelling similar electrode arrays in similar locations in all the cochlear models to isolate the effect of cochlear morphometry on the results.

From these results it was concluded that incorporation of a CI user's cochlear morphometry into a model is essential to predict user-specific outcomes. As user-specific outcomes can be predicted, making use of such a more complex modelling method as opposed to a model based on the morphology of a generic human cochlea is warranted.

The detailed models produced using this method allows the investigation of parameters that cannot be measured from an actual living cochlea. This is either because measuring requires invasive techniques or because measurements do not isolate a single parameter, but are rather a compound response of many parameters such as an ECAP response that contains the response of multiple neurons as well as measuring artefacts and noise. Using the models produced here, predictions of parameters, such as single fibre responses, may be obtained in isolation without measuring artefacts present. This allows the investigation of cochlear systems on a lower level and aids our understanding of the system as a whole. Some of the aspects investigated using these models are described here.

7.2.2 Bone resistivity estimation

A wide range of values have been reported for the resistivity of bone throughout the body. Different studies utilizing VC models of the implanted cochlea have used various resistivity values to describe the bone around the cochlea. This makes the selection of a value to use in a cochlear model difficult. This study (Chapter 4) set out to obtain a resistivity value to use in VC models of the implanted cochlea.

As implementations of the bone surrounding the cochlea and return electrode vary among models, different configurations were investigated. These include a cochlea in an infinitely large bone medium with the return electrode surrounding the model at a distance of infinity, a cochlea in a bone ellipsoid roughly the shape of a human head with the return electrode placed in an accurate location and a detailed model of the head consisting of a skull, brain and scalp with the return electrode in an accurate position.

It was found that modelled intra-cochlear potential and fmSTC widths and slopes are heavily dependent on the value of bone resistivity. A suitable bone resistivity was thus obtained by varying the resistivity of bone until predicted potential and fmSTC widths and slopes matched data from literature. As the widths and slopes from literature represented

the averages of many cochleae, the widths and slopes predicted by all five models in the present study were also averaged to make the data comparable.

Results indicated that neural excitation and intra-cochlear electric field spread are dependent on the detail of the description of the head volume surrounding the cochlea as well as the implementation of the neuron model as different bone resistivities are required in VC models to match measured spread reported in literature. This effect is greater when predicting the neural excitation spread than the electric field spread.

As a starting point for modellers using models to predict neural excitation spread, a bone resistivity value of 10 000 Ω.cm is proposed. A bone resistivity of 6500 Ω.cm is proposed when predicting intra-cochlear electric field spread. Given the sensitivity of the predicted bone resistivity values on the type of head model and neuron model used, optimization of the bone resistivity for a specific model is recommended.

7.2.3 Influence of source position on potential decay

An accurate bone resistivity value to use in cochlear models allows the accurate estimation of the decay of potential fields in the cochlea.

The current from a monopolar stimulating electrode is generally assumed to be decaying at a rate of 3 dB/mm. This value was obtained from animal studies and salt bath experiments and is generally accepted as the monopolar electrical stimulus resolution in cochlear implants (Bingabr et al., 2008). Implant processor analysis filters are also calculated according to this exponential decay of current. This value was derived based on the model of exponential current decay experienced by a source in an isotropic, infinitely large medium that holds well within the cochlear scala. The neural elements are, however, not located in the cochlear scala but rather below the OC inside the bony spiral lamina. It was found that the structures surrounding the neural elements cause the neural elements to

experience a more complex level of decay and that the assumption of a constant 3 dB/mm decay rate does not apply.

It was found that potential from a stimulating electrode does not decay at a constant rate throughout the cochlea, but is highly dependent on the location of the source as well as the cochlear structure in which the potential is measured. When measuring in the spiral lamina where the neural elements are located, it was found that for each source location, the decay is described by a linear function with a large offset and relatively shallow slope. Two simple models were derived to predict the slope and offset of the linear function from parameters describing the location of a source. Four parameters that are easily obtainable form radiographic data are used to describe the location of the source.

This allows the prediction of potential decay at a location along the OC when the location of the source is known. The outcomes have implications for the design of speech processor analysis filters where filter characteristics have to be adapted according to the location of an electrode. Based on the findings, these filters should in general have shallower cut-offs than the 3 dB/mm that is generally used. This may in part explain why speech perception is worse than expected in some users as Bingabr et al. (2008) found that speech perception performance was negatively affected when using very narrow synthesis filters. Individualized filter selection based on electrode location may also aid in better mapping of frequencies in a user's implant.

7.2.4 Estimating the mismatch between perceived frequency and programming maps

It has been shown that a distortion of a frequency map leads to a decrease in speech perception performance (Shannon et al., 1998; Baskent and Shannon, 2003; Başkent and Shannon, 2004). Other studies have, however, found that speech performance of users with distorted frequency maps may improve with time and training (Faulkner, 2006; Rosen et al., 1999; Faulkner et al., 2012; Nogaki et al., 2007; Li et al., 2009). A study by Faulkner

(2006) found that a basal frequency shift of 6 mm between binaurally implanted ears caused listeners to ignore the mismatched information rather than integrating the information. Having a map that more accurately maps frequencies to perceived frequencies should give users a better ability to adapt to the incoming sound as well as lead to proper integration of signals from binaural implants (Stakhovskaya et al., 2007).

It is generally assumed that an electrode will stimulate the neurons closest to it. Using Greenwood's function the pitch perceived by stimulating an electrode may then be determined. This assumption only holds if a neuron is non-degenerate and stimulated at the terminal of the dendrite in the OC near the stimulating electrode. In general this assumption may not hold as a neuron may be degenerate in nature and only be stimulated at the SG or axon. As neurons follow a 'bicycle spoke pattern' from SG to OC as described by Stakhovskaya et al. (2007), Greenwood's function has to be applied at the site on the OC where the dendrite of the stimulated degenerate neuron used to be to predict the perceived frequency. Due to the complex current patterns caused by the non-linear structure of the cochlea, stimulation may also not occur at the neuron closest to the stimulating electrode, but at another more distant site. The five cochlear models constructed in this study were used to determine the sites of neural excitation and the perceived frequencies of all the electrode contacts. The mismatch between the mapping and perceived frequencies of the specific implanted cochleae were then assessed.

It was found that the perceived frequencies differed from the mapped frequencies of four of the five cochleae. The one cochlea that displayed a good match between perceived and mapped frequencies was found to have a very deep insertion that facilitated the match. For both the bilateral users, large mismatches in the perceived frequencies between the left and right ears were found.

This part of the study demonstrates one practical use of user-specific models in predicting user-specific outcomes.

7.3 GENERAL DISCUSSION

7.3.1 Present cochlear implant models

Since the introduction of computational volume conduction models of the auditory periphery by Girzon (1987), various aspects have been incorporated into models to more accurately describe the functioning of the implanted cochlea. Finley et al. (1990) included a basic model of the neural responses to stimulation and later others integrated active neuron models into VC models to predict neural excitation patterns in guinea pig and human cochleae (Frijns et al., 1995; Briaire and Frijns, 2000a; Frijns et al., 2000; Rattay et al., 2001a; Hanekom, 2001a). Much work has also been done in the improvement of the active neuron models in making the dynamics resemble more of the characteristics of mammalian and human cochlear nerve fibres (Frijns et al., 2000; Rattay et al., 2001b; Smit, Hanekom and Hanekom, 2008). These models have contributed to a better understanding of the functioning of the implanted cochlea in general. This includes insight into the effects that electrode placement, stimulation mode, electrode design, neural degeneration and ectopic stimulation, among others, have on neural excitation. These contributions to the field of cochlear implants ultimately lead to improved implants and techniques and implant users being able to perceive sound better.

Sound perception performance does, however, still vary greatly among individual implanted users (Firszt et al., 2004; Kunisue et al., 2007) and even between implanted ears. The effects that contribute to these variations are still not fully understood. In order to use VC models of the cochlea to investigate some of the factors affecting these variations, such models have to incorporate user-specific parameters.

7.3.2 Improvements on present cochlear implant models

This study set out to improve upon present cochlear VC models by describing a detailed method to incorporate user-specificity. Other studies that have incorporated user-specificity into models (Carlyon et al., 2010; Kalkman et al., 2014a) do not provide extensive details of the methodologies followed and assumptions made during model

construction. The present study sets out by firstly incorporating the morphometry of a specific user's cochlea and electrode placement into a model from data obtained non-invasively. It was found that a further improvement in detail is needed especially when predicting neural excitation patterns from monopolar stimulation sources. As monopolar stimulation causes current to flow through structures external to the cochlea, a more detailed description of head volume was incorporated. An accurate return electrode position was also required and incorporated.

Neural excitation due to monopolar stimulation is especially sensitive to the resistivity value used for the bone surrounding the cochlea. As different resistivities have been used in other cochlear models reported in literature (Frijns et al., 1995; Finley et al., 1990; Hanekom, 2001b; Malherbe et al., 2013; Hanekom, 2001a; Briaire and Frijns, 2006; Govindasamy, 2012; Rattay et al., 2001a; Kalkman et al., 2014a; Frijns et al., 2009a; Whiten, 2007), a bone resistivity value was estimated (see Chapter 4) by comparing modelled results to results obtained in literature. A suitable bone resistivity value is dependent on the implementation of the surrounding head structures and return electrode. Different bone resistivities were thus suggested for use in cochlear models where different head volume implementations are used.

7.3.3 Uses of a more detailed model

Having a more detailed model of an implanted cochlea allows the estimation of parameters that are difficult to obtain from the cochlea of a living human. One such application is in the description of monopolar current decay in the stimulated cochlea (as was demonstrated in Chapter 3). It was found that the generally assumed monopolar decay rate of 3 dB/mm, that was measured in physical models containing electrodes in salt solutions (Kral et al., 1998) as well as in the scala of animal models (Kral et al., 1998; O'Leary et al., 1985), does not apply when measured in the human spiral lamina where the neural elements are located and also varies as electrode location varies. This has implications for implant processor

analysis filter designs (Bingabr et al., 2008) where different cut-off frequencies may be needed based on the positions of the electrode contacts inside an individual's cochlea.

7.3.4 Uses for a user-specific model

Cochlear implant users require the mapping of their processor analysis filter bands to their electrode contacts. Stakhovskaya et al. (2007) noted that having a map that accurately maps audible frequencies to perceived frequencies should give users a better chance at adapting to the incoming sound than with mismatched filters. Estimating the absolute perceived frequency of an implanted electrode contact is generally not possible using psychophysical tests where a user does not have residual hearing in one ear. A user-specific model may, however, be used to estimate perceived frequencies. This was demonstrated (in Chapter Chapter 6) where the frequencies predicted by the models were compared to the frequencies of the user's maps. It was found that mapped frequencies were very different from the predicted perceived frequencies in four of the five user cochleae.

Another potential use of a user-specific model is in model predicted mapping (MPM) where a model is used in the determination of mapping parameters that are difficult to obtain using psychoacoustics. This may occur in cases where users are unable to respond to stimuli interactively or are having difficulty comprehending the required tasks (e.g. small children). In such cases a model could be used to predict relative thresholds between electrodes based on electrode location and cochlear morphometry. Such models may also serve as a visual aid of electrode locations relative to other structures and help shed light on irregular electrode behaviour such as that demonstrated by kinked electrode arrays or electrodes located outside of the cochlea. Electrodes causing unwanted facial nerve stimulation may also be identified and compensated for in a user's map by incorporating a facial nerve model into the user-specific model as was demonstrated by Frijns et al. (2009a).

Detailed visualization of a user's cochlear structure may also aid in the construction of space filling electrodes that conform to individual cochlear shapes. Rebscher et al. (2007) demonstrated in guinea pig models that such space filling arrays limit current spread and lower neural threshold currents. User-specific models may also be constructed of cochleae pre-operatively, to aid as a visualization tool in insertion surgery planning, thus minimizing insertion trauma.

Cochlea-specific current pathways can be predicted by user-specific models. These may be employed in determining novel stimulation techniques such as current and beam steering (Bonham and Litvak, 2008; Van Den Honert and Kelsall, 2007; Kalkman et al., 2014b; Frijns, Dekker and Briaire, 2011; Frijns, Kalkman, Vanpoucke, Bongers and Briaire, 2009b) where virtual channels between electrode contacts are created by varying the intensity of the current of various electrodes. In order to accurately determine the virtual channel that will be formed, detailed knowledge of a specific implant's current dispersion is required; an application that VC models are particularly well suited for.

7.3.5 Ease of use

In order to utilize a user-specific model in the scenarios mentioned, such a model should be constructed with relative ease and convenience to the user. As the method developed to construct models described (in Chapter 3), utilizes non-invasive CT scan data that is readily available from routine pre-operative and post-operative scans, the inconvenience to the user is minimal. The method also focussed on the rapid construction of a model. Although the method followed is more involved than using a model based on a generalized cochlear morphology, constructing a model and obtaining user-specific predictions is still less time consuming than approximating these affects using psychophysics or other data.

7.3.6 A tool for researchers

The intention of this study was to create a tool for researchers to probe the implanted cochlea of a specific individual. Having such a tool allows the investigation of parameters

that affects the large variability in hearing perception performance between implant users. Detailed investigation of these parameters using the methods developed in this study is the focus of future work. Future work that may emanate from this study is described in the following section.

7.4 FUTURE DIRECTIONS

This study focussed on the development of a method to create a model of the implanted cochlea of a specific living user. Such a model may then be used as a tool to predict user-specific parameters that cannot be measured in vivo. As these parameters describe the workings of a specific person's cochlea, they may be used to investigate factors that affect sound perception on an individualized basis. Future work includes the determination of these factors, by comparing measured data of individuals to predictions from their respective cochlear models. Measured data may be obtained from the users in the form of ECAP data or perceptual data from psychophysical experiments.

ECAP data may also be used in conjunction with user models to estimate areas of neural degeneration in the cochleae of specific users which could lead to the optimization of individual user maps. User maps may also be optimized from modelled results such as the predicted perception data that was presented in section Chapter 6. Here map frequencies could be adjusted to allow for a more natural mapping between stimulus and perceived frequencies. Investigation of the effectiveness of such map adjustments over time will determine the efficacy of such a method.

Although this method produces more detailed models than other cochlear models presently described in literature, the complexity of the models produced pale in comparison to the complexity of the implanted human cochlea that it is attempting to model. When the model outputs are compared to more measured data, the aspects of the model requiring refinement and expansion should become more evident.

One aspect of the models that presently require refinement is the implementation and selection of the neuron model. In this study it was found that predicted neural excitation is heavily dependent on the type, as well as the state, of the neural degeneration incorporated into the model. Refinement of the neuron model dynamics, as well as the geometric implementation of the individual neurons, should lead to more accurate prediction of neural excitation.

Another area of refinement may be in the incorporation of a user's fine inner cochlear structures into a model. The present method employs scaling of a general description of these structures to fit the outer cochlear dimensions of a specific cochlea. This was done as present imaging techniques do not have the resolution to allow imaging of these structures in-vivo.

In an attempt to predict perceptual outcomes, models of more central processes could be applied to the output of the model of the peripheral auditory system presented here. This includes the modelling of the auditory nucleus, inferior colliculus, and auditory cortex. Unfortunately much less is known of the functioning of these structures than is known of the cochlea making modelling a challenge.

CHAPTER 8 CONCLUSIONS

A method to construct a computational 3D finite element model of the implanted cochlea of a specific living individual from a non-invasive standard CT scan was presented. This method is intended for use as a tool for researchers to probe the cochleae of specific implanted users non-invasively. Models of five implanted cochleae were constructed using this method and it was found that potential field patterns and neural excitation patterns are influenced by cochlear geometry, return electrode location, electrode array location, head geometry, resistivity of the cochlear bone and electrode array location. These models were furthermore used to establish a bone resistivity value for use in volume conduction cochlear models, used to derive a simple model to predict potential decay inside a cochlea as well as to investigate the mismatch between perceived and mapped frequencies of the individual implant users. Having a model that predicts user-specific outcomes paves the way for investigations into the effects that determine inter-user hearing performance variability.

In summary:

- A method was developed to construct a 3D FE model of the implanted cochlea of a specific individual from non-invasive CT scan data.
- These models allow the prediction of cochlear parameters that cannot be measured directly in a living human implant user.
- The user-specificity of the models that are produced is an improvement over existing models based on the geometry of a generic cochlea.
- Modelling of a user-specific cochlea allowed the predictions of user-specific parameters such as intra-cochlear potentials and neural excitation on a single neuron level.
- The individualised models were used to predict the frequency mismatch between perceived frequencies and the programming map of specific individuals. This may have value in a clinical setting where better mapping may be performed in terms of mapped frequencies and the matching of maps between binaural implants.
- Including specificity also resulted in a more detailed model being developed than is currently reported on in literature. This is especially apparent in the addition of a high resolution head model and return electrode placement.

- The level of detail in the model also allowed other factors generally present in a cochlea to be investigated such as the bone resistivity value and potential decay.
- The effect that return electrode configuration and the surrounding head model has on monopolar stimulated potential fields and neural excitation was investigated. From the findings a bone resistivity value to use in modelling studies was derived.
- The potential decay in a cochlear duct was found to be non-linear and highly dependent on electrode location. This is in contrast to the constant monopolar decay rate of roughly 3 dB/mm that is generally assumed in literature. A function was derived to estimate this decay and presented as an alternate method of estimating potential decay in the cochlea. The inputs to this function are easily obtainable from standard radiographic data to ensure ease of use in a clinical setting.
- High resolution models may serve as visual aids to clinicians in indicating the position of the electrode array relative to other cochlear structures during model-based diagnostics.
- Having a tool to predict user-specific outcomes facilitates investigations into the effects that determine inter-user hearing performance variability.

REFERENCES

Adunka, O., Unkelbach, M. H., Mack, M. G., Radeloff, A. and Gstoettner, W. (2005). Predicting basal cochlear length for electric-acoustic stimulation. *Archives of Otolaryngology - Head and Neck Surgery,* **131**(6)**:**488-492.

Akhtari, M., Bryant, H. C., Mamelak, A. N., Flynn, E. R., Heller, L., Shih, J. J., Mandelkem, M., Matlachov, A., Ranken, D. M., Best, E. D., Dimauro, M. A., Lee, R. R. and Sutherling, W. W. (2002). Conductivities of three-layer line human skull. *Brain Topography,* **14**(3)**:**151-167.

Aschendorff, A., Kubalek, R., Hochmuth, A., Bink, A., Kurtz, C., Lohnstein, P., Klenzner, T. and Laszig, R. (2004). Imaging procedures in cochlear implant patients - Evaluation of different radiological techniques. *Acta Oto-Laryngologica, Supplement,* **124**(552)**:**46-49.

Aschendorff, A., Kubalek, R., Turowski, B., Zanella, F., Hochmuth, A., Schumacher, M., Klenzner, T. and Laszig, R. (2005). Quality control after cochlear implant surgery by means of rotational tomography. *Otology and Neurotology,* **26**(1)**:**34-37.

Avci, E., Nauwelaers, T., Lenarz, T., Hamacher, V. and Kral, A. (2014). Variations in microanatomy of the human cochlea. *Journal of Comparative Neurology,* **522**(14)**:**3245-3261.

Balkany, T. J., Eshraghi, A. A. and Yang, N. (2002). Modiolar proximity of three perimodiolar cochlear implant electrodes. *Acta Otolaryngol,* **122:**363-369.

Baskent, D. and Shannon, R. V. (2003). Speech recognition under conditions of frequency-place compression and expansion. *Journal of the Acoustical Society of America,* **113**(4 I)**:**2064-2076.

Başkent, D. and Shannon, R. V. (2004). Frequency-place compression and expansion in cochlear implant listeners. *Journal of the Acoustical Society of America,* **116**(5)**:**3130-3140.

Bettman, R., Beek, E., Van Olphen, A., Zonneveld, F. and Huizing, E. (2004). MRI versus CT in assessment of cochlear patency in cochlear implant candidates. *Acta Oto-Laryngologica,* **124**(5)**:**577-581.

Biedron, S., Westhofen, M. and Ilgner, J. (2009). On the number of turns in human cochleae. *Otology and Neurotology,* **30**(3)**:**414-417.

Bingabr, M., Espinoza-Varas, B. and Loizou, P. C. (2008). Simulating the effect of spread of excitation in cochlear implants. *Hearing Research,* **241**(1-2)**:**73-79.

Blamey, P., Arndt, P., Bergeron, F., Bredberg, G., Brimacombe, J., Facer, G., Larky, J., Lindstr”m, Nedzelski, J., Peterson, A., Shipp, D., Staller, S. and Whitford, L. (1996). Factors Affecting Auditory Performance of Postlinguistically Deaf Adults Using Cochlear Implants. *Audiology and Neuro-Otology,* **1**(5)**:**293-306.

Bonham, B. H. and Litvak, L. M. (2008). Current focusing and steering: Modeling, physiology, and psychophysics. *Hearing Research,* **242**(1-2)**:**141-153.

Bouchard, M. E., Ouellet, C. and Cohen, H. (2009). Speech development in prelingually deaf children with cochlear implants. *Linguistics and Language Compass,* **3**(1)**:**1-18.

Bozorg Grayeli, A., Saint Yrieix, C., Imauchi, Y., Cyna-Gorse, F., Ferrary, E. and Sterkers, O. (2004). Temporal bone density measurements using CT in otosclerosis. *Acta Oto-laryngologica,* **124**(10)**:**1136-1140.

Brackmann, D. E. (1976). The cochlear implant; basic principles. *Laryngoscope,* **86**(3)**:**373-388.

Briaire, J. J. and Frijns, J. H. M. (2000a). 3D mesh generation to solve the electrical volume conduction problem in the implanted inner ear. *Simulation Practice and Theory,* **8**(1-2)**:**57-73.

Briaire, J. J. and Frijns, J. H. M. (2000b). Field patterns in a 3D tapered spiral model of the electrically stimulated cochlea. *Hearing Research,* **148:**18-30.

Briaire, J. J. and Frijns, J. H. M. (2006). The consequences of neural degeneration regarding optimal cochlear implant position in scala tympani: A model approach. *Hearing Research,* **214**(1-2)**:**17-27.

Buchman, C. A., Dillon, M. T., King, E. R., Adunka, M. C., Adunka, O. F. and Pillsbury, H. C. (2014). Influence of cochlear implant insertion depth on performance: A prospective randomized trial. *Otology and Neurotology*.

Burnett, D. S. 1987. *Finite Element Analysis: From concepts to applications*, Addison-Wesley Publishing Company.

Caldemeyer, K. S., Sandrasegaran, L., Shinaver, C. N., Mathews, V. P., Smith, R. R. and Kopecky, K. K. (1999). Temporal Bone: Comparison of Isotropic Helical CT and Conventional DirectAxial and Coronal CT. *Americal Journal of Radiology,* **172:**1675-1682.

Carlyon, R. P., Macherey, O., Frijns, J. H. M., Axon, P. R., Kalkman, R. K., Boyle, P., Baguley, D. M., Briggs, J., Deeks, J. M., Briaire, J. J., Barreau, X. and Dauman, R. (2010). Pitch comparisons between electrical stimulation of a cochlear implant and acoustic stimuli presented to a normal-hearing contralateral ear. *JARO - Journal of the Association for Research in Otolaryngology,* **11**(4)**:**625-640.

Chaturvedi, A., Mohan, C., Mahajan, S. B. and Kakkar, V. (2006). Imaging of cochlear implants. *Indian Journal of Radiology and Imaging,* **16**(3)**:**385-392.

Chen, J. M., Farb, R., Hanusaik, L., Shipp, D. and Nedzelski, J. M. (1999). Depth and quality of electrode insertion: A radiologic and pitch scaling assessment of two cochlear implant systems. *American Journal of Otology,* **20**(2)**:**192-197.

Cheng, A. H. D. and Cheng, D. T. (2005). Heritage and early history of the boundary element method. *Engineering Analysis with Boundary Elements,* **29**(3)**:**268-302.

Chiu, S. Y., Richie, J. M., Rogart, R. B. and Stagg, D. (1979). A quantitative description of membrane currents in rabbit myelinated nerve. *J.Physiol.,* (292)**:**149-166.

Choi, C. T. M., Lai, W. D. and Chen, Y. B. (2004). Optimization of cochlear implant electrode array using genetic algorithms and computational neuroscience models. *IEEE Transactions on Magnetics,* **40**(2 II)**:**639-642.

Chou, C. K. (2007). Thirty-five years in bioelectromagnetics research. *Bioelectromagnetics,* **28**(1)**:**3-15.

Clough, R. W. (1990). Original formulation of the finite element method. *Finite Elements in Analysis and Design,* **7**(2)**:**89-101.

Cohen, L. T. (2009). Practical model description of peripheral neural excitation in cochlear implant recipients: 1. Growth of loudness and ECAP amplitude with current. *Hearing Research,* **247**(2)**:**87-99.

Cohen, L. T., Saunders, E. and Richardson, L. M. (2003). Spatial spread of neural excitation in cochlear implant recipients: comparison of improved ECAP method and psychophysical forward masking. *Hearing Research,* **179:**72-87.

Cohen, L. T., Xu, J., Xu, S. A. and Clark, G. M. (1996). Improved and simplified methods for specifying positions of the electrode bands of a cochlear implant array. *American Journal of Otology,* **17**(6)**:**859-865.

Connor, S. E. J., Bell, D. J., O'Gorman, R. and Fitzgerald-O'Connor, A. (2009). CT and MR imaging cochlear distance measurements may predict cochlear implant length required for a 360º insertion. *American Journal of Neuroradiology,* **30**(7)**:**1425-1430.

Czerny, C., Steiner, E., Gstoettner, W., Baumgartner, W. D. and Imhof, H. (1997). Postoperative Radiographic Assessment of the Combi 40 Cochlear Implant. *American Journal of Roentgenology,* **169**(6)**:**1689-1694.

Dawson, P. W., Blamey, P. J., Rowland, L. C., Dettman, S. J., Clark, G. M., Busby, P. A., Brown, A. M., Dowell, R. C. and Rickards, F. W. (1992). Cochlear implants in children, adolescents, and prelinguistically deafened adults: Speech perception. *Journal of Speech and Hearing Research,* **35**(2)**:**401-417.

Dimopoulos, P. and Muren, C. (1990). Anatomic variations of the cochlea and relations to other temporal bone structures. *Acta Radiologica,* **31**(5)**:**439-444.

Doyle, J. H., Doyle Jr, J. B. and Turnbull Jr, F. M. (1964). Electrical Stimulation of the Eighth Cranial Nerve. *Archives of otolaryngology (Chicago, Ill. : 1960),* **80:**388-391.

Earl, B. R. and Chertoff, M. E. (2012). Mapping auditory nerve firing density using high-level compound action potentials and high-pass noise masking. *Journal of the Acoustical Society of America,* **131**(1)**:**337-352.

Erixon, E., Högstorp, H., Wadin, K. and Rask-Andersen, H. (2009). Variational anatomy of the human cochlea: Implications for cochlear implantation. *Otology and Neurotology,* **30**(1)**:**14-22.

Faulkner, A. (2006). Adaptation to distorted frequency-to-place maps: Implications of simulations in normal listeners for cochlear implants and electroacoustic stimulation. *Audiology and Neurotology,* **11**(SUPPL. 1)**:**21-26.

Faulkner, A., Rosen, S. and Green, T. (2012). Comparing live to recorded speech in training the perception of spectrally shifted noise-vocoded speech. *Journal of the Acoustical Society of America,* **132**(4)**:**EL336-EL342.

Fernandez, C. (1952). Dimensions of the Cochlea (Guinea Pig). *The Journal of the Acoustical Society of America,* **24**(5)**:**519-523.

Finley, C. C. Finite-element model of radial bipolar field patterns in the electrically stimulated cochlea - Two and three dimensional approximations and tissue parameter sensitivities. Annual International Conference of the IEEE Engineering in Medicine and Biology - Proceedings, 1989. 1059-1060.

Finley, C. C., Holden, T. A., Holden, L. K., Whiting, B. R., Chole, R. A., Neely, G. J., Hullar, T. E. and Skinner, M. W. (2008). Role of electrode placement as a contributor to variability in cochlear implant outcomes. *Otology & neurotology : official publication of the American Otological Society, American Neurotology Society [and] European Academy of Otology and Neurotology,* **29**(7)**:**920-928.

Finley, C. C., Wilson, B. S. and White, M. W. 1990. Models of neural responsiveness to electrical stimulation. *In:* MILLER, J. M. and SPELMAN, F. A. (eds.) *Cochlear Implants: Models of the Electrically Stimulated Ear.* New York: Springer-Verlag.

Firszt, J. B., Holden, L. K., Skinner, M. W., Tobey, E. A., Peterson, A., Gaggl, W., Runge-Samuelson, C. L. and Wackym, P. A. (2004). Recognition of speech presented at soft to loud levels by adult cochlear implant recipients of three cochlear implant systems. *Ear and Hearing,* **25**(4)**:**375-387.

FitzHugh, R. 1969. Mathematical models of excitaions and propagation in nerve. *In:* SCHWAN, H. P. (ed.) *Biological Engineering.* New York: McGraw-Hill Book Co.

Frankenhaeuser, B. and Huxley, A. F. (1964). The action potential in the myelinated nerve fiber of Xenopus laevis as computed on the basis of voltage clamp data. *J.Physiol.,* (171)**:**302-315.

Friedland, D. R., Venick, H. S. and Niparko, J. K. (2003). Choice of ear for cochlear implantation: The effect of history and residual hearing on predicted postoperative performance. *Otology and Neurotology,* **24**(4)**:**582-589.

Frijns, J. H. M., Briaire, J. J. and Grote, J. J. (2001). The importance of human cochlear anatomy for the results of modiolus-hugging multichannel cochlear implants. *Otology and Neurotology,* **22**(3)**:**340-349.

Frijns, J. H. M., Briaire, J. J. and Schoonhoven, R. (2000). Integrated use of volume conduction and neural models to simulate the response to cochlear implants. *Simulation Practice and Theory,* **8**(1-2)**:**75-97.

Frijns, J. H. M., de Snoo, S. L. and Schoonhoven, R. (1995). Potential distributions and neural excitation patterns in a rotationally symmetric model of the electrically stimulated cochlea. *Hearing Research,* **87**(1-2)**:**170-186.

Frijns, J. H. M., Dekker, D. M. T. and Briaire, J. J. (2011). Neural excitation patterns induced by phased-array stimulation in the implanted human cochlea. *Acta Oto-laryngologica,* **131**(4)**:**362-370.

Frijns, J. H. M., Kalkman, R. K. and Briaire, J. J. (2009a). Stimulation of the facial nerve by intracochlear electrodes in otosclerosis: A computer modeling study. *Otology and Neurotology,* **30**(8)**:**1168-1174.

Frijns, J. H. M., Kalkman, R. K., Vanpoucke, F. J., Bongers, J. S. and Briaire, J. J. (2009b). Simultaneous and non-simultaneous dual electrode stimulation in cochlear implants: Evidence for two neural response modalities. *Acta Oto-laryngologica,* **129**(4)**:**433-439.

Gabriel, S., Lau, R. W. and Gabriel, C. (1996). The dielectric properties of biological tissues: II. Measurements in the frequency range 10 Hz to 20 GHz. *Physics in Medicine and Biology,* **41**(11)**:**2251-2269.

Geddes, L. A. and Baker, L. E. (1967). The specific resistance of biological material-A compendium of data for the biomedical engineer and physiologist. *Medical and biological engineering,* **5**(3)**:**271-293.

Geers, A., Tobey, E., Moog, J. and Brenner, C. (2008). Long-term outcomes of cochlear implantation in the preschool years: From elementary grades to high school. *International Journal of Audiology,* **47**(SUPPL. 2).

Ghiz, A. F., Salt, A. N., DeMott, J. E., Henson, M. M., Henson, Jr. and Gewalt, S. L. (2001). Quantitative anatomy of the round window and cochlear aqueduct in guinea pigs. *Hearing Research,* **162**(1-2)**:**105-112.

Girzon, G. 1987. *Investigation of current flow in the inner ear during electrical stimulation of intracochlear electrodes.* Master's, M.I.T.

Govindasamy, R. 2012. *Modelling subject-specific electrically evoked auditory neural responses in the guinea pig.* Masters in Engineering Dissertation, University of Pretoria.

Greenwood, D. D. (1990). A cochlear frequency-position function for several species - 29 years later. *Journal of the Acoustical Society of America,* **87**(6)**:**2592-2605.

Gupta, R., Bartling, S. H., Basu, S. K., Ross, W. R., Becker, H., Pfoh, A., Brady, T. and Curtin, H. D. (2004). Experimental Flat-Panel High-Spatial-Resolution Volume CT of the Temporal Bone. *Americal Journal of Neuroradiology,* **25:**1417-1424.

Hanekom, T. 2001a. *Modelling of the eletrode-auditory nerve fibre interface in cochlear prosthesis.* PhD thesis, University of Pretoria.

Hanekom, T. (2001b). Three-dimensional spiraling finite element model of the electrically stimulated cochlea. *Ear and Hearing,* **22**(4)**:**300-315.

Hanekom, T. (2005). Modelling encapsulation tissue around cochlear implant electrodes. *Medical and Biological Engineering and Computing,* **43**(1)**:**47-55.

Hartmann, R. and Klinke, R. (1990). Impulse patterns of auditory nerve fibres to extra- and intracochlear electrical stimulation. *Acta Oto-Laryngologica, Supplement,* **469:**128-134.

Hartmann, R., Topp, G. and Klinke, R. (1984). Discharge patterns of cat primary auditory fibers with electrical stimulation of the cochlea. *Hearing Research,* **13:**47-62.

Hassanzadeh, S., Farhadi, M., Daneshi, A. and Emamdjomeh, H. (2002). The effects of age on auditory speech perception development in cochlear-implanted prelingually deaf children. *Otolaryngology - Head and Neck Surgery,* **126**(5)**:**524-527.

Haueisen, J., Ramon, C., Eiselt, M., Brauer, H. and Nowak, H. (1997). Influence of tissue resistivities on neuromagnetic fields and electric potentials studied with a finite element model of the head. *IEEE Transactions on Biomedical Engineering,* **44**(8)**:**727-735.

Hochmair, I., Hochmair, E., Nopp, P., Waller, M. and Jolly, C. (2015). Deep electrode insertion and sound coding in cochlear implants. *Hearing Research,* **322**(0)**:**14-23.

Hodgkin, A. L. and Huxley, A. F. (1952). A quantitative description of membrane current and its application to conduction and excitation in nerve. *J.Physiol.,* (117)**:**500-544.

Hoekema, R., Wieneke, G. H., Leijten, F. S. S., Van Veelen, C. W. M., Van Rijen, P. C., Huiskamp, G. J. M., Ansems, J. and Van Huffelen, A. C. (2003). Measurement of the conductivity of skull, temporarily removed during epilepsy surgery. *Brain Topography,* **16**(1)**:**29-38.

Hofman, R., Segenhout, J. M. and Wit, H. P. (2009). Three-dimensional reconstruction of the guinea pig inner ear, comparison of OPFOS and light microscopy, applications of 3D reconstruction. *Journal of Microscopy,* **233**(2)**:**251-257.

Jiang, M., Wang, G., Skinner, M. W., Rubinstein, J. T. and Vannier, M. W. (2003). Blind deblurring of spiral CT images. *IEEE transactions on medical imaging,* **22**(7)**:**837-845.

Kalkman, R. K., Briaire, J. J., Dekker, D. M. T. and Frijns, J. H. M. (2014a). Place pitch versus electrode location in a realistic computational model of the implanted human cochlea. *Hearing Research,* **315:**10-24.

Kalkman, R. K., Briaire, J. J. and Frijns, J. H. M. (2014b). Current focussing in cochlear implants: An analysis of neural recruitment in a computational model. *Hearing Research*.

Kan, A., Litovsky, R. Y. and Goupell, M. J. (2015). Effects of Interaural Pitch Matching and Auditory Image Centering on Binaural Sensitivity in Cochlear Implant Users. *Ear and Hearing*.

Kaste, S. C., Young, C. W., Holmes, T. P. and Baker, D. K. (1997). Effect of helical CT on the frequency of sedation in pediatric patients. *Americal Journal of Radiology,* **168**(4)**:**1001-1003.

Ketten, D. R., Skinner, M. W., Wang, G., Vannier, M. W., Gates, G. A. and Neely, G. J. (1998). In vivo measures of cochlear length and insertion depth of nucleus cochlear implant electrode arrays. *Ann Otol Rhinol Laryngol,* **107:**1-16.

Kikidis, D. and Bibas, A. (2014). A Clinically Oriented Introduction and Review on Finite Element Models of the Human Cochlea. *BioMed Research International,* **2014:**8.

Kim, H. N., Shim, Y. J., Chung, M. H., Chang, M. S. and Choi, H. S. (1997). Comparison of speech discrimination scores between SPEAK and MPEAK speech-processing strategies. *Advances in oto-rhino-laryngology,* **52:**110-112.

Klop, W. M. C., Briaire, J. J., Stiggelbout, A. M. and Frijns, J. H. M. (2007). Cochlear implant outcomes and quality of life in adults with prelingual deafness. *Laryngoscope,* **117**(11)**:**1982-1987.

Koizuka, I., Seo, Y., Murakami, M., Seo, R. and Kato, I. (1997). Micro-magnetic resonance imaging of the inner ear in the guinea pig. *NMR in Biomedicine,* **10**(1)**:**31-34.

Kral, A., Hartmann, R., Mortazavi, D. and Klinke, R. (1998). Spatial resolution of cochlear implants: The electrical field and excitation of auditory afferents. *Hearing Research,* **121**(1-2)**:**11-28.

Kujawa, S. G. and Liberman, M. C. (2009). Adding insult to injury: Cochlear nerve degeneration after "temporary" noise-induced hearing loss. *Journal of Neuroscience,* **29**(45)**:**14077-14085.

Kumar, G., Chokshi, M. and Richter, C. P. (2010). Electrical impedance measurements of cochlear structures using the four-electrode reflection-coefficient technique. *Hearing Research,* **259**(1-2)**:**86-94.

Kunisue, K., Fukushima, K., Kawasaki, A., Maeda, Y., Nagayasu, R., Kataoka, Y., Kariya, S., Fukutomi, Y., Takami, H. and Nishizaki, K. (2007). Comprehension of abstract words among hearing impaired children. *International journal of pediatric otorhinolaryngology,* **71**(11)**:**1671-1679.

Lane, J. I., Driscoll, C. W. L., Witte, R. J., Primak, A. and Lindell, E. P. (2007). Scalar Localization of the Electrode Array After Cochlear Implantation: A Cadaveric Validation Study Comparing 64-Slice Multidetector Computed Tomography With Microcomputed Tomography. *Otology & Neurotology,* **28:**191-194.

Lee, J., Nadol Jr, J. B. and Eddington, D. K. (2010). Depth of electrode insertion and postoperative performance in humans with cochlear implants: A histopathologic study. *Audiology and Neurotology,* **15**(5)**:**323-331.

Li, T., Galvin Iii, J. J. and Fu, Q. J. (2009). Interactions between unsupervised learning and the degree of spectral mismatch on short-term perceptual adaptation to spectrally shifted speech. *Ear and Hearing,* **30**(2)**:**238-249.

Loizou, P. C., Stickney, G., Mishra, L. and Assmann, P. (2003). Comparison of speech processing strategies used in the Clarion implant processor. *Ear and Hearing,* **24**(1)**:**12-19.

Luker, G. D., Lee, B. C. P. and Erickson, K. K. (2007). Spiral CT of the temporal bone in unsedated pediatric patients. *Americal Journal of Neuroradiology,* **14:**1145-1150.

Mahmoud, A. F. and Ruckenstein, M. J. (2014). Speech Perception Performance as a Function of Age at Implantation Among Postlingually Deaf Adult Cochlear Implant Recipients. *Otology and Neurotology*.

Majdani, O., Leinung, M., Rau, T., Akbarian, A., Zimmerling, M., Lenarz, M., Lenarz, T. and Labadie, R. (2008). Demagnetization of cochlear implants and temperature changes in 3.0T MRI environment. *Otolaryngology - Head and Neck Surgery,* **139**(6)**:**833-839.

Malherbe, T. K. 2009. *Development of a methods to create subject specific cochlear models for electric hearing.* Masters Dissertation, Department of Electric, Electronic and Computer Engineering, University of Pretoria.

Malherbe, T. K., Hanekom, T. and Hanekom, J. J. (2013). Can subject-specific single-fibre electrically evoked auditory brainstem response data be predicted from a model? *Medical Engineering & Physics,* **35**(7)**:**926-936.

Malherbe, T. K., Hanekom, T. and Hanekom, J. J. (2015). The effect of the resistive properties of bone on neural excitation and electric fields in cochlear implant models. *Hearing Research,* **327:**126-135.

Marshall, D., Johnell, O. and Wedel, H. (1996). Meta-analysis of how well measures of bone mineral density predict occurrence of osteoporotic fractures. *British Medical Journal,* **312**(7041)**:**5.

Mens, L. H. M., Huiskamp, G., Oostendorp, T. and Van Den Broek, P. (1999). Modelling surface potentials from intracochlear electrical stimulation. *Scandinavian Audiology,* **28**(4)**:**249-255.

Mesnildrey, Q. and Macherey, O. (2015). Simulating the dual-peak excitation pattern produced by bipolar stimulation of a cochlear implant: Effects on speech intelligibility. *Hearing Research,* **319:**32-47.

Micco, A. G. and Richter, C. P. (2006). Electrical resistivity measurements in the mammalian cochlea after neural degeneration. *Laryngoscope,* **116**(8)**:**1334-1341.

Michelson, R. P., Merzenich, M. M., Pettit, C. R. and Schindler, R. A. (1973). A cochlear prosthesis: Further clinical observations; preliminary results of physiological studies. *Laryngoscope,* **83**(7)**:**1116-1122.

Milroy, C. M. and Michaels, L. (1990). Pathology of the otic capsule. *Journal of Laryngology and Otology,* **104**(2)**:**83-90.

Misrahy, G. A., Hildreth, K. M., Shinabarger, E. W. and Gannon, W. J. (1958). Electrical properties of wall of endolymphatic space of the cochlea (guinea pig). *The American journal of physiology,* **194**(2)**:**396-402.

Mosnier, I., Sterkers, O., Bebear, J. P., Godey, B., Robier, A., Deguine, O., Fraysse, B., Bordure, P., Mondain, M., Bouccara, D., Bozorg-Grayeli, A., Borel, S., Ambert-Dahan, E. and Ferrary, E. (2009). Speech performance and sound localization in a

complex noisy environment in bilaterally implanted adult patients. *Audiology and Neurotology,* **14**(2)**:**106-114.

Mudry, A. and Mills, M. (2013). The early history of the cochlear implant: A retrospective. *JAMA Otolaryngology - Head and Neck Surgery,* **139**(5)**:**446-453.

Nadol Jr, J. B. (1990). Degeneration of cochlear neurons as seen in the spiral ganglion of man. *Hearing Research,* **49:**141-154.

Nadol Jr, J. B. (1997). Patterns of neural degeneration in the human cochlea and auditory nerve: Implications for cochlear implantation. *Otolaryngology - Head and Neck Surgery,* **117**(3 I)**:**220-228.

Nelson, D. A., Donaldson, G. S. and Kreft, H. (2008). Forward-masked spatial tuning curves in cochlear implant users. *Journal of the Acoustical Society of America,* **123**(3)**:**1522-1543.

Noble, J. H., Gifford, R. H., Hedley-Williams, A. J., Dawant, B. M. and Labadie, R. F. (2014). Clinical evaluation of an image-guided cochlear implant programming strategy. *Audiology and Neurotology,* **19**(6)**:**400-411.

Nogaki, G., Fu, Q. J. and Galvin Iii, J. J. (2007). Effect of training rate on recognition of spectrally shifted speech. *Ear and Hearing,* **28**(2)**:**132-140.

O'Leary, S. J., Black, R. C. and Clark, G. M. (1985). Current distributions in the cat cochlea: A modelling and electrophysiological study. *Hearing Research,* **18**(3)**:**273-281.

Oostendorp, T. F., Delbeke, J. and Stegeman, D. F. (2000). The conductivity of the human skull: Results of in vivo and in vitro measurements. *IEEE Transactions on Biomedical Engineering,* **47**(11)**:**1487-1492.

Parkinson, A. J., Arcaroli, J., Staller, S. J., Arndt, P. L., Cosgriff, A. and Ebinger, K. (2002). The Nucleus® 24 Contour™ cochlear implant system: Adult clinical trial results. *Ear and Hearing,* **23**(1 Suppl)**:**41S-48S.

Poznyakovskiy, A. A., Zahnert, T., Kalaidzidis, Y., Schmidt, R., Fischer, B., Baumgart, J. and Yarin, Y. M. (2008). The creation of geometric three-dimensional models of the inner ear based on micro computer tomography data. *Hearing Research,* **243**(1-2)**:**95-104.

Rattay, F., Leao, R. N. and Felix, H. (2001a). A model of the electrically excited human cochlear neuron. II. Influence of the three-dimensional cochlear structure on neural excitability. *Hearing Research,* **153**(1-2)**:**64-79.

Rattay, F., Lutter, P. and Felix, H. (2001b). A model of the electrically excited human cochlear neuron I. Contribution of neural substructures to the generation and propagation of spikes. *Hearing Research,* **143:**43-63.

Rebscher, S. J., Hetherington, A., Bonham, B., Wardrop, P., Whinney, D. and Leake, P. A. (2008). Considerations for design of future cochlear implant electrode arrays: electrode array stiffness, size, and depth of insertion. *Journal of rehabilitation research and development,* **45**(5)**:**731-747.

Rebscher, S. J., Hetherington, A. M., Snyder, R. L., Leake, P. A. and Bonham, B. H. (2007). Design and fabrication of multichannel cochlear implants for animal research. *Journal of Neuroscience Methods,* **166**(1)**:**1-12.

Roland, J. T., Fishman, A. J., Alexiades, G. and Cohen, N. L. (2000). Electrode to modiolus proximity: a fluoroscopic and histologic analysis. *American Journal of Otolaryngology,* **21:**218-225.

Rosen, S., Faulkner, A. and Wilkinson, L. (1999). Adaptation by normal listeners to upward spectral shifts of speech: Implications for cochlear implants. *Journal of the Acoustical Society of America,* **106**(6)**:**3629-3636.

Rosset, A., Spadola, L. and Ratib, O. (2004). OsiriX: An open-source software for navigating in multidimensional DICOM images. *Journal of Digital Imaging,* **17**(3)**:**205-216.

Rubinstein, J. T. (1993). Axon termination conditions for electrical stimulation. *IEEE Transactions on Biomedical Engineering,* **40**(7)**:**654-663.

Rubinstein, J. T., Parkinson, W. S., Tyler, R. S. and Gantz, B. J. (1999). Residual speech recognition and cochlear implant performance: Effects of implantation criteria. *American Journal of Otology,* **20**(4)**:**445-452.

Ruivo, J., Mermuys, K., Bacher, K., Kuhweide, R., Offeciers, E. and Casselman, J. W. (2009). Cone beam computed tomography, a low-dose imaging technique in the postoperative assessment of cochlear implantation. *Otology and Neurotology,* **30**(3)**:**299-303.

Rush, S. and Driscoll, D. A. (1968). Current distribution in the brain from surface electrodes. *Anesthesia and Analgesia,* **47**(6)**:**717-723.

Saba, R., Elliott, S. J. and Wang, S. (2014). Modelling the effects of cochlear implant current focusing. *Cochlear Implants International,* **15**(6)**:**318-326.

Sakata, M., Hareyama, M., Heil, T. A., Henson, M. M., Henson Jr, O. W., Webber, R. L., Nair, M. K. and Smith, D. W. (2007). High-Resolution in situ Imaging of Cochlear Implant Electrode Arrays in Cat Temporal Bones Using Tuned Aperture Computed Tomography (TACT r). *Ear and Hearing,* **28:**435-443.

Schorr, E. A., Roth, F. P. and Fox, N. A. (2009). Quality of life for children with cochlear implants: Perceived benefits and problems and the perception of single words and emotional sounds. *Journal of Speech, Language, and Hearing Research,* **52**(1)**:**141-152.

Schuknecht, H. F. 1993. *Pathology of the Ear,* Philadelphia, Lea & Febiger.

Schwartz, J. R. and Eikhof, G. (1987). Na currents and action potentials in rat myelinated nerve fibres at 20 and 37 degrees C. *Pflug.Arch.,* (409)**:**469-577.

Seemann, M. D., Seemann, O., Bonel, H., Suckfull, M., Englmeier, K. H., Naumann, A., Allen, C. M. and Reiser, M. F. (1999). Evaluation of the middle and inner ear structures: Comparison of hybrid rendering, virtual endoscopy and axial 2D source images. *European Radiology,* **9**(9)**:**1851-1858.

Seeram, E. 2001. *Computed Tomography: Physical principles, clinical applications and quality control,* Philadelphia, Saunders.

Shannon, R. V., Zeng, F. G. and Wygonski, J. (1998). Speech recognition with altered spectral distribution of envelope cues. *Journal of the Acoustical Society of America,* **104**(4)**:**2467-2476.

Shibata, T., Matsumoto, S., Agishi, T. and Nagano, T. (2009). Visualization of Reissner membrane and the spiral ganglion in human fetal cochlea by micro-computed tomography. *American Journal of Otolaryngology - Head and Neck Medicine and Surgery,* **30**(2)**:**112-120.

Simmons, F. B. (1966). Electrical stimulation of the auditory nerve in man. *Archives of Otolaryngology,* **84**(1)**:**2-54.

Skinner, M. W., Holden, L. K., Whitford, L. A., Plant, K. L., Psarros, C. and Holden, T. A. (2002). Speech recognition with the Nucleus 24 SPEAK, ACE, and CIS speech coding strategies in newly implanted adults. *Ear and Hearing,* **23**(3)**:**207-223.

Skinner, M. W., Ketten, D. R., Holden, L. K., Harding, G. W., Smith, P. G., Gates, G. A., Neely, G. J., Kletzker, G. R., Brunsden, B. and Blocker, B. (2002). CT-Derived Estimation of Cochlear Morphology and Electrode Array Position in Relation to Word Recognition in Nucleus-22 Recipients. *Journal of the Association of Research in Otolaryngology,* **3:**332-350.

Skinner, M. W., Ketten, D. R., Vannier, M. W., Gates, G. A., Yoffie, R. L. and Kalender, W. A. (1994). Determination of the position of nucleus cochlear implant electrodes in the inner ear. *American Journal of Otology,* **15**(5)**:**644-651.

Skpizner, B. A., Holliday, R. A., Roland, J. T., Cohen, N. L., Waltzman, S. B. and Shapiro, W. H. (1995). Postoperative Imaging of the Multichannel Cochlear Implant. *Americal Journal of Neuroradiology,* **16:**1517-1524.

Skrodzka, E. B. (2005). Mechanical passive and active models of the human basilar membrane. *Applied Acoustics,* **66**(12)**:**1321-1338.

Smit, J. E., Hanekom, T. and Hanekom, J. J. (2008). Predicting action potential characteristics of human auditory nerve fibres through modification of the Hodgkin-Huxley equations. *South African Journal of Science,* **104**(7-8)**:**284-292.

Snel-Bongers, J., Briaire, J. J., Van Der Veen, E. H., Kalkman, R. K. and Frijns, J. H. M. (2013). Threshold levels of dual electrode stimulation in cochlear implants. *JARO - Journal of the Association for Research in Otolaryngology,* **14**(5)**:**781-790.

Sorn, P. M. and Curtin, H. D. 1996. *Head and neck imaging,* St. Louis, Mosby-Year Book.

Sparreboom, M., Langereis, M. C., Snik, A. F. M. and Mylanus, E. A. M. (2015). Long-term outcomes on spatial hearing, speech recognition and receptive vocabulary after sequential bilateral cochlear implantation in children. *Research in Developmental Disabilities,* **36**(0)**:**328-337.

Spelman, F. A., Clopton, B. M. and Pfingst, B. E. (1981). Tissue impedance and current flow in the implanted ear. Implications for the cochlear prosthesis. *The Annals of otology, rhinology & laryngology. Supplement,* **98:**3-8.

Spelman, F. A., Clopton, B. M. and Suesserman, M. F. Measurements of the resistivity of bony tissues of the cochlea. IEEE/Engineering in Medicine and Biology Society Annual Conference, 1987. 1911-1912.

Sridhar, D., Stakhovskaya, O. and Leake, P. A. (2006). A frequency-position function for the human cochlear spiral ganglion. *Audiology and Neurotology,* **11**(SUPPL. 1)**:**16-20.

Stakhovskaya, O., Sridhar, D., Bonham, B. H. and Leake, P. A. (2007). Frequency map for the human cochlear spiral ganglion: Implications for cochlear implants. *JARO - Journal of the Association for Research in Otolaryngology,* **8**(2)**:**220-233.

Strelioff, D. (1973). A computer simulation of the generation and distribution of cochlear potentials. *The Journal of the Acoustical Society of America,* **54**(3)**:**620-629.

Suesserman, M. F. and Spelman, F. A. (1993). Lumped-parameter model for in vivo cochlear stimulation. *IEEE Transactions on Biomedical Engineering,* **40**(3)**:**237-245.

Swartz, J. D. (1989). Current imaging approach to the ternporal bone. *Radiology,* **171:**309-317.

Sweeney, J. D., Mortimer, J. T. and Durand, D. (1987). Modeling of mammilian myelinated nerve for functional neuromuscular electrostimulation. *IEEE 9-th ann.conf.Eng.Med.Biol.Soc.Boston***:**1577-1578.

Tang, C., You, F., Cheng, G., Gao, D., Fu, F., Yang, G. and Dong, X. (2008). Correlation between structure and resistivity variations of the live human skull. *IEEE Transactions on Biomedical Engineering,* **55**(9)**:**2286-2292.

Tang, Q., Benítez, R. and Zeng, F. G. (2011). Spatial channel interactions in cochlear implants. *Journal of Neural Engineering,* **8**(4).

Teissier, N., Van Den Abbeele, T., Sebag, G. and Elmaleh-Berges, M. (2009). Computed tomography measurements of the normal and the pathologic cochlea in children. *Pediatric Radiology,* **40**(3)**:**275-83.

Teufert, K. B., Linthicum, Jr. and Connell, S. S. (2006). The effect of organ of Corti loss on ganglion cell survival in humans. *Otology and Neurotology,* **27**(8)**:**1146-1151.

Thorne, M., Salt, A. N., DeMott, J. E., Henson, M. M., Henson, Jr. and Gewalt, S. L. (1999). Cochlear fluid space dimensions for six species derived from reconstructions of three-dimensional magnetic resonance images. *Laryngoscope,* **109**(10)**:**1661-1668.

Van Besouw, R. M., Forrester, L., Crowe, N. D. and Rowan, D. (2013). Simulating the effect of interaural mismatch in the insertion depth of bilateral cochlear implants on speech perception. *Journal of the Acoustical Society of America,* **134**(2)**:**1348-1357.

Van Den Honert, C. and Kelsall, D. C. (2007). Focused intracochlear electric stimulation with phased array channels. *Journal of the Acoustical Society of America,* **121**(6)**:**3703-3716.

Van Der Marel, K. S., Briaire, J. J., Wolterbeek, R., Snel-Bongers, J., Verbist, B. M. and Frijns, J. H. M. (2014). Diversity in cochlear morphology and its influence on cochlear implant electrode position. *Ear and Hearing,* **35**(1)**:**9-20.

Vanpoucke, F. J., Zarowski, A. J. and Peeters, S. A. (2004). Identification of the impedance model of an implanted cochlear prosthesis from intracochlear potential measurements. *IEEE Transactions on Biomedical Engineering,* **51**(12)**:**2174-2183.

Verbist, B. M., Ferrarini, L., Briaire, J. J., Zarowski, A., Dmiraal-Behloul, F., Olofsen, H., Reiber, J. H. C. and Frijns, J. H. M. (2009). Anatomic considerations of cochlear morphology and its implications for insertion trauma in cochlear implant surgery. *Otology and Neurotology,* **30**(4)**:**471-477.

Verbist, B. M., Frijns, J. H. M., Geleijns, J. and van Buchem, M. A. (2005). Multisection CT as a Valuable Tool in the Postoperative Assessment of Cochlear Implant Patients. *Americal Journal of Neuroradiology,* **26:**424-429.

Vincent, C., Ruzza, I., Vaneecloo, F. M. and Dubrulle, F. (2008). Magnetic resonance imaging with the Digisonic SP Neurelec cochlear implant. *European Archives of Oto-Rhino-Laryngology,* **265**(9)**:**1043-1046.

Vladimirescu, A. 1994. *The Spice Book,* John Wiley & Sons, Inc.

Voie, A. H. (2002). Imaging the intact guinea pig tympanic bulla by orthogonal-plane fluorescence optical sectioning microscopy. *Hearing Research,* **171**(1-2)**:**119-128.

Vollmer, M., Beitel, R. E., Snyder, R. L. and Leake, P. A. (2007). Spatial selectivity to intracochlear electrical stimulation in the inferior colliculus is degraded after long-term deafness in cats. *Journal of Neurophysiology,* **98**(5)**:**2588-2603.

von Békésy, G. (1951). The Coarse Pattern of the Electrical Resistance in the Cochlea of the Guinea Pig (Electroanatomy of the Cochlea). *The Journal of the Acoustical Society of America,* **23**(1)**:**18-28.

Wang, G., Vannier, M. W., Skinner, M. W., Cavalcanti, G. P. and Harding, G. W. (1998). Spiral CT Image Deblurring for Cochlear Implantation. *IEEE transactions on medical imaging,* **17**(2)**:**251-262.

Wang, G., Vannier, M. W., Skinner, M. W., Kalender, W. A., Polacin, A. and Ketten, D. R. (1996). Unwrapping Cochlear Implants by Spiral CT. *IEEE Transactions on Biomedical Engineering,* **43**(9)**:**891-900.

Whiten, D. M. 2007. *Electro-anatomical Models of the Cochlear Implant.* PhD, Massachusetts Institute of Technology.

Whiting, B. R., Bae, K. T. and Skinner, M. W. (2001). Cochlear Implants: Three-dimensional Localization by Means of Coregistration of CT and Conventional Radiographs. *Radiology,* **221:**543-549.

Wysocki, J. (1999). Dimensions of the human vestibular and tympanic scalae. *Hearing Research,* **135**(1-2)**:**39-46.

Xu, J., Stevenson, A. W., Gau, D., Tykocinski, M., Lawrence, D., Wilkins, S. W., Clark, G. M., Saunders, E. and Cowan, R. S. (2001). The role of radiographic phase-contrast imaging in the development of intracochlear electrode arrays. *Otol Neurotol,* **22:**862-868.

Xu, J., Xu, S. A., Cohen, L. T. and Clark, G. M. (2000). Cochlear view: Postoperative radiography for cochlear implantation. *American Journal of Otology*, **21**(1)**:**49-56.

Yang, S., Wang, G., Skinner, M. W., Rubinstein, J. T. and Vannier, M. W. (2000). Localization of cochlear implant electrodes in radiographs. *Medical Physics,* **27**(4)**:**775-777.